A Multi-Scale Iterative Approach for Finite Element Modeling of Thermal Contact Resistance

by

Mary Kathryn Thompson

B.S., Massachusetts Institute of Technology, 2002
M.S., Massachusetts Institute of Technology, 2004

Submitted to the Department of Mechanical Engineering
in Partial Fulfillment of the Requirements for the Degree of

Doctor of Philosophy in Mechanical Engineering

at the

Massachusetts Institute of Technology

September 2007

Signature of Author.....
Department of Mechanical Engineering
August 9, 2007

Certified by.....
Alexander H. Slocum
Professor of Mechanical Engineering
Thesis Supervisor

Accepted by.....
Lallit Anand
Professor of Mechanical Engineering
Chairman, Committee for Graduate Students

A Multi-Scale Iterative Approach for Finite Element Modeling of Thermal Contact Resistance

by

Mary Kathryn Thompson

Submitted to the Department of Mechanical Engineering
on August 9, 2007 in Partial Fulfillment of the
Requirements for the Degree of Doctor of Philosophy in
Mechanical Engineering

ABSTRACT

Surface topography has long been considered a key factor in the performance of many contact applications including thermal contact resistance. However, essentially all analytical and numerical models of thermal contact resistance and thermal contact conductance either neglect surface topography or make simplifications and assumptions about the nature of the surface. This work combines measured surface geometry with an iterative thermal/structural finite element model to more accurately predict microscopic and macroscopic thermal contact resistance. A commercial power electronics module which exhibits both macroscopic surface form and micro scale surface roughness is analyzed using three different macro scale surface models to verify the accuracy of the model and to demonstrate the impact of geometric surface assumptions. Finally, the factors influencing the thermal/structural behavior of bolted plates are examined and recommendations for reducing both contact resistance and the overall thermal resistance of bolted plate systems are presented.

Thesis Supervisor: Alexander H. Slocum

Title: Neil and Jane Pappalardo Professor of Mechanical Engineering

Acknowledgements

I can recall quite clearly sitting on my parents's bed as a very small child with my mother telling me that one day I would get a Ph.D. from MIT. I am not certain that I fully understood what a Ph.D. was at the time. I am certain that I had never heard of MIT. But the message was clear: You can be anything you want to be. We will help you.

Twenty some years later, I find myself writing the acknowledgements section for my doctoral dissertation from MIT. I find it ironic that my mother's prediction came true, but not surprising. My parents and my sister have helped, supported, taught, advised, and loved me every step of the way. This work is dedicated to them.

I would like to thank my committee: Prof. David M. Parks, Prof. Borivoje Mikic, Prof. Alexander H. Slocum, and Prof. Nam P. Suh for their mentorship, encouragement, guidance, input and discussion in all aspects of this project. It would not have been possible without them.

I would like to thank ABB Inc. for sponsoring this research.

I would like to thank Jerry Bittner from ANSYS Inc. who has been unfailingly supportive of my research for almost a decade. I would also like to thank the following people from ANSYS Inc. for their help over the years: Paul Lethbridge, Chokri Guetari, Sheryl Ackerman, Dino Ciabattoni, John Dulis, Rich Lange, Dave Looman, George Karnos, Beth Mazurak, Diana Cooney, Shane Moeykens, Matt Madore, John Kiefer and everyone in Technical Enhancements and Customer Support at ANSYS Corporate Headquarters.

This research required an enormous number of surface measurements, often with equipment that I did not have access to on campus. I would like to thank Amy McClung from Zygo Inc., Jeffrey Grissom from Corning Tropel, Prof. Christopher Brown and Brendan Powers from the WPI Surface Metrology Lab, Randall Leifheit from Solarius Development, Nabeel Sufi and Don Roberts from ADE Phase Shift, and David Main and Paul Beaulieu at Excel Technologies for their help in obtaining the measurements that I needed.

I would like to thank Karta Khalsa from Zygo Inc. for working with me to develop a method for transferring Zygo surface data directly into an ANSYS array. Without his help, the surface importation work would have been possible, but not practical. I hope that we can continue to work together in the future.

I would like to thank Prof. Sanjay Sarma, Prof. Alex Techet, and Dr. Nannaji Saka from MIT and Prof. Norbert Huber and Dr. Vishwanath Hegadekatte from the GKSS Forschungzentrum in der Helmholtz-Gemeinschaft for their conversations about my research.

I would like to thank Dr. Joseph Foley, Dr. Edwin Karat, Dr. Andrew “Zoz” Brooks, Dr. Thomas Mack and Antonio Vicente for their help with various aspects of this thesis.

I would like to thank Prof. Rohan Abeyaratne, Prof. Wesley Harris, Sandra Harris, and Prof. Chrys Chryssostomidis for being phenomenal mentors over the years.

I would like to thank Beth Weinstein, Emily Thornett, and Valerie Laird for making the preliminary publication of this work a pleasure.

Finally, I would like to thank the teaching, technical, administrative and support staff in the Mechanical Engineering Department at MIT, especially Maureen Lynch, Ray Hardin, Tony Pulsone, Lori Hyke, Mark Belanger, Dick Fenner, Bob Nuttall, Bob Gersten, Steve Haberek, Joe Cronin, Pierce Hayward, Mike Maier, Leslie Regan, Joan Kravit, Peggy Garlick, Meg Gross, Caroline Johnston, Maureen DeCourcey, Joan Hutchins, Franz Hover and Christiaan Adams. Without them, nothing would ever get done.

Contents

Chapter 1: Introduction

1.1 Overview

Surface topography has long been considered a key factor in the performance of many contact applications including thermal contact resistance. Many attempts have been made to model and predict thermal contact resistance, but this work has been limited by the ability to create models that accurately describe the behavior of interacting asperities at the surface.

Traditionally, surfaces were modeled analytically using assumptions and simplifications. Asperities were modeled as a variety of geometric shapes. Surface asperity heights and contact patterns were treated as probability distributions. The behavior of a single pair of interacting asperities was often extrapolated to describe the behavior of a pair of interacting surfaces covered in asperities. These assumptions were not made because they were shown to accurately represented the system of interest, but because they made modelling possible. In the 1950's and 60's when much of this work was done, there was no alternative.

There have been many advances in technology in the past seventy years, especially in surface metrology and numerical analysis techniques. It is now possible to optically measure micro and macro scale surface features and record the surface data digitally. Numerical and finite element modeling permit multi-physics contact simulations with complex geometry, boundary conditions, material properties and material models. It seems logical to combine the digital surface data with numerical analysis techniques to create more accurate models of surface phenomena like thermal contact resistance. However, the assumptions and simplifications about surface topography that were developed for analytical modeling are prevalent in numerical models today, primarily because the historical computational costs associated with solving problems with real surface geometry were prohibitive. In 2001, Peng et al. argued that “for 3D rough surface contact problems with many asperities of arbitrary shape, [the] requirement of large number[s] of mesh elements makes the finite element approach unfeasible.”[1] Marchand, et al. echoed this sentiment in 2000.[2] It seems that statements like these have discouraged researchers from periodically checking to see if they are still true.

This work demonstrates that finite element models with real surface topography can be created and solved today. This technology is then applied to predict thermal contact resistance at the macro and micro scales.

Chapter 2 presents a method for importing surface measurement data into a finite element program and two methods for creating surface geometry using the imported data. It is shown that it is possible to solve relatively small contact problems with real surface geometry on a desktop computer. (Larger problems could be solved on industrial

computers with or without parallel processing capability today if desired.) The results of mechanical contact analyses with imported surface geometry are shown to qualitatively match expectations.

Chapter 3 presents a multi-scale iterative approach to model thermal contact resistance on the macro and micro scale to be used in conjunction with the finite element surface modeling methods developed in the previous chapter. The assumptions and limitations of the model are discussed and future improvements to the model are suggested.

In Chapter 4, a commercial power electronics module (PEM) which exhibits both macroscopic surface form and micro scale surface roughness is analyzed using three different macro scale surface models and three different interstitial materials to demonstrate the method, to verify the accuracy of the model and to demonstrate the impact of geometric surface assumptions. The PEM base plate, which is bolted to an ideal heat sink, is modeled as ideal (perfectly flat), idealized (sinusoidal) and real (imported) with vacuum, air, and thermal grease in the interface.

The predicted macro scale contact patterns for the three models are shown to be similar to the measured contact pattern, but the contact pattern from the imported surface model is shown to be the best match. The results of the imported thermal/structural analysis on the macro scale with air (R = 1.61e-2 K/W) and thermal grease (R =3.91e-3 K/W) bound the experimental measurements (R = 9e-3 K/W) as expected. The micro scale analysis predicts a thermal contact resistance per unit area that is similar to experimental values from the literature.

Both the thermal and structural results are qualitatively similar for all three surface models, but quantitatively the results differ by up to 98%. In addition, the ideal and idealized surface models do not bound the experimental measurement of total thermal resistance for the PEM. The upper bound simulations with air as the interstitial material ($R_{air,ideal}$ = 7.16e-3 K/W and $R_{air,idealized}$ = 7.32e-3 K/W) are 20% lower than the experimental value. This shows that the ideal and idealized surface models cannot be used to accurately predict the thermal resistances for the case study and validates the need for better surface modeling.

In Chapter 5, the factors influencing the micro and macro scale thermal/structural behavior of bolted plates are examined and recommendations for reducing both contact resistance and the overall thermal resistance for the case study are presented. It is shown that the micro scale system is insensitive to the nature of the applied thermal load as long as the results from the macro scale model for the elements in contact are used. The micro scale system is sensitive to applied structural load, surface roughness and nano scale thermal boundary resistance. The applied load and thermal boundary resistance seem to exhibit a threshold type behavior while the relationship between thermal contact resistance and surface roughness seems to be linear. The choice of surface sample and imported lateral resolution seem to have a relatively small effect on the model. The effects of the surface modeling parameters will be explored further in future work.

It is shown that the macro scale system is relatively insensitive to the nature of the applied thermal load, the applied structural load, the micro scale thermal contact resistance and the thickness of the heat sink. The thermal resistances are sensitive to base plate thickness, the amplitude of the surface form and the thermal and mechanical material properties of the base plate and the heat sink. The applied load and micro scale thermal contact resistance both exhibit a threshold type behavior. The macro scale system also exhibits strong coupling between the thermal and structural solutions, especially for the surface form amplitude and the base plate thickness, which can make it difficult to predict the effect that altering certain parameters will have on the thermal resistances in the model. It is shown that the thermal contact resistance on the macro scale contributes approximate 25% to the total thermal resistance of the system regardless of interstitial material. It is also shown that one dimensional thermal conduction resistances (L/KA) apply only for the cases where thermal grease is present at the interface.

Finally, it is shown that the PEM system for the case study can be improved by up to 153% if the applied structural load is increased, the surface form (bow) is eliminated, the micro scale thermal contact resistance is reduced and the base plate and heat sink materials are replaced with copper.

In chapter 6, the contributions and conclusions of the work are presented and recommendations for improving the performance of the PEM bolted joint system based on the results of chapter 5 are made.

A lengthy discussion of future work for modeling surface topography is presented. It is proposed that the length scale dependence of certain aspects of surface importation methods be investigated including: the required minimum imported lateral resolution; the minimum surface sample size to produce a representative micro scale mode; and the relationship between the length scale(s) of the imported surfaces and the length scales of the finite element mesh and the so-called pinball region. It is suggested that more advanced material models (plasticity, viscoelasticity, viscoplasticity), temperature dependent material properties, thermal expansion, and surface coatings be included in future work. It is also suggested that traditional surface models be compared to imported surface models to determine the quality of the historical models and propose improvements in surface modeling.

Finally, a length discussion of future work for modeling the thermal contact resistance of bolted plates is presented. It is proposed that alternate solutions to reducing the total thermal resistance of bolted plate systems be considered including: the use of micro and meso scale surface texturing to reduce thermal contact resistance between the two plates; and the removal of the heat sink altogether to permit the use of forced air cooling to remove the heat from the base plate. It is suggested that the modeling of the bolted regions be improved and the effect of bolt hole geometry on total thermal resistance and thermal contact resistance be investigated. It is suggested that local results be used in the place of averaged results during the iteration between length scales. Finally, it is suggested that the

results of this work be compared to historical analytical and experimental correlations and the thermal and structural results of this work be compared further to propose new correlations if applicable.

1.2 Choice of Finite Element Program

The finite element method can be applied either by writing a custom finite element program or by using a commercial finite element program. There are advantages and disadvantages to both approaches. Commercial finite element packages have a large number of built in features, including pre-defined elements to simulate various physics regimes, solid modeling capabilities and a graphical user interface. The larger codes are able to model many problems of interest with a wide variety of physics environments, so the user does not need to spend time and energy developing the capabilities that they need for their application. Commercial codes are also used extensively in industry so innovative modeling techniques developed with commercial codes can easily be transferred to industry. The disadvantages of commercial codes are the cost of purchasing the software and a steep initial learning curve.

Custom finite element codes can be less expensive in terms of time and money to write if the user is well versed in finite element theory and a relatively small variety of problems need to be solved. Custom codes may be more user friendly if designed for a specific type of application. A custom code may also be necessary if the physics necessary is not available in the commercial codes.

Some of the available commercial finite element programs have also incorporated features that permit the user to customize or modify the program to increase the capabilities and flexibility of the program. This allows the programs to bridge the gap between commercial and custom codes. ANSYS and ABAQUS are two of the leaders in this area. In ANSYS, these capabilities include a scripting language called the ANSYS Parametric Design Language (APDL) and User Programmable Features which allow the user to write FORTRAN routines to create a custom version of ANSYS.

The cost and learning curve associated with using a commercial code with customization features are far outweighed by the benefit of adapting these types of programs for non-traditional contact and tribological applications. For this work, the ANSYS finite element program will be used although the methods should be applicable to a wide range of finite element programs.

References:

1. Peng, W. and Bhushan, B. “A numerical three-dimensional model for the contact of layered elastic/plastic solids with rough surfaces by variational principle.” Trans. AMSE, J. Tribology 123 (2002) 330-342.
2. Marchand, A. S. and Raynaud, M. “Numerical Determination of Thermal Contact Resistance for Nonisothermal Forging Processes.” Trans. ASME, J. Heat Transfer 122 (2000) 776-784.

References:

Chapter 2: Surface Modeling and Importation

This chapter presents a method for importing surface measurement data into a finite element program and two methods for creating surface geometry using the imported data. It is shown that it is possible to solve relatively small contact problems with real surface geometry on a desktop computer. (Larger problems could be solved on industrial computers with or without parallel processing capability today if desired.) The results of mechanical contact analyses with imported surface geometry are shown to qualitatively match expectations.

2.1 Challenges for Modeling Surfaces

There are a number of challenges associated with modeling surfaces and systems where the behavior at the surface is critical. First, the geometry at the surface is often irregular and complex. Surface damage such as pitting or scratching can further increase the complexity of the surface topography, making it difficult to formulate a geometric model that accurately describes the surface topography.

Surface chemistry may have a large effect on the behavior of surfaces in contact. Adhesion and molecular bonding between surfaces may contribute to the contact forces holding the surfaces together. Adsorption, absorption, oxidation and corrosion may change the chemical composition and the material properties at the surface. Material properties are also temperature and length scale dependent which further complicates the model.

In addition to natural oxides, other surface layers both intentional and unintentional may be present at the surface. Protective oxides may be placed on the surface through anodizing operations. Surfaces may be coating with pure metals such as copper and gold to increase the electrical or thermal conductivity of the surface. Compounds such as titanium carbide may be added to increase the hardness. It is often difficult to judge the thickness and material properties of these surface layers and the resulting layers may not be uniform in thickness or in quality.

Sub-surface imperfections such as voids or cracks may be present in surfaces. These can have a significant impact on the behavior of the surface and lead to phenomena such as delamination wear, however they are difficult to measure and predict.

Materials such as air, lubricants, dirt and wear particles may be present in the interface between two surfaces which can affect the mechanical, thermal, and electrical behavior at the interface. Materials can also transfer from one surface to another across an interface.

Sporadic contact between rough surfaces can result in very high localized loading between two surfaces in contact which can require the inclusion of more advanced modeling including plasticity, fracture and creep.

Finally, real surfaces often require multi-physics modeling to describe mechanical, thermal, electrical and fluid behavior at or near the interface.

Addressing all of these issues in a single model is very difficult, so most surface models focus on one of these challenges and neglect the rest. One of the most common issues to address is surface topography.

2.2 Prior Art: Traditional Geometric Surface Models

Traditionally, surfaces were modeled analytically by ignoring the surface details, including the details by using experimentally derived coefficients, or simplifying the surface geometry. Surface asperities have been modeled using a variety of geometric shapes and the behavior of a single pair of interacting asperities was often assumed to describe the behavior of a pair of interacting surfaces covered in asperities.[1-4] Surfaces have also been modeled using probability distributions [5-7] and by using fractals.[8-10] In most cases, these assumptions were not made because they were shown to accurately represent the system of interest, but because they made modeling possible.

More recently, numerical contact simulations have been used to model surface phenomena. Some researchers choose to write custom programs to perform the numerical analysis [9,11,12] while others have chosen to use commercial finite element programs.[13,14] However, the geometric assumptions used in the analytical models have followed into the numerical models primarily because the computational costs associated with solving increasingly complex geometry were considered to be prohibitive.[15,16]

2.3 Improving Geometric Surface Models

For some of the simpler geometric surface models, it is possible to determine qualitatively that they are not a good representation of a real surface by visually comparing a measured surface to a modeled surface. For example, most real surfaces are not covered in hemispherical shaped asperities. (Shot peened surfaces are one notable exception.) However, for many of the more complicated surface models, including models that use probability distributions and fractals, the quality of the assumptions are less clear.

To improve the quality of geometric surface models, it is necessary to determine the quality of the current model, and then improve the assumptions in the model if possible. It will never be possible to completely remove geometric assumptions, so the goal should be to create a model that is closest to reality that is still within our ability to solve.

In this work, real measured surface geometry is incorporated into finite element models. The use of real surface data to create surface geometry significantly improves the quality of the assumptions in the models and the quality of the model results. This in turn enables predictive modeling for surface phenomena that have been limited to experimental coefficients in the past.

In future work, these imported surfaces will be compared to historical surface modeling techniques to evaluate their quality. Imported surfaces may also help us to develop new geometric surface models which are similar to the real surfaces but have lower computational costs.

2.4 Overview of Surface Modeling Using Real Surface Data

The procedure for creating and importing surface data for finite element analysis has four basic steps:

1. Gather information about the surface geometry.
2. Transfer information into the finite element program as a 2D array.
3. Operate on array values (if desired).
4. Apply array values for modify finite element model or to create solid model.

Each of these steps are discussed in detail below.

2.5 Gathering Information about the Surface

When gathering information about surface topography for importation into a finite element model, it is desirable to obtain high resolution digital data without damaging the sample. For this reason, optical surface metrology methods are recommended.

Optical surface metrology methods include: white light phase shifting optical profilometers, grazing incidence profilometers, confocal white light profilometers, and confocal laser scanning profilometers. The first two methods are true three dimensional measurement techniques that use optical fringes to determine the surface heights. The last two methods are two dimensional measurement techniques which can be used to build three dimensional images. Each method has advantages and disadvantages. For this work, a phase shifting optical profilometer is used to measure micro scale surface topography and a grazing incidence profilometer is used to measure macro scale geometry. The other methods were also used in the course of this work but those measurements are not presented.

2.6 Transferring Surface Information

Many finite element programs, including ANSYS, ABAQUS and MATLAB, have the ability to create models using a series of plain text commands instead of using the graphical user interface. These commands can then be read into the program either as input files or as batch files. This ability to import collections of commands as input files also permits surface data to be easily imported.

The surface transfer process has four steps:

1. Prepare the surface data for export
2. Export the surface data into a portable file format
3. Use the surface data to create the input commands
4. Import the commands into the finite element program.

2.6.1 Preparing the Surface Data for Export

Most surface metrology software has the ability to repair, modify and filter surface data, while most finite element programs do not. For this reason, these operations should be performed before the data is exported.

2.6.1.1 Data Drop Out

All optical metrology tools have limitations, and many surface have features or properties that are difficult to measure. When a metrology tool cannot get a signal for a given pixel or area on the surface, no data is recorded for that location; that data point simply “drops out” of the data set.

After the surface data is obtained, the analyst should determine the extent and location of the data drop out points so they can make an engineering decision about the quality of the data set. If the data drop out points are relatively few and far away from areas of interest, then the data set may be acceptable for use in finite element analysis. Too many data drop out points or a number of drop out points clustered around an important surface feature may require additional measurements or a different measurement technique. Once the data set is determined to be acceptable, then the data fill tools included with the surface metrology software may be used to repair the missing data.

2.6.1.2 Measurement Artifacts

In addition to having missing surface data due to data drop out phenomena, it is also possible to have anomalous data included that is a result of measurement artifacts or foreign objects (dust, dirt, etc.) on the surface. Often measurement artifacts appears as isolated tall thin spikes on the surface. Real spikes on the surface would be rapidly broken off or worn away with handling and use and are unlikely to be present on the surface.

Measurement artifacts can often be avoided by carefully cleaning the sample surface before imaging the surface. They can also be removed after the measurement is taken by filtering the data to remove statistical outliers and replacing them with a more probable value through a data fill process.

2.6.1.3 Alignment Errors

Finally, alignment errors between the measurement device and the sample can cause planar surface form to be included in the surface data even if it is not present in the sample. This planar surface form can also be removed by filtering the surface data before it is exported.

2.6.2 Exporting Surface Data

To import surface data into a finite element program, the data recorded by the measurement device must first be exported from its native file format into a portable (open) file format. Most software programs output the surface metrology data to a file that has an enriched data format which permits the generation of surface data, surface plots, 2D and 3D images, calculated parameters and more. The files may have extensions like .dat, .sur, and .map and may be either binary or ascii. These native file formats are generally for the convenience of the generating program and are usually not intend for use with any other software. Although some programs can read the native file formats of other programs, many cannot so most surface metrology software also has capabilities to export the surface data in a variety of formats including as an ascii plain text file.

One common format for exported data is the “xyz” or “triplet” format. The file for xyz data contains three columns of data: the first column contains the x index or coordinate for each data point recorded, the second column contains the y index or coordinate, and the third column contains the z coordinate or surface height. The column data may be space delimited, comma delimited or tab delimited. If x and y indices are provided instead of coordinates, they may be multiplied by the lateral resolution of the measurement to convert them to x and y coordinates.

For this work, all surface data was exported in triplet format.

2.6.3 Creating the Input Commands

After the surface data is exported in a portable format, it must be reformatted as commands that can be interpreted by the finite element program. The commands required will depend on the particular finite element code being used. For this work, a two dimensional array parameter is defined in ANSYS and the surface data is used to populate the array. The row and column indices are the x and y indices for the surface data. The cells in the array contain the surface height (z coordinate) information.

An example of converting xyz data to an ANSYS array is shown in Figure 2-1. The original data is listed on the left, while the commands to create the surface data array are on the right.

```
0 0 10.1186
1 0 10.1154
2 0 10.1168
3 0 10.1023
4 0 10.1145
5 0 10.1192
6 0 10.12
7 0 10.1197
8 0 10.1205
9 0 10.1174
10 0 10.1114
```

```
numrow = 10
numcol = 1
*dim,surfdata,array,numrow,numcol

surfdata ( 1 , 1    ) = 10.1186
surfdata ( 2 , 1    ) = 10.1154
surfdata ( 3 , 1    ) = 10.1168
surfdata ( 4 , 1    ) = 10.1023
surfdata ( 5 , 1    ) = 10.1145
surfdata ( 6 , 1    ) = 10.1192
surfdata ( 7 , 1    ) = 10.12
surfdata ( 8 , 1    ) = 10.1197
surfdata ( 9 , 1    ) = 10.1205
surfdata ( 10 , 1   ) = 10.1174
surfdata ( 11 , 1   ) = 10.1114
```

Figure 2-1: Surface Data: XYZ Format (Left), ANSYS Array Format (Right)

Surface data can be formatted manually using a variety of software programs and scripting languages, however this can be time consuming and cumbersome. To facilitate this work, Karta Khalsa of Zygo Inc. created a translator program which automatically converts the Zygo native file format (.dat) to a plain text file (.txt) suitable for use as an ANSYS input file. All surface data for this work was imported using this translator program.

2.6.4 Importing the Input Commands

Finally, the commands and surface data are saved as an input file and read into the finite element program. The details of how to do this will vary depending on the finite element program being used.

2.7 Operating on Surface Data in ANSYS

Once the surface data has been exported from the measurement software, some secondary operations may need to be performed on the surface data before creating solid model or finite element model geometry. Examples of these operations include: re-centering the data, combining surface arrays, mirroring surface arrays, scaling surface arrays, and enabling interpolation of the array. These operations may be performed by an external program if desired. For this work, the ANSYS Parametric Design Language (APDL) is used to perform these operations within the finite element program.

2.7.1 Re-Centering Surface Arrays

Surface data is often based on relative measurements instead of absolute measurements and the reference plane for relative measurements can be somewhat arbitrary. It may vary some sample to sample, and from measurement to measurement. It is recommended all data sets be re-centered about the mean surface height after importation into the finite element program. This ensures that the mean surface coincides with the nominal surface in the model.

2.7.2 Mirroring Surface Arrays

Numerical surface data is not only relative to a vertical plane, it is also relative to the coordinate system being used. The location of the origin relative to the surface data and the direction of the normal vectors impacts how the data is recorded, viewed, exported, and ultimately used to construct surface geometry. If data is exported into a different coordinate system without taking the differences into account, many characteristic parameters like average roughness, rms roughness and the surface height distributions will be the same, but the imported data will no longer resemble the original surface. Analyses that depend on both the surface heights and their locations will be invalidated.

Some surface metrology tools display the surface data in a coordinate system that is different than the one that is used to record the data. If the data is imported into the finite element program using the recorded coordinate system instead of into the display coordinate system, the generated surface will be valid for analytical purposes, but the surface generated in the finite element program may appear to be rotated from or the mirror image of the surface map generated by the surface metrology program.

The data may be rotated or mirrored into an alternate configuration if desired, but the user should know which surface is the “real” surface and which is the altered (rotated or mirrored surface) and if the rotation can be permitted. All surfaces in this work are imported using the measurement (“real”) coordinate system, instead of the display coordinate system. For this reason, some imported surfaces will appear as vertical mirror images of the measured surfaces. Surfaces that exhibit this mirrored effect were measured using a Zygo New View optical interferometer. Surfaces that do not exhibit the mirrored effect were measured using a Corning Tropel Flat Master grazing incidence interferometer.

2.7.3 Combining Surface Arrays

There are many reasons why it would be desirable to combine surface arrays. First, very few real surfaces exhibit features on a single length scale. For example, many micro scale surfaces exhibit roughness, waviness, and surface form. Since each of these features has a different range of characteristic frequencies, it may not be possible to capture them all with a single measurement. Instead, they could be measured separately, imported into separate surface data arrays, and then combined before the model geometry is created.

Figure 2-2 shows examples of surfaces that were created by combining two separate arrays which describe different frequencies. The models have the same dimensions (50 x 50 x 10 um) but the surface on the left is four times rougher than the surface on the right.

In addition, it may be desirable to modify the surface topography to reflect operations (intentional or unintentional) performed on the surface such as lapping, grinding, or wear. Each operation may have its own characteristic distribution which could be subtracted from the data to produce a machined or polished version of the original surface.

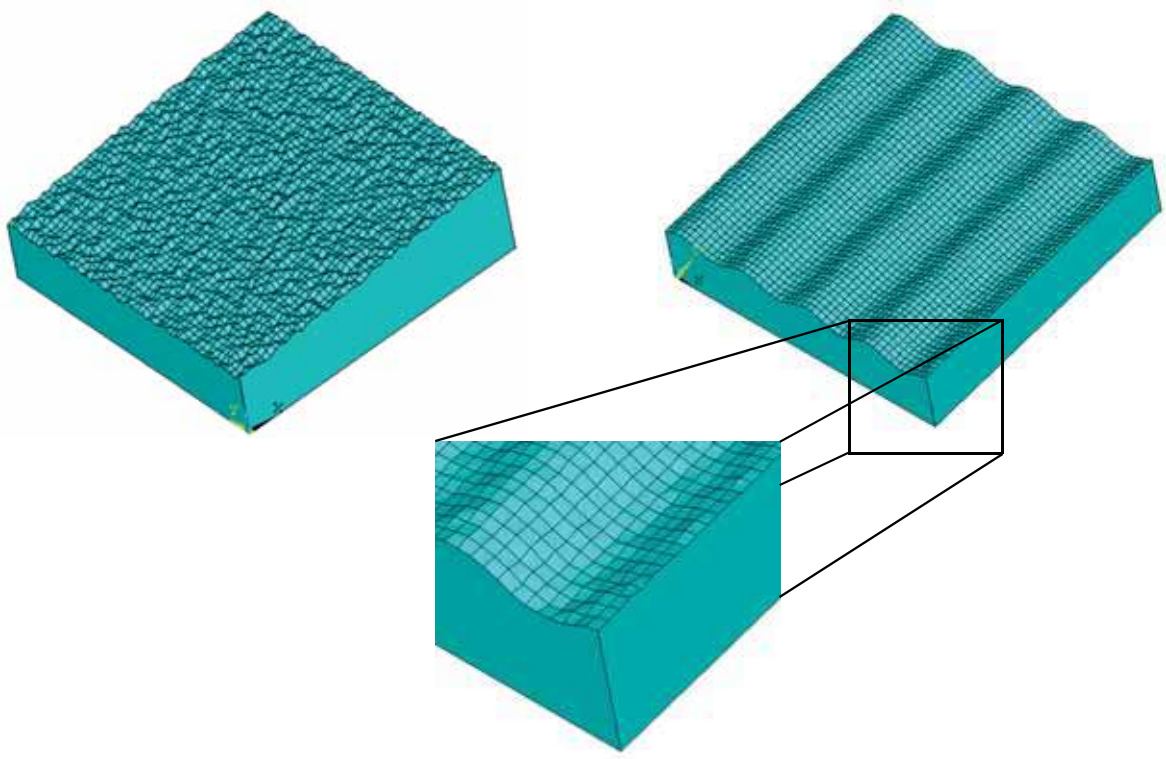

Figure 2-2: Combined Surfaces: Roughness and Surface Form (left), Roughness and Waviness (right)

2.7.4 Scaling Surface Arrays

It may be desirable to determine how a given measured surface would behave if the surface features were scaled up or down to create a rougher or smoother surface. In this case, the surface array may be multiplied by some value to scale the values in the array.

2.7.5 Enabling Interpolation

There may be instances when more surface data is available than can be incorporated and solved in a given model. Conversely, there may be instances when the characteristic length of the finite element mesh (average element edge length) is much shorter than the

length between data points. In these cases, it is very unlikely that the locations of entities in the model (keypoints, nodes, etc.) will line up exactly with the locations of the measured data points. By enabling interpolation between data points, surface heights can be retrieved based on the location of the model entities to be created or modified. This significantly increased the flexibility of the method and decouples the finite element mesh from the imported lateral resolution for surfaces that are created by modifying the mesh.

In ANSYS, the simplest way to enable linear interpolation is to transfer the surface data into an ANSYS table parameter. An ANSYS table parameter is similar to an array parameter except that table indices may be real numbers rather than limited to integers and linear interpolation between the cells is permitted when extracting values from the table. All models presented in this work have been transferred from their original surface arrays into surface tables.

2.8 Methods for Creating Geometry from Surface Data

After the surface data array has been created, imported into ANSYS and all operations have been completed, the surface geometry must be created. Two methods of creating surface geometry from surface data were developed for this work. The first method modifies the finite element model by moving all of the nodes or all of the surface nodes in the model. The second method uses bottom up solid modeling to create the solid model geometry.[17]

2.8.1 Procedure for Moving Nodes

To create a rough surface by moving nodes in the model:

1. Create a volume (solid model geometry).
2. Mesh the volume to create nodes and elements.
3. Detach the finite element model from the solid model.
4. Select every node[9] (or every surface node) by location and move the z coordinate of that node by a fraction of the asperity height value (or the full asperity height) for that (x,y) location.

This procedure is shown in Figure 2-3 and Figure 2-4 for a uniform brick mesh with surface nodes modified and an arbitrary tetrahedral mesh with all nodes modified.

The main benefits of this procedure are its robustness and flexibility. It can be used on arbitrary geometry including on models that have been imported from an external CAD package. It is also slightly less complicated and quicker procedure to perform. The disadvantages of this procedure are a lack of user-friendliness. After the rough surface is created, the model cannot be re-meshed (only modified manually by moving nodes and

elements). And, finite element entities (nodes and elements) can no longer be selected based on their attachment to solid model entities. Careful planning is, therefore, required when modifying the finite element mesh.

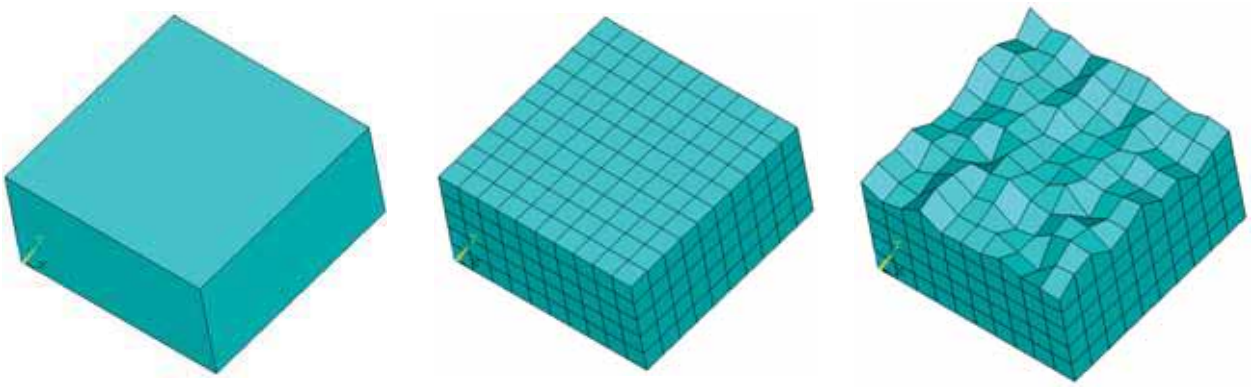

Figure 2-3: Stages of Creating Rough Surface by Moving Nodes (Brick Mesh)

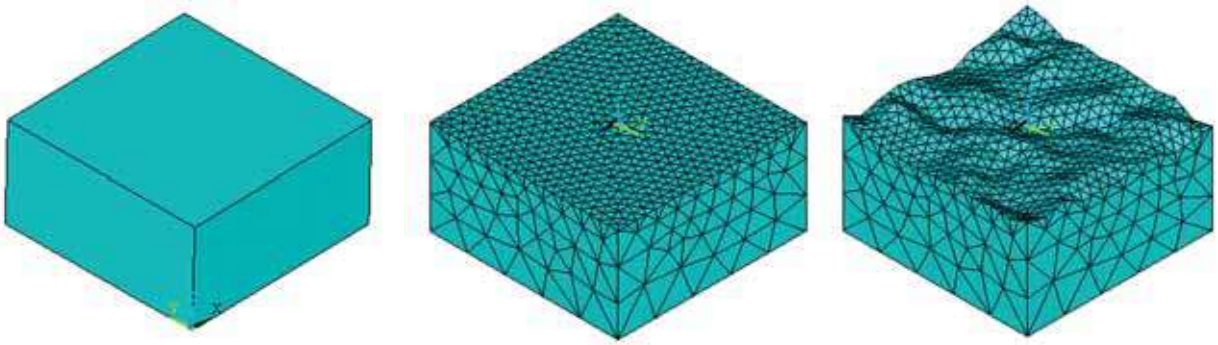

Figure 2-4: Stages of Creating Rough Surface by Moving Nodes (Tet Mesh)

2.8.2 Procedure for Creating Keypoints

To generate a rough surface by creating keypoints:

1. Create key points using the values in the array.
2. Create lines between key points in the x and y directions.
3. Create areas.
4. Use bottom up solid modeling to complete the block volume.
5. Mesh the volume to create nodes and elements.

Since the key points are not co-planar, ANSYS uses Coons patches to generate the surfaces.

Step 1.

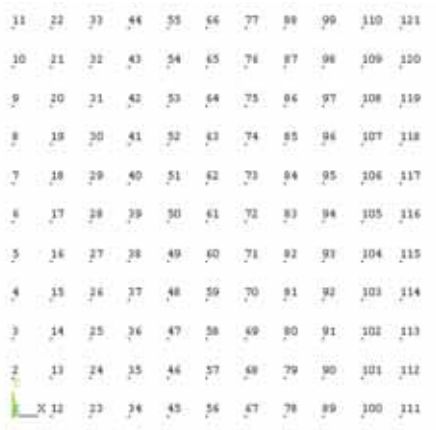

Step 2a.

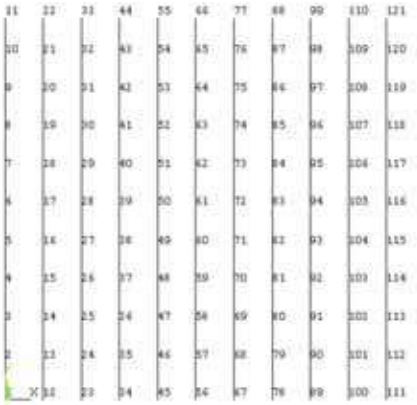

Step 2b.

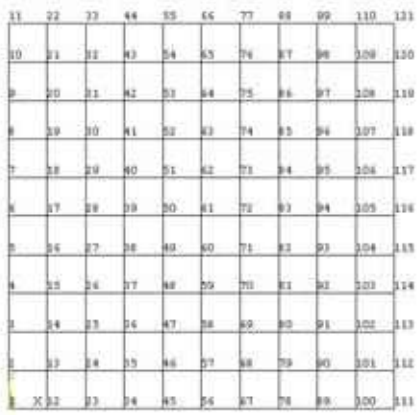

Step 3.

Step 4.

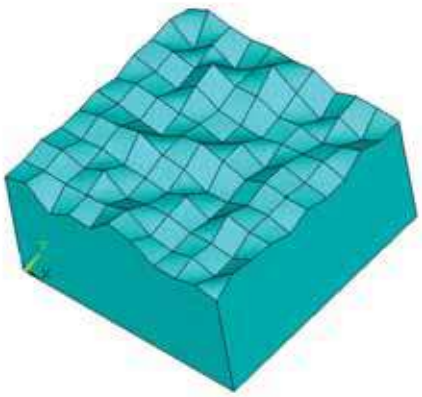

Step 5.

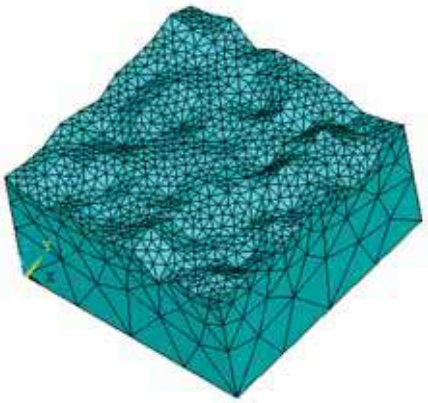

Figure 2-5: Procedure for Creating Rough Surface by Keypoints

The primary advantage of using this method are its robustness and the fact that the solid model can be meshed and re-meshed. However, the creation of Coons patches can be very time consuming and it may be difficult to create complicated geometries using bottom up solid modeling techniques.

2.9 Example Imported Surface Roughness Measurement

Three sets of surface metrology data, all from a Gar microfinish surface comparator, were imported, used to generate surface models, and solved to demonstrate the techniques described above qualitatively verify the quality of the model. The measured surfaces were the 2L, 4L sample, and 8L sample (Figure 2-6). These were the three smoothest surfaces available on the surface comparator.

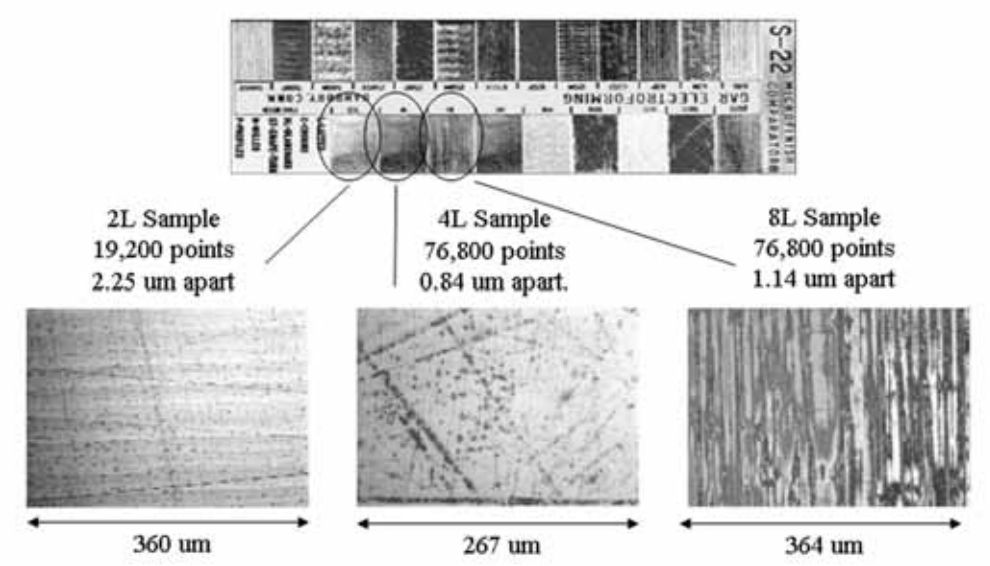

Figure 2-6: Surface Comparator

2.9.1 Measured Surface Data Sets

The 2L sample data set was taken from a lapped surface with a roughness average of 2 micro inches (0.05 um) and a peak to valley roughness value of 3.07 um. The 2L sample data set contained 19,199 measured data points with a lateral resolution of 2.24 um. The data set contained one data drop out point which was repaired manually. The data was filtered to remove planar surface form.

The 4L sample data set was taken from a lapped surface with a roughness average of 4 micro inches (0.1 um) and a peak to valley roughness value of 4.36 um. The 4L sample data set contained 76,800 measured data points with a lateral resolution of 0.835 um.The data set contained no data drop out points and was filtered to remove planar surface form.

The 8L sample data set was taken from a lapped surface with a roughness average of 8 micro inches (0.2 um) and a peak to valley roughness value of 1.39 um. The 8L sample data set contained 76,795 measured data points with a lateral resolution of 1.136 micrometers. The data set contained 75 data drop out points and was repaired using a data fill tool. The data was filtered to remove planar surface form.

The surface maps for the three measured surfaces are shown in Figure 2-7. The surface heights in the z direction are shown 1000 times larger than the lengths in the x and y directions.

2.9.2 Imported Sample Data Sets

Each of the three data sets were imported into ANSYS using a lateral resolution of 3 um. The full data set was not used because of the time and disk space required to solve the larger problems on a PC. The rough surface was created by modifying the finite element model.

The major geometric features of all three imported surfaces are visible in both the surface map and the imported surface geometry. For the 2L sample, there are two major geometric features.There is a tall peak on the left hand side of the surface, circled in black.There is also a triangular shaped depression at the bottom of the surface map and at the top of the imported image, outlined with a black rectangle.

For the 4L sample, there are five major geometric features (valleys or scratches) visible in both the surface map and the imported surface geometry. Black lines have been placed along the features in both the surface map and imported image to highlight their location.

For the 8L sample, there are two major geometric features. First, the valley in the center of the sample seems to be the deepest and widest. The intersection of that valley with the edge of the sample is circled on both the surface map and the imported surface. In addition, there is a depression in the center of the left-most line of data. The depression is indicated with an arrow. Unlike the 2L and 4L samples, the 8L sample exhibits surface lay and there is a clear directionality to the surface features.

The surface geometry created with the imported data from the three surface data sets are shown in Figure 2-8. The surface heights in the z direction are shown 1000 times larger than the lengths in the x and y directions.

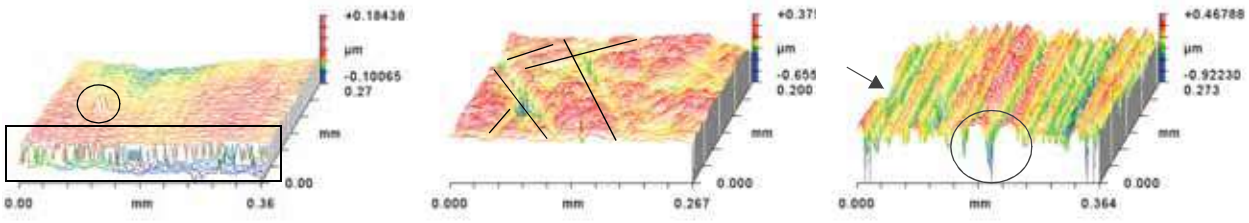

Figure 2-7: Measured Surface Geometry: 2L Sample (left), 4L (middle), 8L (right)

Figure 2-8: Imported Surface Geometry: 2L Sample (left), 4L (middle), 8L (right)

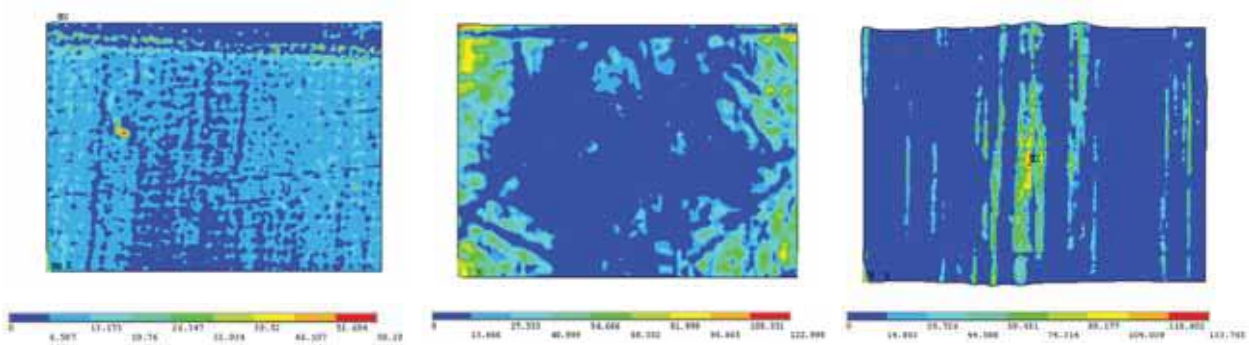

Figure 2-9: Contact Pressure (MPa): 2L Sample (left), 4L (middle), 8L (right)

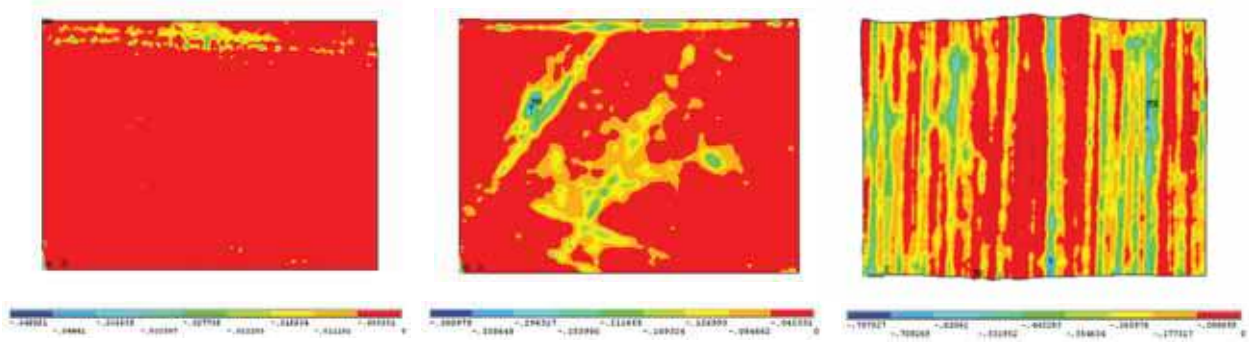

Figure 2-10: Contact Gap (um): 2L Sample (left), 4L (middle), 8L (right)

2.9.3 Analysis

Mechanical contact analyses were performed for the three models with imported surfaces. The roughened bodies were meshed with three dimensional 8-noded structural solid elements. The rough surface was then covered with three dimensional 4-noded surface-to-surface contact elements to provide a deformable contact surface.

A second smooth, infinitely stiff contact surface was created opposite the rough surface. The second surface was meshed with a single three dimensional 4-noded target element. By making the second surface ideal and rigid, we ensure that the results of the analysis will reflect only the behavior of the roughened surface. A pilot node was created at one corner of the infinitely stiff contact surface to permit boundary conditions to be applied to that surface.

Isotropic linear elastic material properties were assigned (somewhat arbitrarily) based on polyetheretherkeytone (PEEK, E = 4.6 GPa, ν = 0.4) to ensure that stresses remained in the linear elastic regime.

A zero displacement constraint in x was placed on all nodes at x = 0. Similarly, zero displacement constrains in y and z were placed on all nodes at y = 0 and z = 0 and the pilot node was also constrained in x and y. Finally, a downward pre-load force of 0.75 N was applied to the pilot node. Since each of the three samples had different surface areas, the nominal contact pressures applied by the smooth, rigid surface were: 7.72 MPa (2L sample), 14.0 MPa (4L sample) and 7.55 MPa (8L sample).

2.9.4 Results

The plots of the contact pressure and contact gap for the three imported rough surfaces are shown in Figure 2-9 and Figure 2-10. For all three surfaces, the plots indicate high contact pressures for tall features and large contact gaps for scratches or depressions in the surface.

The contact pressure for the 2L sample ranges from 0 to 59.28 MPa. The contact pressure distribution is relatively uniform, with high contact pressure where the tall peak makes contact with the opposite surface and little or no contact pressure in the region of the depression. The contact gap for the 2L sample ranges from 0 to -0.05 um and is also very uniform across the surface. These results are consistent with expectations for a very smooth, soft surface.

The contact pressure for the 4L sample ranges from 0 to 123 MPa. The contact pressure distribution is relatively high and uniform around the perimeter. The contact pressure is low and relatively uniform pressure in the center. Regions of low pressure are seen crossing the high contact pressure areas. These correspond to small scratches on the surface that can be seen in the surface plot and the imported surface geometry. The contact

gap for the 4L sample ranges from 0 to -0.38 um. The largest contact gaps are seen in the center of the sample and correspond to large scratches on the surface which are visible in the surface plot and the imported surface geometry.

The contact pressure for the 8L sample ranges from 0 to 133.77 MPa and the contact gap ranges from 0 to -0.80 um. The 8L sample has few areas of contact, all running along the direction of lay. The contact pressure is high along the ridges of the surface. The contact gap is large along the valleys between the ridges. The largest (and second deepest) valley is indicated by the region with the largest contact gap in the center of the sample.

The contact pressures and gaps for the 2L sample are much smaller than for the 4L and 8L sample which is to be expected as the 2L sample is much smoother than the other two. The results for the 4L and 8L sample, however, are relatively similar in magnitude indicating that the difference between the two samples may be more a results of the surface lay (surface roughness pattern) than of the magnitude of the surface roughness.

The results of the contact analyses are an excellent match with expectations and qualitatively show that surface importation is a viable surface modeling option.

2.10 Conclusions

This chapter discussed the challenges associated with incorporating real surface topography into finite element models and past attempts to model ideal and idealized surface geometry. A method for importing real surface measurement data into a finite element program and two methods for creating surface geometry using the imported data were presented. Three relatively small finite element models were constructed using real surface data and the methods presented in this chapter. These models were used in contact simulations to demonstrate the methods and show that the results qualitatively matched expectations.

References:

1. J. F. Archard, "Contact and Rubbing of Flat Surfaces," J. App. Physics Vol. 24 No. 8, (1953).
2. Madhusudana, C.V., Thermal Contact Conductance, Springer-Verlag, New York (1996) 9 - 44.
3. Blencoe, K. A., et al., "The influence of lubricant rheology and surface topography in modelling friction at concentrated contacts" Proc. Instn. Mech. Engrs. Vol. 212 Part J.
4. Greenwood, J. A., 1966, "Constriction Resistance and the Area of Real Contact," Br. J. Appl. Phys., 17 (1996) 1621-1632.
5. Greenwood, J. A., and Williamson, J. B. P., 1966, "The Contact of Nominally Flat Surfaces," Proc. R. Soc. London, Ser. A, 295, (1966) 300-319.

6. S K Chilamakuri and B Bhushan, "Contact analysis of non-Gaussian random surfaces," Proc. Instn. Mech. Engrs. Vol. 212, Part J, (1998).
7. Peng, W. and Bhushan, B. A numerical three-dimensional model for the contact of layered elastic/plastic solids with rough surfaces by variational principle. Trans. ASME, J. Tribology 123 (2001) 330-342.
8. J. F. Archard, "Elastic Deformation and the Laws of Friction," Proceedings of the Royal Society of London. Series A, Mathematical and Physical Sciences, Vol.243, No. 1233. (Dec. 24, 1957), 190-205.
9. Hyun, S. "Finite-element analysis of contact between elastic self-affine surfaces." Physical Review E 70, 026117, (2004).
10. Brown, C.A. et al. "Fractal analysis of topographic data by the patchwork method." Wear, 161 (1993) 61-67.
11. Karpenko, Y. A. and Akay, A. "A Numerical Method for Analysis of Extended Rough Wavy Surfaces in Contact." J. Tribology 124 (2002) 668-679.
12. Kim, T. W. and Bhushan, B. "Generation of Composite Surfaces with Bimodal Distribution and Contact Analysis for Optimum Tribological Performance." J. Tribology 128 (2006) 851-863.
13. Tang, J. et al. "Modelling of Oxide Scale Surface Roughness in Hot Metal Forming." Journal of Materials Processing Technology 177 (2006) 126-129.
14. Glynn, M. L. et al. "Modeling Effects of Material Properties and Three-Dimensional Surface Roughness on Thermal Barrier Coatings." Mat. Res. Soc. Symp. Proc. Vol. 645E (2001).
15. Peng, W. and Bhushan, B. A numerical three-dimensional model for the contact of layered elastic/plastic solids with rough surfaces by variational principle. Trans. ASME, J. Tribology 123 (2001) 330-342.
16. Marchand, A.S. and Raynaud, M. "Numerical Determination of Thermal Contact Resistance for Nonisothermal Forging Processes." J. Heat Transfer, Vol. 122 (2000) 776-784.
17. Thompson, M.K. "Methods for the Generation of Rough Surfaces in ANSYS." Proceedings of the 2006 International ANSYS Users Conference & Exhibition, Pittsburgh, PA. 16 pages.

References:

Chapter 3: Multi-Scale Modeling of Thermal Contact Resistance

This chapter presents a multi-scale iterative approach to model thermal contact resistance on the macro and micro scale to be used in conjunction with the finite element surface modeling methods developed in the previous chapter. The assumptions and limitations of the model are discussed and future improvements to the model are suggested.

3.1 Thermal Resistance at the Interface

3.1.1 Thermal Contact Resistance

An analogy is often made between the electrical and thermal domains to permit a discussion of "thermal circuits" and "thermal resistances." In the electrical domain, electrical resistance "is a measure of the degree to which an object opposes the passage of an electric current"[1] and is a function of both geometry and material properties. Ohm's law relates the current and voltage drop in the electrical circuit to the resistance:

$$\Delta V = IR \qquad [3.1]$$

where Δ V is the voltage drop in the circuit [volts V], I is the current in the circuit [amps] and R is the resistance [ohms].[2]

In the thermal domain there are thermal impedances which oppose the flow of heat. These impedances are again a function of both geometry and material properties. Modifying Ohm's Law for thermal systems yields:

$$\Delta T = QR \qquad [3.2]$$

where Δ T is the temperature drop in the circuit [K], Q is the heat flow in the circuit [W] and R is the so-called thermal resistance of the thermal circuit [K/W]. Rewriting Equation [3.2] to resemble Fourier's Law and Newton's Law of Cooling yields:

$$Q = \frac{1}{R}\Delta T \qquad [3.3]$$

Thermal resistances behave like their electrical counterparts; thermal resistors in series add:

$$R_{total} = R_1 + R_2 + R_3 + \ldots \quad [3.4]$$

while thermal resistors in parallel add as inverses:

$$\frac{1}{R_{total}} = \frac{1}{R_1} + \frac{1}{R_2} + \frac{1}{R_3} + \ldots \quad [3.5]$$

The electrical analogy for heat transfer is a quasi-one-dimensional model. It assumes that heat in each resistor flows uniformly in one direction and that the same amount of heat flows through each resistor in series. It is also assumed that the temperatures of the bodies perpendicular to the heat flow are also uniform. In the cases where this is not true, an averaged temperature must be used in the thermal circuit.

For continuum thermal systems, the major modes of heat transfer (conduction, convection and radiation) can all be represented as thermal resistors. For example, the thermal resistance for conduction in a simple one dimensional (1D) system in cartesian coordinates is:

$$R_{cond} = \frac{L}{kA} \quad [3.6]$$

where L is the length or distance that the heat must flow [m], k is the thermal conductivity of the material through which the heat flows [W/mK], and A is the cross sectional area through which the heat flows [m^2].[3]

Similarly, a temperature drop is observed between two surfaces in contact, even when the contact is ideal. The impedance or resistance to heat flow across the interface between two surfaces in contact which causes the temperature drop is referred to as “thermal contact resistance” (TCR).

Consider the system in Figure 3-1. Heat flows from surface 11 to surface 22 through the bulk of body 1, across the interface, and through the bulk of body 2. The amount of heat that flows through each body and through the interface must be the same and is equal to the difference between the average surface temperatures and the resistances by the following relation:

$$Q = \frac{1}{R_1}(\overline{T_{11}} - \overline{T_{12}}) = \frac{1}{R_{contact}}(\overline{T_{12}} - \overline{T_{21}}) = \frac{1}{R_2}(\overline{T_{21}} - \overline{T_{22}}) \quad [3.7]$$

where T_{11} is the average temperature of the outer surface of top body (body 1), T_{12} is the average temperature of the contact surface for the top body and T_{21} is the average temperature of the contact surface for the bottom body (body 2), and T_{22} is the average temperature of the outer surface of the bottom body.

The total thermal resistance for the system is given by:

$$Q = \frac{1}{R_{Total}}(\overline{T_{11}} - \overline{T_{22}}) \qquad [3.8]$$

The heat transfer across the interface may be either via solid conduction where the bodies touch or via interstitial heat transfer through the gaps. In cases where the contacting surfaces are very rough or non-conforming, the average temperature drop across the interface can be significantly greater than the temperature drop in the bulk.

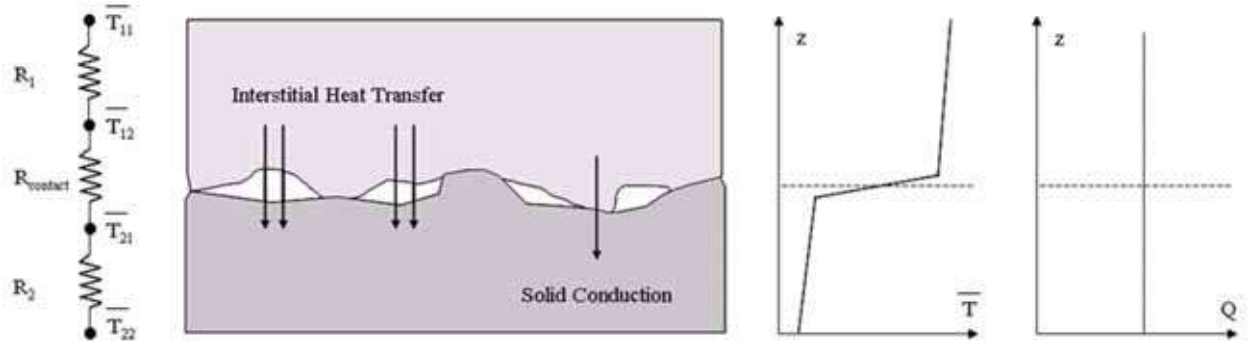

Figure 3-1: Schematic of System with Thermal Contact Resistance

3.1.2 Thermal Contact Resistance per Unit Area

In the previous section, thermal contact resistance was presented as the total contact thermal resistance across the interface [K/W]. The total resistance ($R = R_1 + R_{contact} + R_2$ [K/W]) and the total contact resistance ($R_{contact}$ [K/W]) are often desirable to know when measuring or designing relatively uniform macro scale devices. However, on the micro scale, often only a portion of the total surface is examined, modeled or measured and the results are assumed to be representative for the entire surface. For this reason, it is often useful to measure or calculate the thermal contact resistance per unit of micro scale surface area ($r_{contact}$ [Km^2/W]).

For this work, thermal contact resistance on the macro scale will be given as the total TCR and on the micro scale it will be given as TCR per unit area.

3.1.3 Thermal Boundary Resistance

Thermal boundary resistance (TBR) is a small magnitude thermal resistance present at all physical interfaces or boundaries, regardless of temperature, contact pressure, or the state of the contacting bodies (solid, liquid, gas). Thermal boundary resistance is caused by scattering, reflection and refraction of energy carriers at an interface. It is a nano scale (quantum) effect and occurs even for ideal contact between two identical materials.

Thermal boundary resistance "is defined as the ratio of the temperature discontinuity at the interface and the heat power per unit area flowing across the interface" and is described by the following equation:

$$r_{boundary} = \Delta T / (Q / A_c) \quad [3.9]$$

where r is the thermal boundary resistance per unit area, ΔT is the steady state difference between the temperatures on each side of the interface, Q is the heat flow across the projected area and A_c is the contact area perpendicular to the flow of heat.[4]

The term "thermal contact resistance" is occasionally used to describe nano scale boundary resistances, but the term "thermal boundary resistance" is hardly ever used to describe resistances at the micro or macro scales. For this work, the term "thermal contact resistance" will be used to describe continuum thermal resistances at boundaries or interfaces where micro scale (> 1e-7 m) surface roughness heavily influences the behavior at the interface. The term "thermal boundary resistance" will be used to describe thermal resistances at boundaries or interfaces where scattering, reflection and refraction due to atomic and nano scale surface topography.

3.1.4 Experimental Values of Thermal Resistances at the Interface

When modeling or predicting phenomena, it is often helpful to have an idea of the range of values expected so the quality of the model may be verified. Based on experimental values obtained at room temperature from the literature, thermal boundary resistance has an approximate range of1e-7 to 1e-9 m^2K/W. [5-7] Thermal contact resistance between metals (copper, steel, and aluminum paired with various materials), also based on experimental values obtained from the literature, has an approximate range of 1e-4 to 1e-6 Km^2/W. [8]

3.2 Challenges for Modeling Thermal Contact Resistance

There are a number of challenges associated with modeling thermal contact resistance and systems where thermal contact is significant.

First, the electrical analogy is, of course, an approximation. Heat flows from one surface to another along the path of least resistance, which may be in any direction or at any angle that maximizes energy transfer across the interface. Temperatures in both bodies may also vary in three dimensions. While many systems can be accurately approximated as one dimensional systems using methods like the electrical analogy, true three dimensional systems must be modeled using three dimensional techniques. If the model geometry is complex, a three dimensional solution may require the use of numerical techniques. And, in some cases it may be difficult to define a thermal contact resistance because the path of the heat is not well defined. It may also be necessary to define a series of local thermal contact resistances which are based on their location, the local temperature(s) and the local heat flux at the contact surface.

The mechanisms which transfer heat between the two surfaces depend on the temperature(s) of the system. For example, at very low temperatures phonon wavelengths are long and the scattering of phonons at a boundary can be considered specular and elastic. Thus, thermal boundary resistance can be estimated based on the acoustic mismatch model.[9] At room temperature, quantum effects may be neglected even at relatively small length scales and continuum relations apply. Thermal conduction and convection are the dominant heat transfer mechanisms across the gaps; thermal radiation is negligible. At very high temperatures, thermal radiation is the dominant heat transfer mechanism across the gaps.[10]

Other factors in the system also depend on temperature. Mechanical and thermal material properties, such as Young's Modulus and thermal conductivity are temperature dependent. Density is also a function of temperature, so thermal expansion in the system may change the nature of the mechanical contact between surfaces. It may also be necessary to consider phenomena such as thermally induced cracking and thermally induced creep.

The mechanisms which transfer heat between two surfaces also depends on the length scale of the geometric features (surface layers, gaps, etc.) which are parallel to the heat flow. For example, at the nano scale there are relatively few gaps and thermal boundary resistance is attributed to scattering of phonons and electrons at the boundary between the surface surfaces.[11] At the micro scale, we view the system as being continuum and heat transfer through the gaps tends to be due to conduction across the material (air, grease, etc.) in the gaps.[12] At the macro scale, heat transfer through the gaps is due to conduction for relatively small gaps and due to natural convection for slightly larger gaps. The transition from conduction to natural convection for unstable systems (where the bottom surface is warmer than the top surface) is determined by the critical Rayleigh number.[13] (Natural convection currents will not form in a thermally stable system.) At very large length scales, forced convection and radiation dominate heat transfer across the gap.

Next, thermal contact problems are fundamentally a thermal/structural problem. As the two surfaces are brought together, they deform mechanically altering the contact pattern between the two surfaces. Since, the heat transfer across the interface depends on the shape and size of the contact patterns, the mechanical contact must be taken into account

to obtain a thermal solution. It is possible to solve a thermal contact problem iteratively, solving the structural problem first and then using the solution of the mechanical problem as the input for the thermal problem. However, in many cases it is simpler to solve the two problems simultaneously.

Finally, thermal contact problems require analysis over multiple length scales. As surfaces are brought together on the macro scale, they make contact. Each contact patch has a certain shape, size, and area. The sum of these areas is the apparent area of contact. If these contact patches were examined on the micro scale, it would be clear that both surfaces were covered with micro asperities - surface roughness - which make contact. Each of these micro scale contact patches also has a certain shape, size and area. The sum of these areas is often considered the real area of contact. This procedure may be repeated again for the nano scale and eventually down to the atomic scale.

The nano asperities must support the load from the micro scale, and the micro scale asperities must support the load from the macro scale. Thus, the load applied to the contact surfaces on the shorter (smaller) length scales depends on the contact pressure at the longer length scales.

Similarly, the resistance to heat transfer across the contacting areas at the macro scale depends on the ratio of solid to interstitial conduction at the micro scale, and thus on the surface topography at the micro scale. The resistance to heat transfer across the contacting asperities at the micro scale depends on the ratio of solid to interstitial conduction at the nano scale. Thus, the thermal behavior at longer length scales depends on the thermal behavior at the shorter length scales.

The behavior of the system over the various length scales is fundamentally coupled; all of the asperities on all of the length scales are deformed simultaneously. However, we do not currently have the capability to build and solve models with surface topography spanning more than three orders of magnitude in length scale so it is not possible to create and solve a model with the nine orders of magnitude in question.

From this discussion, it is clear that surface topography plays a major role in both the mechanical and thermal aspects of thermal contact. So in addition to the challenges discussed above, thermal contact resistance also has all of the challenges associated with modeling surface topography mention in the previous chapter.

3.3 Prior Art: Modeling Thermal Contact Resistance

Discussions of thermal contact often can be divided into three sections: surface analysis, deformation analysis and thermal analysis.[14]

Many of the same assumptions used to model surfaces and surface topography discussed in the previous chapter have been used to model thermal contact systems. Surface asperities have been modeled using a variety of geometric shapes including hemispheres,[15] half cylinders[16], cones[17], squares[18], and saw tooth patterns.[19] They have also been modeled as random Gaussian or near-Gaussian distributions.[20] Some past works have neglected both the surface analysis and the deformation analysis in favor of assumptions about the shape, size and distribution of contact spots.[21] Circular or disc contact spots (both regularly[22] and randomly[23] distributed) are particularly popular and imply a hemispherical asperity shape assumption.

Once the surfaces are analyzed and characterized, a mechanical contact or deformation analysis is usually performed to determine the nature (size, shape and distribution) of the contact areas. The deformation analysis may be analytical or numerical. Herztian contact is frequently used, as is the concept of a “plasticity index” first introduced by Greenwood.[24] Often only one of the two contact surfaces is rough[18] or deformable.[15] In many cases, the goal of the deformation analysis is to determine the ratio of real to apparent area of contact.[26,27]

Next, the thermal constriction resistance of a single contacting region (heat channel) is modeled. This analysis assumes that the thermal effect of adjacent contact patches can be neglected.[29] Heat channels have been modeled as cylinders, semi-infinite cylinders, plates, cylinders ending in cones contacting against plates, coaxial cylinders,[14] and hemispheres.[30] Interstitial heat transfer around the heat channel is often neglected.[14,18,25] Thermal resistances between the contacting heat channels or asperities are also often neglected. Finally, the results of the surface, deformation and mechanical analyses are combined to produce an estimate of the thermal contact resistance (or its inverse: thermal contact conductance).

Numerical models for the thermal analysis typically use the results of the mechanical analysis directly, rather than using the ratio of real to apparent area of contact or another derived result.[18,20,28]

3.4 Improving Models for Thermal Contact Resistance

To improve the quality of thermal contact resistance models, it is again necessary to improve the assumptions in the model. By using the surface modeling methods developed in the previous chapter, it is possible to greatly improve the assumptions about asperity shape, size and distribution. This, in turn, permits the analyst to solve for the true contact pattern instead of relying on assumptions and probability arguments to determine the nature of the contact regions. By using numerical methods such as finite element analysis, three dimensional thermal contact models may be created and solved using realistic

geometry and the true contact pattern. Finally, interstitial heat transfer and thermal boundary resistance at the solid-solid interfaces can be included to more accurately reflect the thermal behavior at the interface.

3.5 A Multi-Scale Iterative Approach for Finite Element Modeling of Thermal Contact Resistance

A new method for modeling thermal contact resistance was developed to address the challenges of modeling TCR discussed in Section 3.2 while incorporating the improvements suggested in Section 3.4.

Recall that the thermal and mechanical behavior of the system over the various length scales is fundamentally coupled, but that we do not have the capability to build and solve models with surface topography spanning more than three orders of magnitude or so in length scale. Since we cannot create and solve models that are coupled over the require length scale, we must solve each length scale (~ 3 orders of magnitude) independently with the results from the next larger and smaller length scale models applied as loads, boundary conditions, or real constants.

Recall also that the load applied to the contact surfaces on the shorter (smaller) length scales depends on the contact pressure at the longer length scales and the thermal behavior at longer length scales depends on the thermal behavior at the shorter length scales. Since the thermal and mechanical problems have opposite length scale dependencies, an iterative model is required.

The result is a three dimensional, coupled thermal/structural, multi-scale, iterative finite element model which uses imported surface geometry at each length scale and accounts for both solid/solid and interstitial heat transfer.

3.5.1 Overview of the Modeling Procedure

The procedure for the new method has six steps:

1. Guess the value for micro scale thermal contact resistance per unit area. Create and solve the macro scale thermal/structural model using imported surface geometry.
2. Create the micro scale thermal/structural model using imported surface geometry. Apply the average contact pressure and the average contact temperature from the macro scale model as the mechanical and thermal loads for the micro scale model.
3. Solve the micro scale thermal/structural model.
4. Calculate the micro scale thermal contact resistance per unit area. Apply this value to the macro scale model and re-solve the macro scale model.
5. Compare the results of the 1st and 2nd macro scale models.
6. Iterate if necessary.

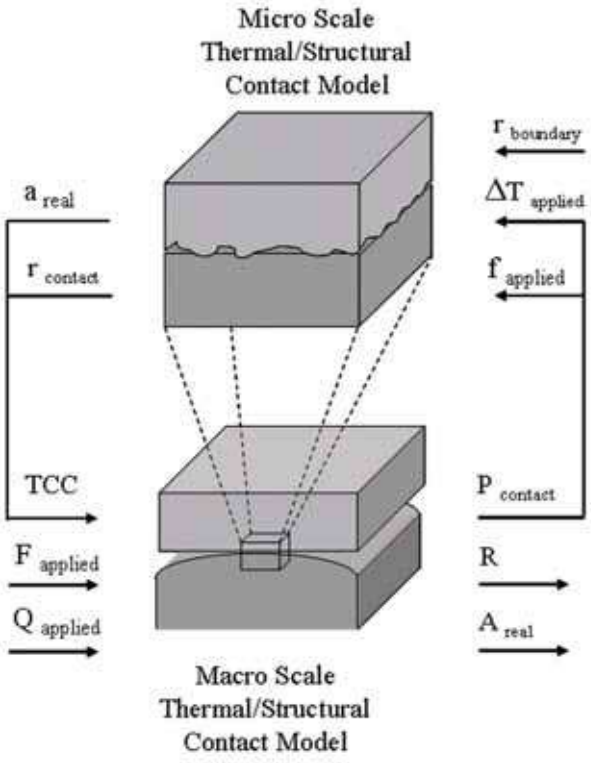

Figure 3-2: Schematic of Multi-Scale Iterative TCR Model

3.5.2 Initial Macro Scale Thermal/Structural Model

The macro scale thermal/structural model requires three major inputs: applied mechanical load, applied thermal load, and a value for thermal contact conductance. The results of the model supply three values: total thermal resistance of the system, total thermal contact resistance of the system, and average contact pressure.

At each length scale, the model must have an applied mechanical load, an applied thermal load, structural boundary conditions and thermal boundary conditions. At the macro scale, it is assumed that the both the mechanical applied load ($F_{applied}$) and thermal applied load ($Q_{applied}$) are specified and determined by the application. The mechanical applied load may be a force or pressure. The thermal applied load may be a temperature or a heat flux.

The mechanical boundary conditions are usually displacements in the x, y, and z direction which fix the model entities in space. The thermal boundary condition is often a temperature on the opposite side of the model from the applied thermal load.

Finally, the thermal contact conductance (TCC) [W/m^2K], which is the inverse of thermal contact resistance per unit area, is applied to the model as a real constant. Real constants in finite element models are solution independent values that are required to solve the model

but are not provided elsewhere. Examples include the thickness of shell elements and the moment of inertia of beam elements. The TCC real constant, which accounts for the resistance to solid-solid conduction at the macro scale, includes the effects of micro scale asperities and the real area of contact and is known to be solution dependent. (The micro scale thermal contact resistance depends on the applied pressure at the micro scale which is a function of the mechanical contact solution at the macro scale.) Since this coupled effect cannot be modeled over the length scales required (100 mm to 100 nm), the solution is decoupled by solving the model on the macro and micro scale. An iteration loop is used to link the macro and micro scale models together and ensure self-consistency between the two models. This, in turn, makes the TCC value solution independent for the purposes of this analysis.

For the first iteration of the macro scale thermal/structural model, the TCC value is guessed based on experimental values from the literature. Since the values from the literature range between 1e-4 and 1e-6 [Km^2/W], an initial value of 1e-5 was used in all initial models.

The structural results of the macro scale model will include deformations, stresses, contact status and contact pressure on a nodal and element basis. The thermal results will include temperatures and heat fluxes, including heat flux across the interface.

The areas for each element in contact may be summed to determine the apparent area of contact ($A_{apparent}$) for the macro scale model. The contact pressure for each contact element can be multiplied by the area of that element and then summed and divided by the apparent area of contact to determine the average contact pressure ($P_{contact}$) for the macro scale model.

The temperatures for the outer (11 and 22) surfaces and for the contact (12 and 21) surfaces may be multiplied by their areas, summed and divided by the surface area to determine the average temperatures for those surfaces ($\overline{T_{11}}$, $\overline{T_{12}}$, $\overline{T_{21}}$, and $\overline{T_{22}}$). The heat flux for each contact element may be multiplied by its area and then summed to determine the total heat flow across the interface. Finally, the total contact resistance (R) for the macro scale system can be determined by dividing the difference of average temperatures across the interface by the heat flow across the interface. Similarly, the total thermal resistance ($R_{contact}$) for the macro scale system can be determined by dividing the different of average temperatures across the outer surfaces by the heat flow across the interface.

3.5.3 Micro Scale Thermal/Structural Model

The micro scale thermal/structural model requires three major inputs: applied mechanical load, applied thermal load, and a value for thermal boundary resistance. The results of the model supply two values: thermal contact resistance per unit area and real area of contact.

At the micro scale, the mechanical applied load ($f_{applied}$) is equal to the average contact pressure ($P_{contact}$) from the macro scale analysis multiplied by the surface area on the micro scale. The mechanical boundary conditions are again displacements in the x, y, and z direction which fix the model entities in space.

The thermal applied load is equal to the average temperature at one side of the interface ($\overline{T_{12}}$). The thermal boundary condition is the average temperature at the other side of the interface ($\overline{T_{21}}$).

Finally, thermal boundary resistance ($r_{boundary}$) [Km^2/W] is applied to the model as a real constant to model the resistance to solid/solid conduction on the nano scale. The value used for thermal boundary resistance is chosen based on experimental data from the literature.

Again, the areas for each element in contact may be summed to determine the real area of contact (a_{real}) for the micro scale model. And, the temperatures for the outer surfaces are again multiplied by their areas, summed and divided by the surface area to determine the average temperatures for those surfaces. The heat flux for each contact element may be multiplied by its area and then summed to determine the total heat flow across the interface. Finally, the thermal contact resistance per unit area ($r_{contact}$) for the micro scale system can be determined by dividing the difference of average temperatures at the outer surfaces by the heat flow across the interface.

3.5.4 Iteration Loop

The calculated value for thermal contact resistance per unit area from the micro scale model can then be used to update the guessed value of TCC in the macro scale model. If the two values are sufficiently close, then the macro scale results from the initial model may be used. Otherwise, the models must be re-run using the new values until the solutions converge.

If desired, the micro scale value for real area of contact may be used to estimate the real area of contact at the macro scale.

The multi-scale finite element model presented here was formulated with the intent of using it with a fully-coupled thermal/structural problem which might include temperature dependent material properties and permit thermal expansion behavior. And, the models solved for the case study in the next two chapters are demonstrated using the iterative approach. However, the case study models include many simplifications for convenience which do not strictly require iteration. For these types of de-coupled or minimally coupled models, it would be possible to solve the macro scale problem once to determine the applied thermal and structural loads on the micro scale. As long as the micro scale solutions are not temperature dependent and not sensitive or dependent on the applied

temperature difference, it should be possible to create a look-up table based on the micro scale results. The macro scale model can then be-resolved using the micro scale look-up table to obtain the final solution.

3.5.5 Assumptions and Limitations

The model presented here has a number of assumptions and limitations. Some of these limitations are fundamental limitations of the method, while others may be addressed in future work.

3.5.5.1 Material Properties

The base plate is assumed to be made from AlSiC (E = 183 GPa, ν = 0.25, k = 175 W/mK). The heat sink is assumed to be made from 6061-T6 aluminum (E = 68.9 GPa, ν = 0.33, k = 167 W/mK). In Chapter 5, the base plate and heat sink are also considered to be made from copper (E = 175 GPa, ν = 0.33, k = 385 W/mK).

All materials in the finite element models are assumed to demonstrate linear elastic behavior and assumed to have no temperature dependence. Thermal expansion was not permitted and no thermal expansion coefficient was defined. For the system of interest in the case study, the temperatures are reasonably low (between 300 and 425 K) and the temperature difference between the two surfaces are small (< 30 K) so the assumptions made are reasonably valid. This may not be the case for many other systems that could be modeled. Future analyses could incorporate material non-linearities (plasticity, viscoelasticity, viscoplasticity, etc.), thermal expansion and temperature dependent material properties if desired.

3.5.5.2 Surface Considerations

Surface considerations including surface chemistry (adhesion and adsorption), coatings, oxides, other intentional or unintentional surface layers, and sub-surface cracks and flaws are all neglected. The viability of including one or more of these considerations in the model will be explored in future work.

3.5.5.3 Estimating Thermal Boundary Resistance

The value used for thermal boundary resistance in the model was chosen based on experimental data from the literature. This assumption could be improved by measuring the thermal boundary resistance for the system of interest, although the cost of this improvement may be substantial and not feasible. There are currently no good analytical models for predicting thermal boundary resistance at room temperature.

3.5.5.4 Applicable Temperature Range

The model was developed assuming that the temperature of the system would be near room temperature (between 0 and 125 C) so thermal radiation between the surfaces was neglected. If higher model temperatures (> 300 C) were required, thermal radiation could be added.

3.5.5.5 Applicable Length Scale

The model that was developed is fundamentally a continuum model. As the gap size between the contact surfaces becomes smaller than the mean free path of the molecules in the gap, it is possible that the model will vastly overestimate the heat transfer across the interface. Although this effect was found to only have a small impact (1 - 3%) on the thermal contact resistance, all gaps in the model that were less than the calculated mean free path were reset to the value of the mean free path.

In addition, it is assumed that all gaps in both the macro and micro scale models will be less than or equal to a few millimeters. Thus, all interstitial heat transfer is gap dependent thermal conduction. Thermal convection in the gap could be added if larger gaps were present.

Although some finite element programs, including ABAQUS, support gap dependent thermal conduction, ANSYS does not at this time. However, ANSYS does support convection across the gap. So for each contact element, a “convection” coefficient was defined equal to the thermal conductivity of the material in the gap (vacuum, air or thermal grease) divided by the calculated gap length to permit gap dependent conduction.

3.5.5.6 Applicable Time Range

The model that was developed and solved is a steady-state model. In the future, this model could be modified to include time dependence and this may be necessary if thermal expansion considerations are to be included.

3.5.5.7 Averaging

Finally, the model developed for this work includes significant averaging between the macro and micro scale. For example, the applied load on the micro scale is determined by the average contact pressure on the macro scale. However, the contact pressure on the macro scale is not a constant. The contact pressure may vary significantly in x and y, so there is actually a range of contact pressures which could be used as the input for the micro scale model.

Similarly, the thermal contact resistance per unit area that is applied to the macro scale model is applied to all contacting regions regardless of contact pressure. However, thermal contact resistance is a function of mechanical contact pressure.

It may be better to solve the micro scale thermal/structural problem for the full range of mechanical contact pressures and then apply appropriate TCC real constant values to the macro scale model based on contact pressure. This is a non-trivial addition to the model but it should be possible to remove some of these averaging assumptions in future work.

3.6 Conclusions

This chapter discussed the challenges associated with predicting thermal contact resistance and past attempts to model thermal contact resistance. A multi-scale iterative method for predicting thermal contact resistance using imported real surface measurement data in a finite element model was presented and the assumptions, limitations and possible improvements to the model were discussed.

References:

1. http://en.wikipedia.org/wiki/Electrical_resistance
2. R. J. Fowler, Electricity: Principles and Applications 5th Ed., (New York: Glencoe/ McGraw Hilll, 1999) 41-42.
3. J. H. Lienhard (IV), J. H. Lienhard (V), A Heat Transfer Textbook, (Cambridge, MA: Phlogiston Press, 2003), 62.
4. Gmelin J., “Thermal boundary resistance of mechanical contacts between solids at sub-ambient temperatures,” Phys. D: Appl. Phys. 32 (1999) R19–R43.
5. Behkam, B., Yang, Y., Asheghi, M. “Thermal Property Measurement of Thin Aluminum Oxide Layers for Giant Magnetoresistive (GMR) Head Applications,” International Journal of Heat and Mass Transfer 48 (2005) 2023-2031.
6. Filippov, K., Balandin, A. “Thermal Boundary Resistance and Heat Diffusion in AlGaN/GaN HFETs,” Mat. Res. Soc. Symp. Proc. Vol. 764 (2003).
7. Marshall, C. D., et al. “Thermal Boundary Resistance and Diffusivity Measurements on Thin YBa2Cu3O7-x Films with MgO and SrTiO3 Substrates Using the Transient Grating Method,” J. App. Phys. 73 (15 January 1993) 850 - 857.
8. Gmelin J., “Thermal boundary resistance of mechanical contacts between solids at sub-ambient temperatures,” Phys. D: Appl. Phys. 32 (1999) R19–R43.
9. G. Chen, Nanoscale Energy Transport and Conversion, (New York: Oxford University Press, 2005) 182.
10. C. V. Madhusudana, Thermal Contact Conductance (New York: Springer Verlag, 1996) 1.
11. G. Chen, Nanoscale Energy Transport and Conversion, (New York: Oxford University Press, 2005) 182.

12. C. V. Madhusudana, Thermal Contact Conductance (New York: Springer Verlag, 1996) 1.
13. A. F. Mills, Heat Transfer 2nd Ed., (Upper Saddle River, NJ: Prentice Hall, 1999) 334.
14. Shai, I., and Santo, M., "Heat Transfer with Contact Resistance." Int. J. Heat Mass Trans. Vol. 25 No. 4 (1982) 465-470.
15. Singhal, V., et al. "An experimentally validated thermo-mechanical model for the prediction of thermal contact conductance." Int. J. Heat and Mass Trans. 48 (2005) 5446-5459.
16. Heichal, Y., and Chandra, S., "Predicting Thermal Contact Resistance Between Molten Metal Droplets and a Solid Surface." J. Heat Transfer Vol. 127 (2005) 1269 - 1275.
17. Kumar, S. S. and Ramamurthi, K. "Prediction of Thermal Contact Conductance Using Monte Carlo Simulation." J. Thermophysics and Heat Trans. Vol 15. No. 1 (2001) 27 - 33.
18. Salti, B. and Laraqi, N., "3-D numerical modeling of heat transfer between two sliding bodies: temperature and thermal contact resistance." Int. J. of Heat and Mass Trans. 42 (1999) 2363-2374.
19. Prasher, R. "Surface Chemistry and Characteristics Based Model for the Thermal Contact Resistance of Fluidic Interstitial Thermal Interface Materials." J. Heat Transfer Vol. 123 (2001) 969 - 975.
20. Zhang, X., et al. "A new method for numerical simulation of thermal contact resistance in cylindrical coordinates." "Int. J. Heat and Mass Trans. 47 (2004) 1091-1098.
21. C. V. Madhusudana, Thermal Contact Conductance (New York: Springer Verlag, 1996) 23-28.
22. Tio, K. K., and Sadhal, S. S., "Thermal constriction resistance: effects of boundary conditions and contact geometries." J. Int. Heat Mass Trans. Vol. 35 No. 6 (1992) 1533-1544.
23. Laraqi, N. and Bairi, A., "Theory of thermal resistance between solids with randomly sized and located contacts." Int. J. Heat Mass Trans. 45 (2002) 4175 - 4180.
24. Greenwood, J.A., "The Area of Contact Between Rough Surfaces and Flats." Trans. AMSE J. Lub. Technol 89 (1967) 81-91.
25. Wang, H. and Degiovanni, A., "Heat transfer through periodic macro-contact with constriction." Int. J. Heat and Mass Trans. 45 (2002) 2177-2190.
26. C. V. Madhusudana, Thermal Contact Conductance (New York: Springer Verlag, 1996) 29-30.
27. Wolff, E.G. and Schneider, D.A., "Prediction of thermal contact resistance between polished surfaces." Int. J. Heat Mass Trans. 41 (1998) 3469-3482.
28. Marchand, A.S. and Raynaud, M. "Numerical Determination of Thermal Contact Resistance for Nonisothermal Forging Processes." J. Heat Transfer, Vol. 122 (2000) 776-784.
29. C. V. Madhusudana, Thermal Contact Conductance (New York: Springer Verlag, 1996) 9.
30. Marotta, E.E., et al. "Thermal Contact Resistance Modeling of Non-Flat Roughened Surfaces with Non-Metallic Coatings." J. Heat Transfer 123 (2001) 11 - 23.

References:

Chapter 4: Case Study: Thermal Contact Resistance of Bolted Joint Systems

In chapters 4 and 5, the methods developed in chapters 2 and 3 are applied to a case study of a bolted joint system. In chapter 4, the performance of the as-designed system is analyzed to demonstrate the multi-scale iterative finite element model for thermal contact resistance, to verify the accuracy of that model, and to demonstrate the impact of geometric surface assumptions used in conjunction with the model. In chapter 5, various parameters associated with the bolted joint system from the case study are varied to optimize the performance of the system.

The bolted joint system for the case study involves a commercial power electronics module (PEM) which exhibits both macroscopic surface form and micro scale surface roughness and its corresponding heat sink. The PEM base plate, which is bolted to an ideal heat sink, is modeled as ideal (perfectly flat), idealized (sinusoidal) and real (imported). Three different interstitial materials (vacuum, air, and thermal grease) are assumed to be present at the interface between the PEM base plate and the ideal heat sink.

It is shown that the multi-scale iterative finite element model in conjunction with the imported surface geometry can be used to accurately predict the thermal contact resistance of bolted joint systems. The predicted macro scale contact patterns for the imported surface model are shown to match well with the experimental contact pattern. The results of the imported thermal/structural analysis on the macro scale are shown to bound the experimental measurements as expected. And, the micro scale analysis predicts a thermal contact resistance per unit area that is similar to experimental values from the literature.

It is also shown that while the ideal and idealized models produce results that are qualitatively similar to the imported surface model, quantitatively the results differ by up to 98%. In addition, it is shown that the ideal and idealized surface models fail to accurately predict the thermal contact resistance of the case study system which validates the need for better surface modeling.

4.1 Introduction

Power electronics modules (PEMs) are a type of housing for power circuitry such as the large power transistors used in electric vehicles. The modules protect the electronic components inside, provide robust terminals for connecting input and output lines, and remove the heat produced inside. Since PEMs have large amounts of current flowing through them, there is a large amount of heat generated inside. The performance of PEMs is often limited by the internal temperature of the module, so increasing the efficiency of heat removal of PEMs can greatly increase their overall performance.

The amount of heat that can be removed from a PEM is a function of the total thermal resistance for the PEM. While many components contribute to the total thermal resistance, one of the biggest resistances occurs between the base plate of the PEM and an external heat sink. The base plate is a metal plate with the inner surface connected to the electronic components and the outer surface exposed to the environment. Heat is conducted from the circuitry through the base plate to the environment. When the base plate is attached to a heat sink, the heat is transferred from the base plate to the heat sink and then removed from the heat sink by forced convection.

This case study examines the nature and behavior of the mechanical and thermal contact between a commercial PEM and an aluminum heat sink and propose changes that can be made to the design to decrease thermal contact resistance at the interface and improve the overall module performance.

4.2 Description of the System of Interest

The PEM of interest is roughly 140 x 180 mm and stands nearly 40 mm thick (Figure 4-1). The base plate of the PEM is 5mm thick and composed of aluminum silicon carbide (AlSiC). AlSiC is a composite matrix material frequently used in electronics thermal management applications. It has a relatively high thermal conductivity (~ 175 W/mK) and a relatively low coefficient of thermal expansion (5e-6 - 15e-6/° C, depending on the amount of silicon carbide present by volume).[1] A thin (5 - 10um) metal Ni/P coating has been applied to the outer layer of the AlSiC base plate. The presence of this coating was neglected for this work. The base plate has 8 through holes around the perimeter which may be used to mount the PEM to the heat sink. The holes are suitable for 1/4-20 machine screws and are not tapped. The housing of the PEM is composed of a glass fiber reinforced plastic. The sidewalls of the housing are roughly 3mm thick and the PEM is hollow inside. During operation, the PEM can generate 600 W and the inside surface of the base plate can reach 125 C. Internal temperatures above 125 C are not permitted.

Figure 4-1: Power Electronics Module: Top (left), Bottom (center), and Test Heat Sink (right)

The PEM of interest is usually attached to a water cooled aluminum heat sink. Applications that require multiple PEMs may mount several PEMs on a single large heat sink. The heat sink is expected to be flat to within 30 um and have an average surface roughness less than 10 um. Heat sinks are not supplied by the PEM manufacturer and the choice of heat sink is up to the user. For this work, a test heat sink was machined from a single piece of 6061-T6 aluminum for use in measuring the mechanical contact between the PEM and a heat sink (Figure 4-1).

During operation, a thin layer of thermal paste or grease is typically placed in the interface between the PEM base plate and the heat sink to promote heat transfer between the two surfaces. While this layer may improve thermal performance, it adds uncertainty to the system. Thermal pastes and greases may not be evenly distributed across the surface, causing non-uniform heat transfer. The paste may migrate during operation. Its chemical composition may break down over time. The paste can also collect debris and can complicate maintenance.

4.3 Behavior of Bolted Joints

The mechanical behavior of bolted joints is relatively well understood. The contact area between two plates joined by a central bolt is “limited to a relatively small annulus around the bolt hole” and the contact pressure decreases from a maximum near the edge of the bolt hole to nearly zero within a short radial distance.”[2] (Figure 4-6 shows that the contact pressure drops dramatically after two bolt diameters away from the center of the bolt hole.)

The thermal behavior of bolted joints is somewhat more complicated. Some of the parameters which influence the thermal contact resistance in bolted joints include: plate thickness, flatness, and roughness; presence, thickness and radius of washers; radius of bolt holes and bolt hole spacing; mechanical properties of the bodies involved; thermal properties of the bodies and interstitial materials involved; and the applied mechanical loads.[3] It has been shown experimentally that contact pressure increases with applied load and decreases with surface roughness and thermal contact resistance has a strong dependence on contact pressure.[4]

Several numerical studies have been performed to simulate the thermal/structural behavior of bolted joints, however the bolted plates are typically smooth and flat with surface roughness neglected[3] or included as an experimentally derived coefficient.[5]

4.4 Macro Scale Thermal/Structural Analysis

4.4.1 Macro Scale Surface Geometry

A representative PEM was measured using a Corning Tropel Flat Master laser grazing incidence interferometer to obtain the surface data for the model. The data was saved in the Zygo.dat native format and the Zygo MetroPro software was used to prepare the data for export to the finite element model. The surface map for the measured PEM base plate is shown in Figure 4-2. The measurement reveals a surface bow of 208.761 um roughly centered on the base plate. The PEM typically has a surface bow of +/- 100 um so the measurement matches expectations.

The PEM base plate measurements shows significant data drop out on the left side of the sample. Grazing incidence interferometers, like the Flat Master, project the light source at a very small angle relative to the surface of interest (typically 1 to 3 degrees) rather than projecting it at an angle nearly normal to the surface of interest. This increases the distance that the reflected light travels and increases the signal that can be detected. However, the measurement is dependent on the incident light reaching the entire surface. Surface features that are very tall can block the incident light from reaching areas in its shadow, preventing those areas from being imaged. This is the case with the surface bow on the PEM. In addition, the surface map seems to be distorted. The base plate along the left edge appears to be longer than the right edge and the top edge is clearly sloping to the right.

The Flat Master is typically used to measure surface form of silicon wafers up to 200 mm in length with a resolution of 5 nanometers and was intended to measure relatively flat surfaces. The PEM base plate was very near the limit of what can be measured using the Flat Master both in terms of lateral and vertical dimensions. To obtain a more complete data set, a laser scanning profilometer would have to be used. However, there would be tradeoffs in terms of lateral resolution, vertical resolution and measurement speed.

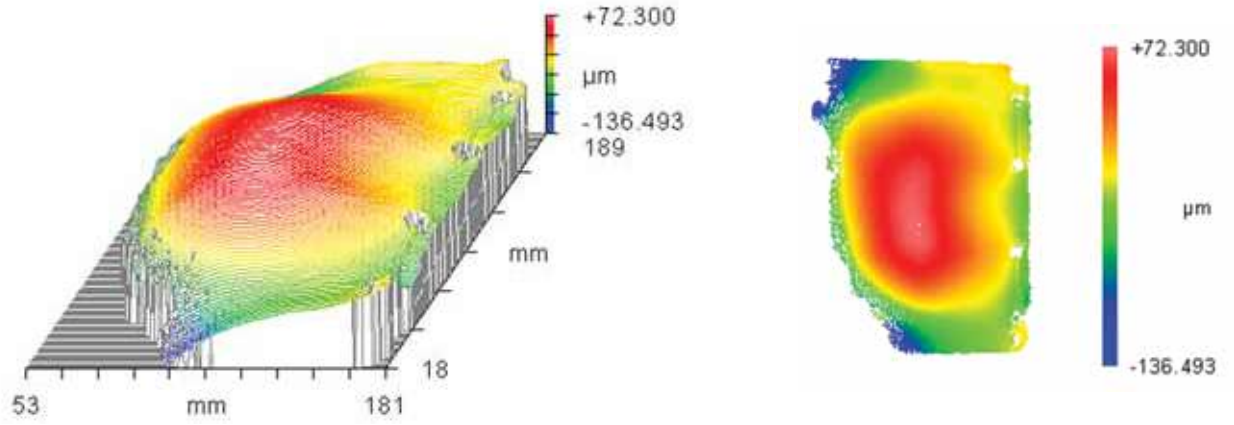

Figure 4-2: PEM Base Plate Surface Form: Orthographic View (left) and Top View (right)

4.4.2 Macro Scale Surface Modeling

The geometry for the macro scale thermal/structural analysis includes only the PEM base plate and the heat sink. The plastic housing for the PEM is thin walled and hollow with a relatively low Young's Modulus. It is assumed that it does not contribute to the structural behavior of the PEM and is not included in the model. The electronic components inside the PEM are also assumed to make no contribution to the structural behavior of the system.

The PEM base plate for the finite element analysis is modeled with ideal (perfectly flat) geometry, idealized (sinusoidal) geometry, and real (imported) geometry (Figure 4-3). The ideal base plate is generated by creating a block and eight cylinders and then subtracting the cylinders from the block to create the bolt holes. The idealized base plate is generated by using bottom up solid modeling techniques to create the lines and the areas for the bottom surface. Boolean operations are again used to subtract eight cylinders from the bottom areas. Finally, the bottom areas are extruded to create the plate thickness. The real base plate was generated by creating an ideal meshed base plate and then moving the surface nodes based on the surface measurement data. The idealized and real surface geometries are shown with the vertical dimensions enlarged 250x.

Figure 4-3: Base Plate Surface Models: Flat (left), Sinusoidal (center), and Imported (right)

Before the surface data could be imported, a data fill operation was used to repair the data set and replace missing data. The data that was missing from the shadow of the surface bow was too extensive and could not be replaced without drastically changing the shape of the surface and thus changing the problem. Instead, a symmetric half model was created and solved. The distortion of the base plate mentioned in the previous section also made it necessary to remove the bolt holes from the measured data using a data fill operation. The bolt holes were added back into the finite element model manually.

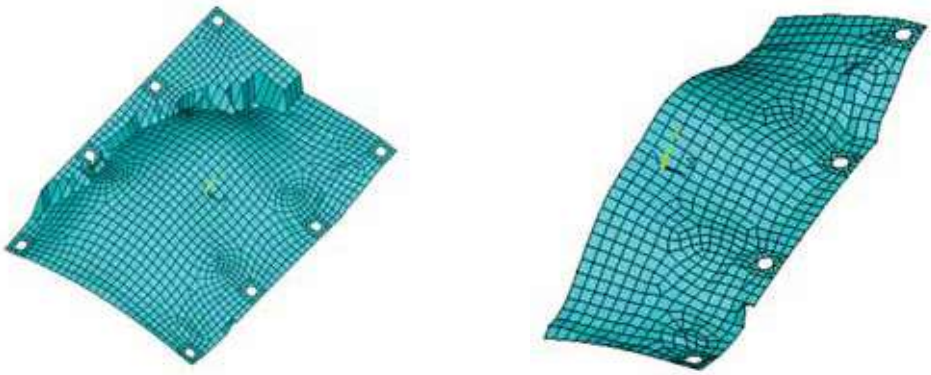

Figure 4-4: Imported Surface Model: Full Model (left) and Symmetric Model (right)

The heat sink is modeled as an ideal (perfectly flat) plate with a matching bolt hole pattern. Although the true heat sink may have internal channels to permit water cooling, these channels will be relatively thin and well supported and it is assumed that they do not contribute to the structural behavior of the heat sink. Instead, the heat sink is modeled as a solid block of aluminum 10 mm thick. The thickness was chosen based on the thickness of a heat sink that is commonly used with the PEM.

The bolts are assumed to transmit an insignificant amount of heat and are not included in the model. They will be considered in future work.

4.4.3 Experimental Procedure

The mechanical contact between the PEM and the test heat sink was measured using carbon paper and Pressure-X pressure sensitive film[6]. The paper or film was placed between the sample PEM and the test heat sink and then the two were bolted together using 5 Nm of torque in an alternating criss-crossing pattern. The results is an estimate of the mechanical contact between the two plates.

The carbon paper and pressure sensitive film tend to over estimate the contact between the plates because they act as a gasket in the interface and will tend to record contact gaps smaller than the thickness of the gasket layer as being “in contact” when they would not otherwise be in contact. They also tend to under estimate the contact between the plates because both the carbon paper and the film have a minimum marking pressure so areas that are in contact but with contact pressures lower than the marking pressure don’t record when they should. In addition, the films record contact for all time so if areas come into contact because of the assembly or disassembly process, they will indicate contact even if those areas are not in contact during steady state operation. Finally, the test heat sink has a surface form of 100 um, which is much less than the surface form of the PEM base plate (208 um) but is much larger than the specification for the heat sink (30 um). For all of these reasons, the experimental contact measured can only be used for qualitative comparisons.

4.4.4 Analysis Procedure

The base plate models were meshed with three dimensional 8-noded (brick) coupled-field solid elements and the heat sink models were meshed with 10-noded (tetrahedral) coupled-field solid elements. Only four degrees of freedom were required (x, y, z and temperature) but this subset could not be chosen so all degree of freedom (x, y, z, temperature, voltage and scalar magnetic potential) were selected. The extra degrees of freedom (volt and mag) are removed from the solution through boundary conditions. The base plates were covered with three dimensional 4-noded surface-to-surface contact elements to provide a deformable contact surface. The heat sinks were covered with three dimensional target segments to provide a deformable target surface.

Linear elastic material properties for the base plate were assigned based on AlSiC: Young’s Modulus of 183 GPa, Poisson’s Ratio of 0.25 and a thermal conductivity of 175 W/mK. Linear elastic material properties for the heat sink were assigned based on Aluminum: Young’s Modulus of 68.9 GPa, Poisson’s Ratio of 0.33 and a thermal conductivity of 167 W/mK. An initial TCC value of 1e5 W/m^2K was assumed.

The voltage and magnetic degrees of freedom for all nodes on both bodies were set to zero to remove those degrees of freedom from the solution. The sidewalls of the bolt holes on both bodies were constrained in x and y to mimic the role of the bolts. The nodes located on the backside of the heat sink were constrained in z to finish locating the heat sink in space and assigned a temperature of 300 K.

The structural load was applied to the nodes along the lines that define the bolt holes on the back side of the heat sink. The magnitude of the load applied to each bolt was determined by the following relation:[7]

$$T = KF_i d \qquad [4.1]$$

where T is the torque applied to the bolt, K is the torque coefficient, F_i is the applied axial force and d is the nominal major diameter of the bolt. The manufacturer specifies that each bolt should be subject to 5 Nm of torque during assembly. 1/4-20 bolts were used so the diameter value is 0.25 inches or 6.35 mm. The value of the torque coefficient is on the order of 0.2 for zinc plated bolts with an assumed frictional coefficient of 0.15 regardless of bolt size.[8] The value of the torque coefficient was assumed to be exactly 0.2. This yields an applied load of 3937 N per bolt. Since there are eight bolts in the model, a total load of 32,000 is applied to the model. The total load was divided by the number of nodes on the selected lines and then evenly distributed to each node.

It should be noted that more accurate models exist for calculating the applied axial from the applied torque, including one offered by Slocum.[9] It should also be noted that by excluding the bolts from the simulation and including the bolt effects through the applied loads and boundary conditions, the nature of the contact has been altered. In the true system, the bolts will have room to shift inside the bolt holes and will provide less of a constraint than has been applied. Thermal expansion effects will cause the applied mechanical load to be larger than is assumed in this model. In addition, the bolts themselves may transfer heat between the two bolted plates. In this work, the omission of the bolts and the assumptions made about the behavior of the bolts was made for convenience and to permit solution convergence. Kim, et al. present a very nice discussion of four methods that can be used for finite element modeling of bolted joints and the accuracy and advantages of the various methods.[10] Similar modeling techniques for the bolted joints and more accurate bolt torque-force relations should be used in future work.

The thermal load was applied to six regions on the backside of the base plate which represent the locations where the circuitry is located and where the heat is generated (Figure 4-5). The load was applied as both a temperature with the contact resistance calculated from the predicted heat flow across the contact surface ($Q_{contact)}$ and as a heat flow with the contact resistance calculated from the average temperatures at the interface ($\overline{T_{12}}$ and $\overline{T_{21}}$). The second applied boundary condition (applied heat flow) is more realistic since it is known that the PEM generates 100 W per heat generation region (600 W total) and will be used for most of the results presented.

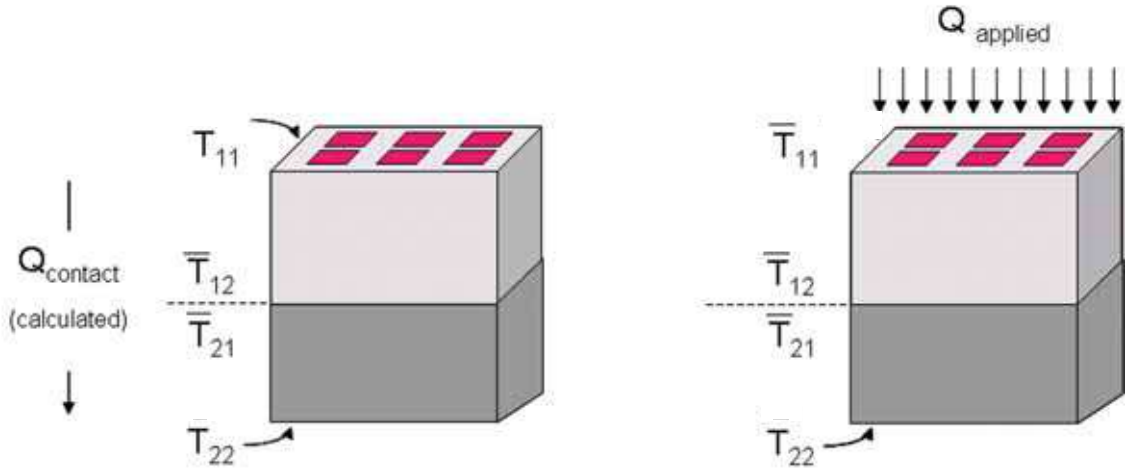

Figure 4-5: Applied Thermal Loads: Temperature (left) and Heat Flow (right)

Finally, the effect of three different materials located in the interface between the base plate and heat sink were considered: vacuum, air and thermal grease. For the first case, only solid/solid conduction was considered. No heat transfer was permitted across the gaps. In the second case, the air was assumed to have a thermal conductivity of 0.03 W/mK. In the third case, the grease was assumed to have a thermal conductivity of 1 W/mK and be perfectly distributed. In the real system, it is possible to have regions where there is no thermal grease or where it has built up so the gap is larger than it would be without the grease. For these reasons, this analysis provides a lower bound (best case) estimate of the thermal contact resistance with thermal grease.

For the second and third cases, gap dependent thermal conduction was implemented by applying a thermal convection load for all contact elements that are not in contact. The thermal "convection" coefficient was defined as the thermal conductivity divided by the gap length as discussed in Section 3.5.5.5.

4.4.5 Structural Results

4.4.5.1 Qualitative Results

Contact status and contact pressure plots for the three surface models (ideal, idealized and imported) and the measured contact are shown in Figure 4-6. The darker (orange) areas on the contact status plots indicate where contact has occurred. There is no contact in the lighter areas. Similarly, the darker areas (red for the pressure sensitive film and dark grey for the carbon paper) indicate contact for the measured surfaces. The darker the color, the higher the contact pressure.

For the simulated contact pressure plots, the higher colors (turqoise, then green, then yellow, then red) indicate areas of high contact pressure. The darker color (dark blue) indicates little or no contact pressure. The color scales for the contact pressure for each of the three cases (flat, sinusoidal and imported) are shown at the bottom. The units are in MPa.

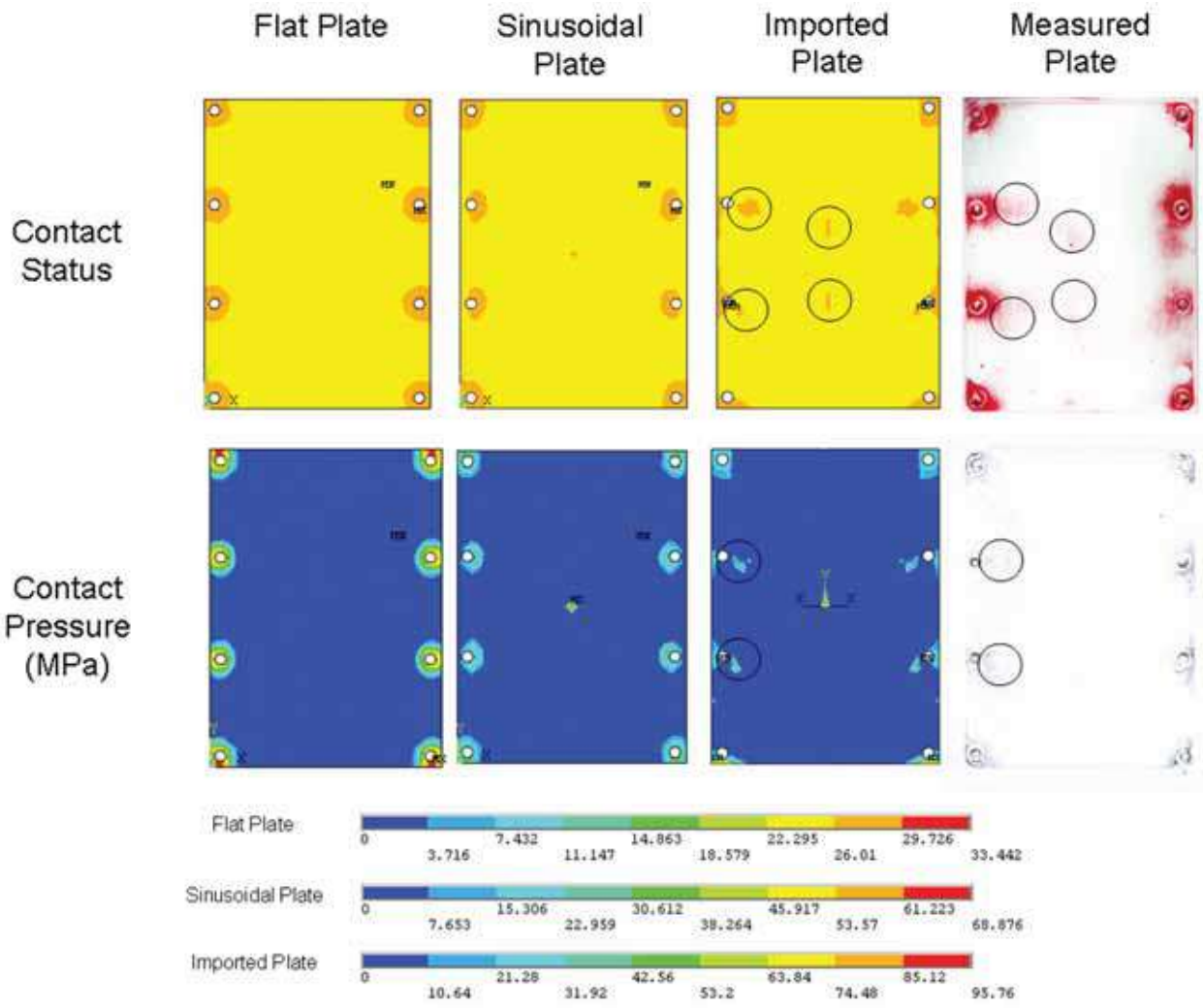

Figure 4-6: Contact Status and Contact Pressure for Simulated and Measured Contact

Qualitatively, the structural results for the three surface models are very similar and match the measured contact well. The mechanical contact is primarily limited to the areas around the bolt holes. For the flat base plate, the contact is centered around each bolt hole which is predicted by historical analytical models.

For the sinusoidal base plate, the contact is still centered around the bolt holes, however the contact areas for the four middle bolt holes are skewed slightly towards the center. This is because the sinusoidal surface is slightly taller near the inner edges of the bolt holes than at the outer edges. The sinusoidal base plate also has a small area of contact at the center of the PEM base plate where the top of the sinusoid is located.

The behavior of the imported surface is slightly more complicated. The contact is still primarily around the bolt holes but it is much less regular and well defined. The contact near the four middle bolt holes is skewed more significantly towards the center. This is because there are depressions visible in the regions around the bolt holes, so the heat sink will make contact more towards the center than directly around the bolt holes. There are also two regions of contact in the center instead of one. These correspond to a very slight double hump which is visible in Figure 4-4.

The measured contact for both the carbon paper and the pressure sensitive film show contact patterns that are most similar to the imported surface.The contact is primarily centered around the bolt holes, however there are also small contact regions between the bolt holes, especially in the middle, and the contact for the middle bolt holes is skewed towards the center. There are also two contact patches in the center of the base plate. The skewed and center contact regions for the imported and measured contact are circled.

This leads to the conclusion that all three surface models produce qualitatively similar results but the imported geometry produced the best match with the measured contact.

4.4.5.2 Quantitative Results

Some characteristic structural results (apparent area of contact, average contact pressure and average contact gap) are shown in Table 4-1. The apparent area of contact (AAoC) is calculated by summing the areas for all of the elements that are in contact in the model. The average contact area is calculated using a weighted average by area of the contact pressures for the elements in contact. The contact gap is similarly calculated by weighted average by area of the contact gaps for the elements that are not in contact.

The total surface areas available for contact of the macro scale models are: 2.54e10 um^2 (flat and sinusoidal), and 1.27e10 um^2 (imported). So the percentage of the surfaces that are in contact after the mechanical load is applied are: 7.94% (flat plate), 7.38% (sinusoidal plate) and 11.35% (imported plate.)

Table 4-1: Characteristic Parameters for Structural Results

	Apparent Area of Contact (um^2)	Average Contact Pressure (MPa)	Average Contact Gap (um)
Flat Plate	2.014e9	15.89	2.95
Sinusoidal Plate	1.87e9	17.10	9.35
Imported Plate	1.44e9	22.24	16.68
(Imported – Flat) / Imported	-30% Difference	-29% Difference	-82% Difference
(Imported – Sine) / Imported	-40% Difference	-23% Difference	-44% Difference

Quantitatively, the results for the three models are less similar. The AAoC for the sinusoidal and flat models are 30% and 40% smaller than for the imported plate respectively. The average contact pressures are 23% and 29% less for the sinusoidal and flat models than for the imported model. The average contact gaps are also 44% and 82% less for the sinusoidal and flat models than for the imported model. There is a clear difference in the structural results for the various surface models which supports the assertion that more accurate surface modeling is needed.

4.4.6 Thermal Results

4.4.6.1 Qualitative Results

Plots of thermal flux across the interface for the three surface models (ideal, idealized and imported) and for the three interstitial conditions (vacuum, air and thermal grease) are shown in Figure 4-7. The dark (red) areas indicate regions of low or zero heat flux. The lighter regions (orange, yellow, and green) indicating increasing heat flux. The darker (blue) regions indicate regions of very high heat flux. The corresponding color scales are shown at the bottom in units of W/m^2.

The results for each of the three models with no interstitial heat transfer are qualitatively very similar. Thermal conduction occurs in the contact regions and the surfaces are insulating everywhere else. The differences in the contact heat flux plots are identical to the differences in the contact status and pressure plots. The maximum local value of heat flux for each of the three models are: 5.39e5 W/m^2 (flat), 9.91e5 W/m^2 (sinusoidal) and 9.95e5 W/m^2 (imported). The sinusoidal and ideal cases are more similar because of the contact regions in the center of the plates. The heat flux here will tend to be higher than elsewhere in the model because of its proximity to the heat generation regions.

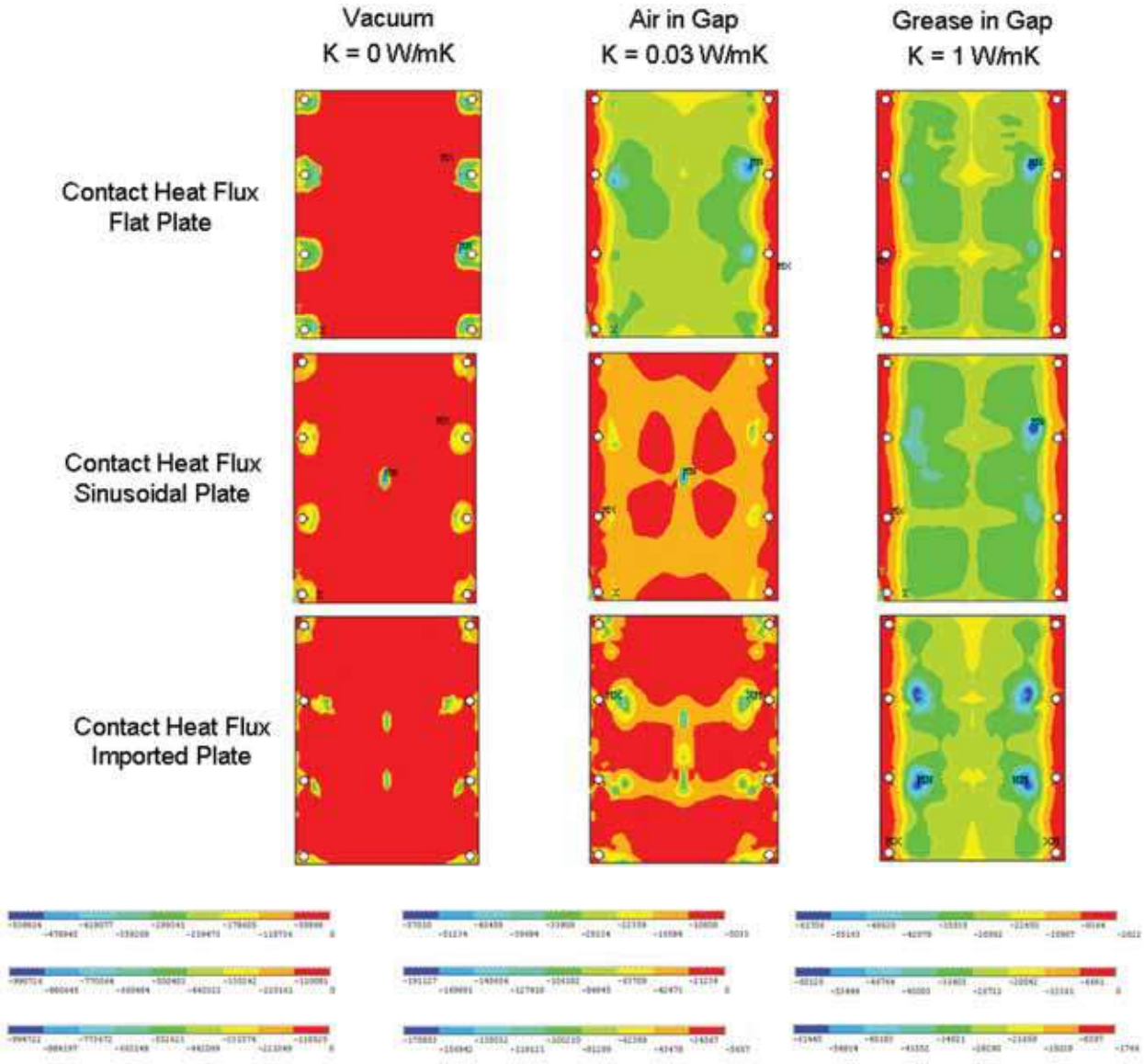

Figure 4-7: Thermal Flux at the Interface for the Three Surface Models and Interstitial Materials

The results for the three models with air in the interface are more complicated. The air tends to "smear" the heat transfer at the interface; thermal conduction occurs at the contact locations and the regions near the contact locations where the gaps are relatively small. Areas where the gaps are relatively large are still insulating. The sinusoidal model, and to a lesser extent the imported model, have higher areas of heat flux near the regions in contact and in the areas connecting the contact regions. The ideal flat geometry, however, has a nearly uniform heat flux in the center of the plate with almost no heat flux at the edges. This is because the average contact gap is so small in the ideal case that the air can effectively "smear" the entire surface. The maximum local value of heat flux for each of

the three models are: 5.70e4 W/m^2 (flat), 1.91e5 W/m^2 (sinusoidal), and 1.76e5 W/m^2 (imported). Here the maximum heat flux in the ideal cases is substantially lower than for the other two geometries because the heat transfer is much more uniform across thee surface.

The results for the three models with thermal grease at the interface are also very similar. The thermal grease effectively smears the entire surface and the heat flux is relatively uniform at the interface. The outline of the heat generation regions can be seen clearly for all three models. The maximum local value of heat flux for each of the three models are: 6.17e4 W/m^2 (flat), 6.01e4 W/m^2 (sinusoidal) and 6.15e4 W/m^2 (imported). The three values are very similar due to the smearing effect which makes the heat transfer relatively uniform over the entire surface.

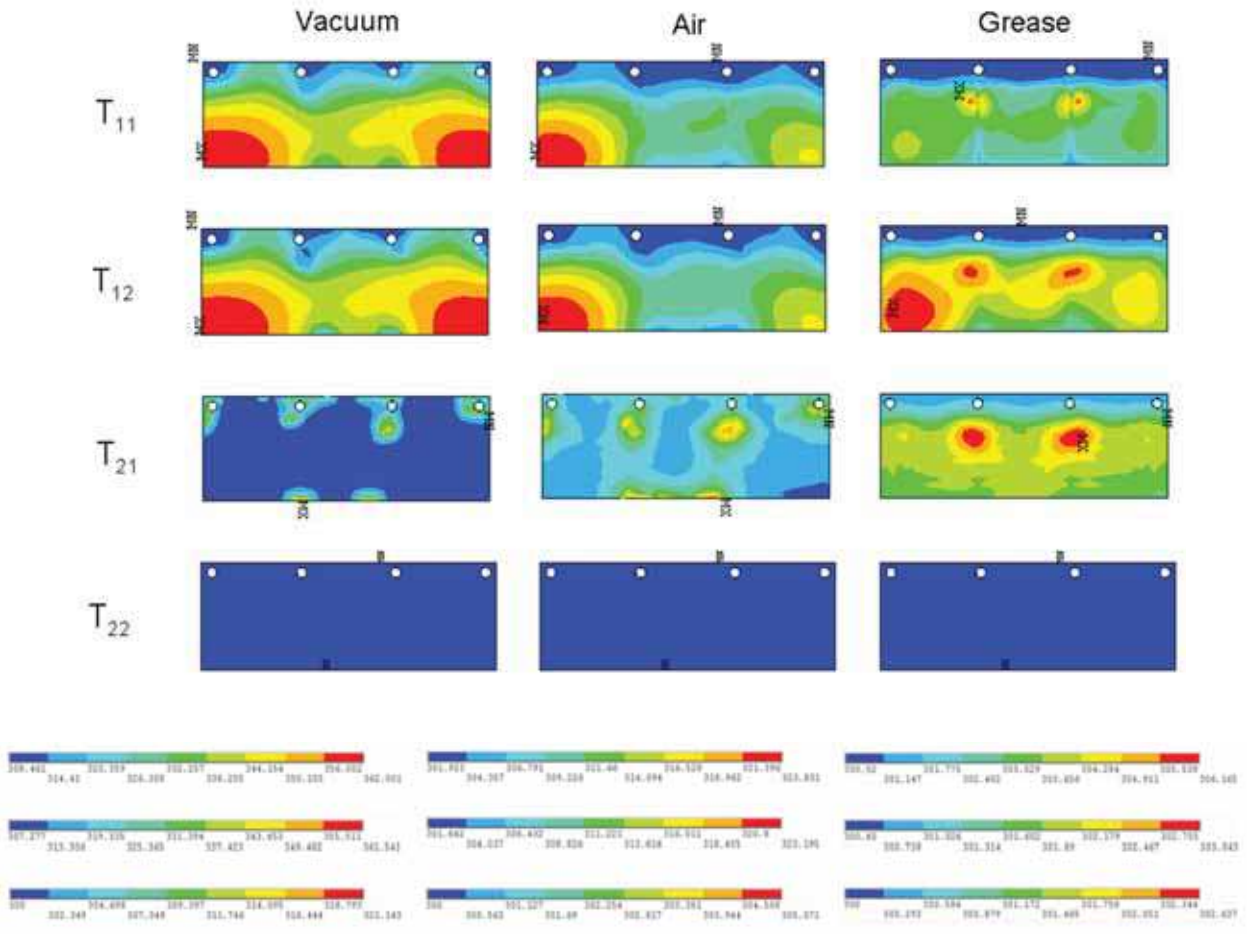

Figure 4-8: Cross Sectional Temperatures for the Imported Model with Three Interstitial Conditions: Vacuum (left), Air (center), and Grease (right)

The smearing effect of the interstitial materials can also be seen in the temperature variation across several planes in the model. Figure 4-8 shows the temperature plots for the imported surface model with vacuum, air and thermal grease for the outer surface of the base plate (T_{11}), for the inner contact surface of the base plate (T_{12}), for the inner contact surface of the heat sink (T_{21}) and for the outer surface of the heat sink (T_{22}). A red color indicates high temperatures while a blue color indicates low temperatures. The imported surface model is a symmetric model; only one half of the model is shown here. The color scales for the first three surfaces (11, 12 and 21) are shown below the temperature plots.

For the vacuum case, the temperatures distributions at the inner and outer surfaces of the base plate look identical (although the two surfaces have different temperature values). The lowest temperatures are at the outer edges because of the conduction through the contact patches near the bolt holes. There are also two local minimums on the center line in the middle where the other two contact patches are located. The maximum temperatures are located at the center line near the edges away from the two middle contact patches due to the heat generation near the center. The temperatures at the inner surface of the heat sink are higher only at the contact areas where the heat is conducting through from the base plate. The temperature at the outer surface of the heat sink is fixed at 300 K and is completely uniform.

The temperature distributions for the air case are similar to the vacuum case. The temperatures for the base plate are lowest near the bolt holes and highest on the center line away from the center contact regions. The temperature near the center contact regions is clearly more uniform than in the vacuum case. The temperatures on the inner surface of the heat sink are again highest near the contact regions but the temperature is more uniform with higher temperatures linking the various contact regions.

The temperature distributions for the thermal grease case are more uniform for all surfaces in the model. This is especially clear for the outer surface of the base plate and the inner surface of the heat sink.

4.4.6.2 Quantitative Results

The total thermal resistance and thermal contact resistance for the three surface models and interstitial materials are listed in Table 4-2 and Table 4-3. Recall that the total thermal resistance for the macro scale model is determined by dividing the difference between the average temperatures at the two outer surfaces ($\overline{T_{11}}$ and $\overline{T_{22}}$) by the total heat flow through the contact surface. The thermal contact resistance for the macro scale model is determined by dividing the difference between the average temperatures at the two inner surfaces ($\overline{T_{12}}$ and $\overline{T_{21}}$) by the total heat flow through the contact surface.

As expected, the total thermal resistance and the thermal contact resistance for all three surface models are highest for the models with vacuum as an interstitial material, smaller for the models with air at the interface and lowest for the models with thermal grease. Both the total and contact resistances for the flat plate with vacuum at the interface are higher than the sinusoidal and imported case. This is because is no contact at the center of the flat plate so the heat has to travel much further to cross the interface than for the other two surface models. For the rest of the interstitial materials, the resistances for the flat and sinusoidal plates are 10 - 98% lower than for the imported model. This is because the flat and sinusoidal models have high average contact areas and lower average contact gaps so the interstitial heat transfer is much more efficient. The differences between the various surface models are significant enough to support the assertion that better surface modeling is required.

Table 4-2: Total Thermal Resistance for the Various Macro Scale Models

	Total Resistance Vacuum (K/W)	Total Resistance Air (K/W)	Total Resistance Grease (K/W)
Flat Plate	8.69e-2	7.16e-3	3.52e-3
Sinusoidal Plate	4.9e-2	7.32e-3	1.86e-3
Imported Plate	6.2e-2	1.61e-2	3.91e-3
(Flat - Imported) / Imported	40% Difference	-56% Difference	-10% Difference
(Sine - Imported) / Imported	-21% Difference	-55% Difference	-52% Difference

Table 4-3: Thermal Contact Resistance for the Various Macro Scale Models

	Contact Resistance Vacuum (K/W)	Contact Resistance Air (K/W)	Contact Resistance Grease (K/W)
Flat Plate	1.79e-2	7.49e-4	2.90e-5
Sinusoidal Plate	1.54e-2	2.16e-3	3.35e-5
Imported Plate	1.55e-2	4.33e-3	1.35e-3
(Flat - Imported) / Imported	15% Difference	-83% Difference	-98% Difference
(Sine - Imported) / Imported	-1% Difference	-50% Difference	-98% Difference

The experimental value of total thermal resistance for the overall system provided by the manufacturer is 9e-3 K/W. This value should fall somewhere between the value for the model with air at the interface (upper bound solution) and the value for the model with thermal grease at the interface (lower bound solution). However, this is only true for the imported surface geometry. The flat and sinusoidal surface geometry under predict the total thermal resistance of the system by at least 20%. For this case study, and perhaps for many other systems, the true surface geometry must be used to generate a realistic model of the system.

Finally, the average temperatures across the imported surface model are listed in Table 4-4. The average temperatures were calculated using a weighted average by area of the elements at each of the surfaces. The elements themselves were selected by their z coordinate in the model and contact status was not considered. However, the average contact temperature at the interface was calculated using a weighted average by area of only the elements in contact.

Table 4-4: Average Temperature Differences for the Imported Surface Model

	Vacuum	Air	Grease
$\overline{T_{11}} - \overline{T_{22}}$	37.127	9.663	2.346
$\overline{T_{12}} - \overline{T_{21}}$	9.295	2.594	0.810
Contact $\overline{T_{12}} - \overline{T_{21}}$	0.347	0.050	0.006

As expected, the average total temperature drop across the model is much larger than the average temperature drop at the interface. The average temperature drops for the vacuum case are also larger than those for air, which in turn are large than those for the grease. The interesting result, however, is how much smaller the average contact temperatures at the interface are compared to the average interfacial temperatures. This highlights the effect of solid/solid conduction through the interface. Since the micro scale analysis will determine the resistance to solid/solid conduction at the interface, the average contact temperature (or average contact heat flux) will be used as the applied thermal loads instead of the average interfacial temperatures.

4.5 Micro Scale Thermal/Structural Analysis

4.5.1 Micro Scale Surface Geometry

Two areas on the PEM base plate and two areas from the test heat sink were measured using a Zygo New View 500 white light optical interferometer. Photographs, surface plots and the imported surface geometry for each of the four measured surfaces are shown in Figure 4-9 and Figure 4-10. Each sample was 353 x 265 um. The base plate samples had peak-to-valley surface roughnesses of 13.72 um and 13.22 um. The heat sink samples had peak-to-valley surface roughness of 11.28 um and 14.56 um. The surface roughness in the surface plots is shown at a 1000:1 scale relative to the horizontal axes. The imported surfaces are shown at true scale.

The surface data from each sample had a small data fill operation performed on it before it was imported into the finite element program. The surface geometry was created using a lateral resolution of 10 um (one data point every 10 um) by moving the surface nodes based on the surface data. The blocks for each half of the micro scale model are 100 um thick.

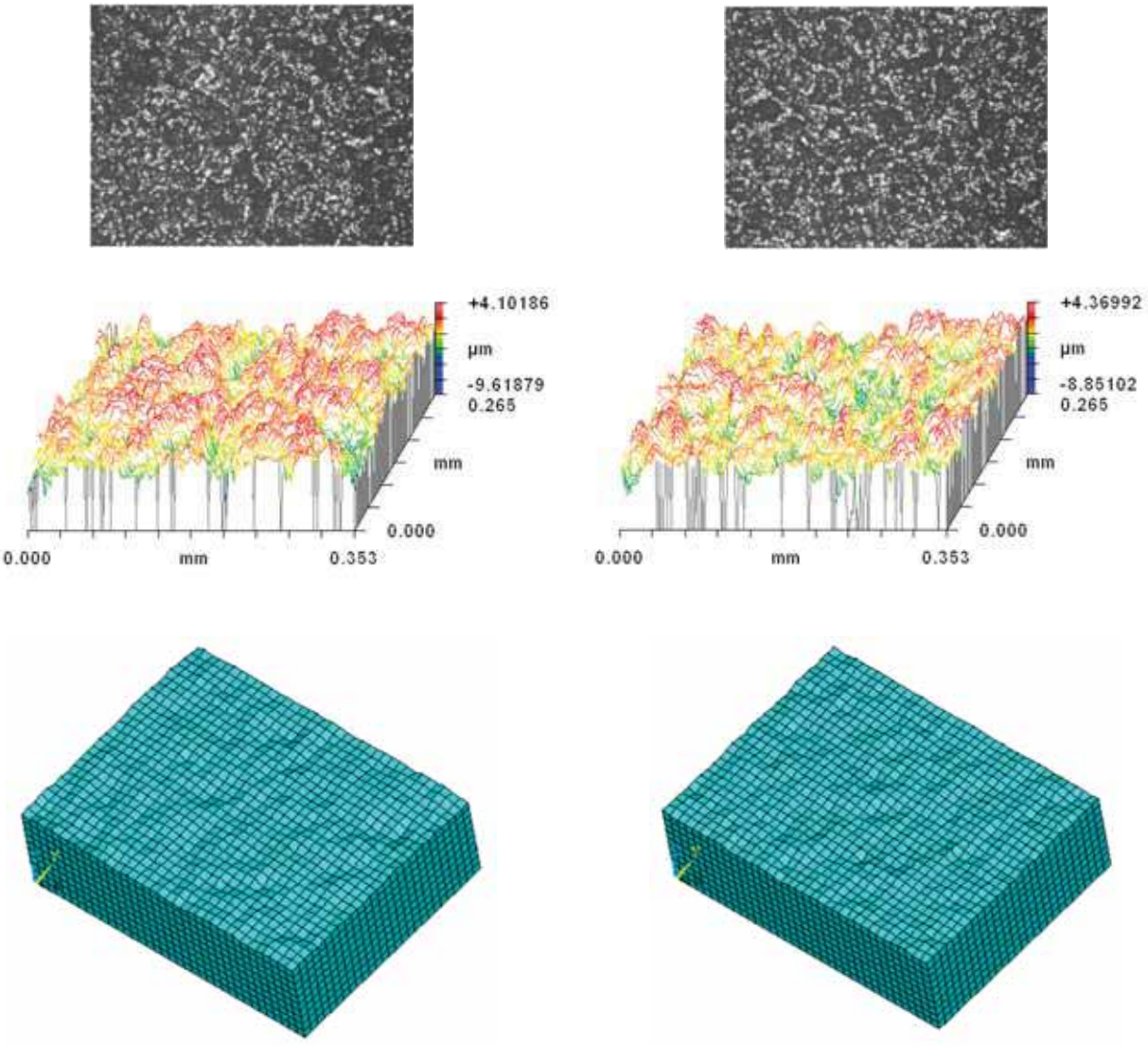

Figure 4-9: Micro Scale Surface Samples from the PEM Base Plate: Photographs of Surface (top), Surface Plots (center), and Imported Surface Geometry (bottom)

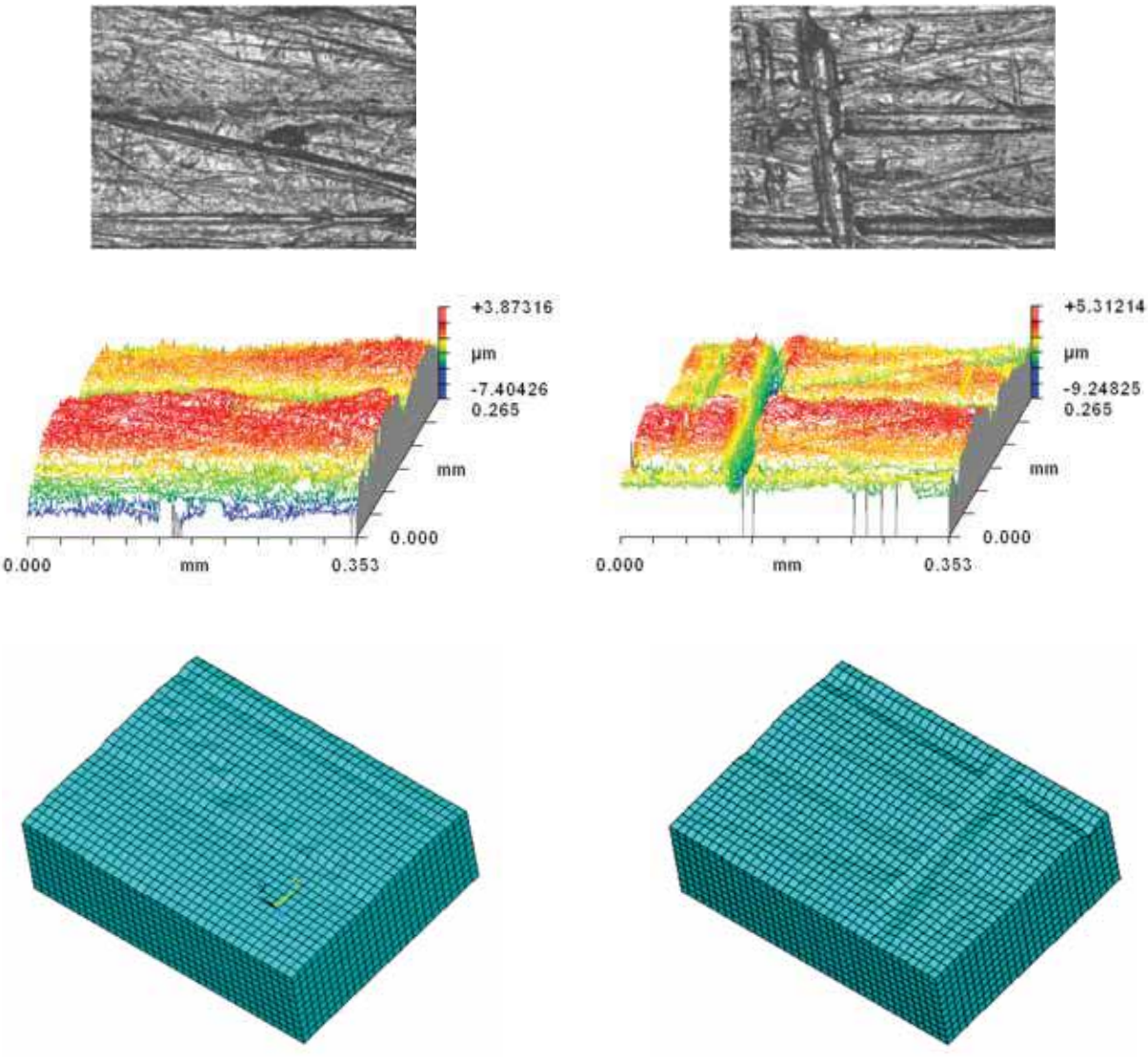

Figure 4-10: Micro Scale Surface Samples from the Test Heat Sink: Photographs of Surface (top), Surface Plots (center), and Imported Surface Geometry (bottom)

4.5.2 Analysis Procedure

The analysis procedure for the micro scale thermal/structural model is very similar to the one used for the macro scale model. Each half of the model was meshed with three dimensional 8-noded (brick) coupled-field solid elements with all degrees of freedom active. The base plate samples were covered with three dimensional 4-noded surface-to-surface contact elements to provide a deformable contact surface. The heat sinks samples were covered with three dimensional target segments to provide a deformable target surface.

Material properties were identical to those used earlier. An initial TCC value of 1e9 W/ m^2K was assumed to represent the thermal boundary resistance at the solid/solid interfaces.

The voltage and magnetic degrees of freedom for all nodes on both bodies were set to zero to remove those degrees of freedom from the solution. The nodes on both bodies along the x planes (x = 0 and x = 353 um) were constrained in the y direction. The nodes on both bodies along the y planes (y = 0 and y = 265 um) were constrained in the x direction. The nodes located on the backside of the base plate sample were constrained in z to finish locating the heat sink in space. The nodes located on the backside of the heat sink were assigned a constant temperature of 0 K. This was done to highlight the temperature drop across the surface.

A uniform structural load was distributed across all of the nodes on the backside of the heat sink. The magnitude of the structural load was equal to the average contact pressure from the macro scale simulation (22.24 MPa) multiplied by the nominal contact area of the samples (363 x 265 um).

The thermal load was applied uniformly to the backside of the base plate. The load was applied as both a temperature calculated from the average temperature of the elements in contact at the interface of the macro scale model and as a heat flux also calculated from the average heat flux of the elements in contact at the interface of the macro scale model.

4.5.3 Results

The contact status and contact pressure for first base plate and first heat sink samples for the micro scale thermal/structural analysis are shown in Figure 4-11. The contact gap and the heat flux at the interface for the same samples are shown in Figure 4-12. The contact status for any contact system in ANSYS is determined by the position of a contact element relative to its target element and can be: open far-field contact, open near-field contact, sliding contact or sticking contact. The contact for the micro scale model is either in sliding contact, in near contact (within the pinball region but not actually in contact), or in far open contact (not within the pinball region). The pinball region in ANSYS is a fixed radial distance from the integration point of each contact element. The size of the pinball region is controlled by a real constant and can be modified if desired.[11]

The two bodies in the micro scale model are in contact over relatively small areas scattered over the surface. The real area of contact was less than 1% of the total surface area available for contact which is typical for two metals in contact. The contact pressure for most of the surface is relatively low with regions of very high contact (1500+ MPa) at many of the contact locations. The gaps between the surfaces at the interface are up to 10 um wide with an average gap of 3.5 um. The contact gap plot shows the extend to which the contact geometry is irregular and complex. The contact flux plot shows that heat flow

is primarily limited to the contact regions and areas with very small contact gaps near the contact regions. The heat flux plot shown is for the vacuum case. The plots for the air and thermal grease cases look identical with solid/solid conduction dominating.

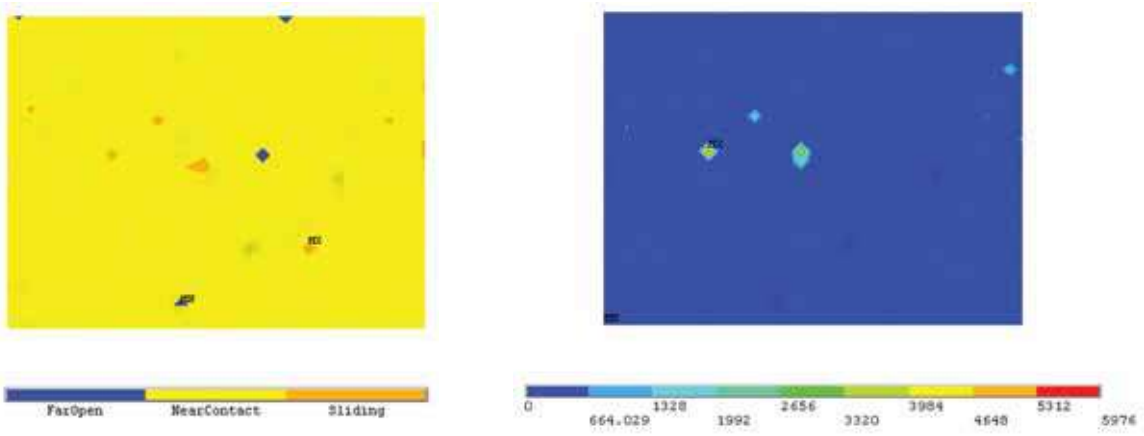

Figure 4-11: Contact Status (left) and Contact Pressure (right) for the Micro Scale Analysis

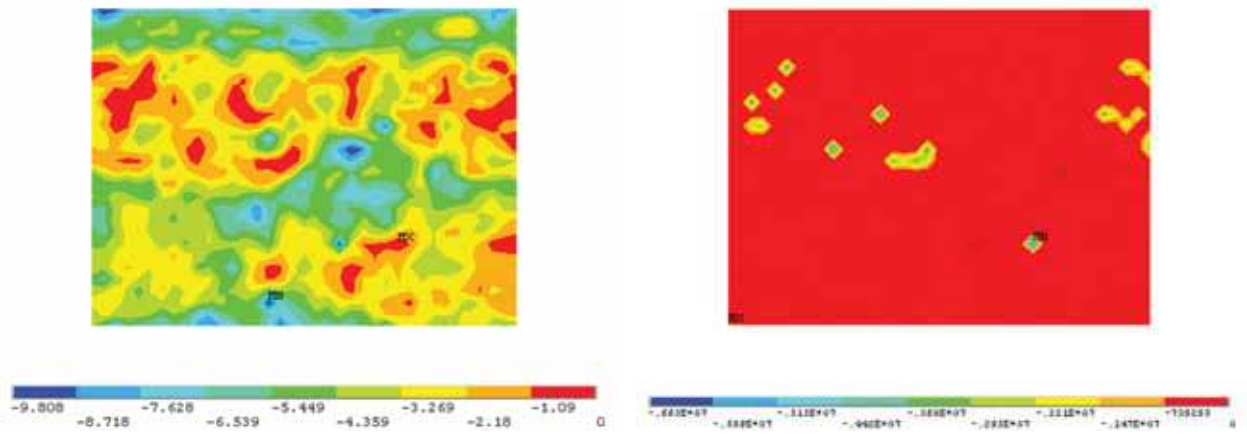

Figure 4-12: Contact Gap (left) and Contact Heat Flux in Vacuum (right) for Micro Scale Analysis

The interfacial temperature plots for the three interstitial materials are shown in Figure 4-13, Figure 4-14, and Figure 4-15. The plots for all three cases are very similar, although the temperature variations across the surface are almost an order of magnitude lower for the air case than for the vacuum case, and the temperature variations across the surface are another order of magnitude lower for the thermal grease case than for the air case. The highest temperatures are again clustered around the contact locations and the regions with very small interstitial gaps.

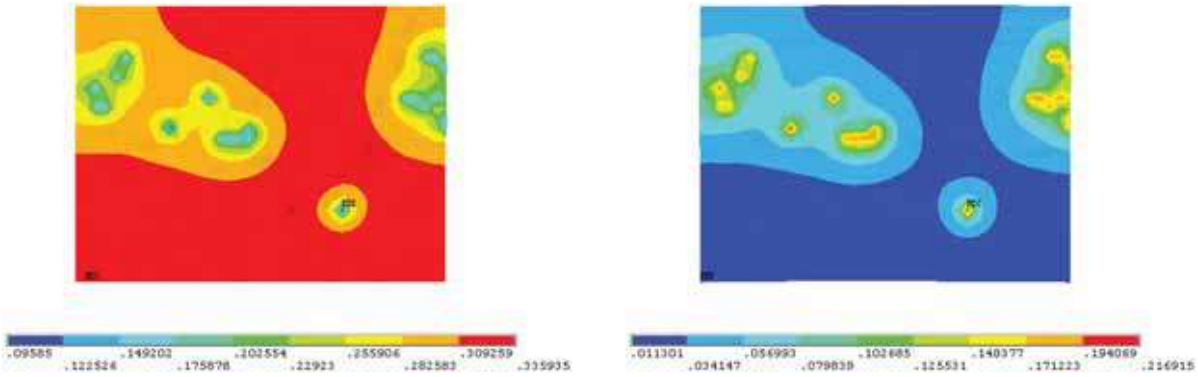

Figure 4-13: T_{12} (left) and T_{21} (right) Temperature Plots for Micro Scale Vacuum Case

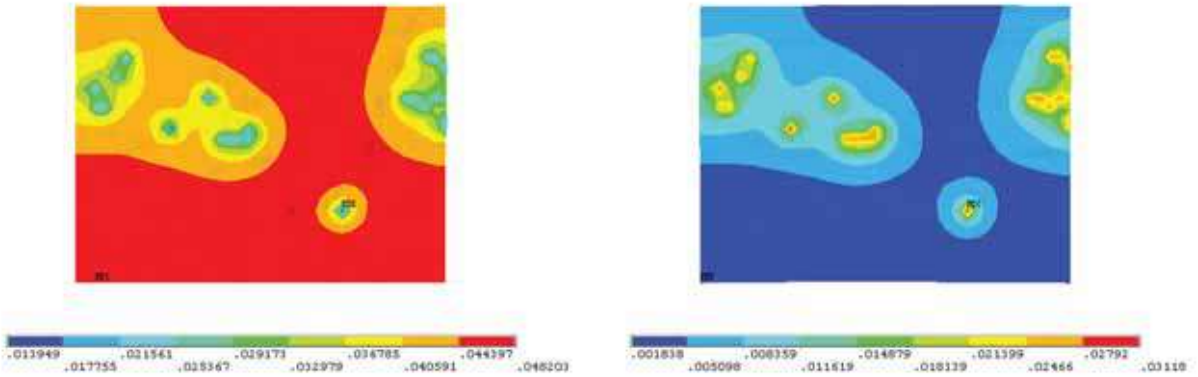

Figure 4-14: T_{12} (left) and T_{21} (right) Temperature Plots for Micro Scale Air Case

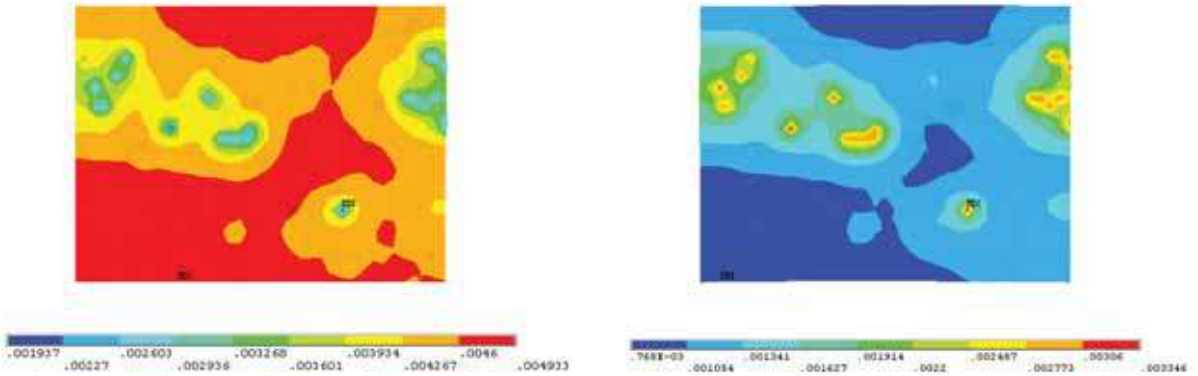

Figure 4-15: T_{12} (left) and T_{21} (right) Temperature Plots for Micro Scale Grease Case

Table 4-5 shows the applied thermal loads and the resulting micro scale thermal contact resistance per unit area.The thermal contact resistance per unit area for the vacuum case was the lowest of the three materials (5.01e-6 Km^2/W) while the resistance for the thermal grease was the highest (2.74e-6 Km^2/W). There were no experimental values from this work to use to verify the micro scale thermal contact resistance results. The closest values from the literature were 1.11e-6 and 4e-6 Km^2/W for aluminum-aluminum contacts at 28 MPa at 326 and 355 K respectively.[12] The interstitial conditions were not reported and are assumed to be air. This model was for AlSiC-aluminum contacts at 22.24 MPa between 300K and 330 K so the two systems should be close enough to compare. The results of the micro scale model are the same order of magnitude as the values reported in the literature, so the micro scale results should be valid at least as approximations. More work to validate the micro scale results will be done in future work.

Table 4-5: Applied Thermal Loads and Micro Scale Thermal Contact Resistance

	Applied ΔT [K]	or	$q_{applied}$ [W/m^2]	$r_{contact}$ [Km^2/W]
Vacuum	0.347		2.37e4	5.01e-6
Air	0.05		3.53e3	4.84e-6
Grease	0.006		6.17e2	2.74e-6

For the micro scale model, different values for temperature or heat flux must be used for each interstitial material based on the results from the macro scale model which makes it difficult to make a direct comparison of the results. The heat for the vacuum case is completely transmitted across the interface due to solid/solid conduction, while the heat for the thermal grease case is transmitted primarily across the gap. The different heat conduction paths change the amount of heat traveling across the solid/solid contacts on the macro scale and changes the applied load on the micro scale. For this reason, the applied thermal load was much higher for the vacuum case than for the air case, and the applied thermal load for the air case was higher than the grease case, resulting in lower thermal contact resistance for the vacuum case than for the other two cases.

4.6 Iteration Loop

The micro scale thermal contact resistances calculated from the first iteration loop were applied as the TCC real constant for the solid/solid contact resistance at the macro scale and the macro scale thermal/structural model was solved for a second time. The results for the vacuum case between the first and second iterations shows a 9% difference, while the

difference in results for the air and thermal grease cases were less than 1%. The results of the second macro scale iteration were then fed back into the micro scale model. The results of the second micro scale iteration were identical to the first micro scale simulation and the second set of results from the micro and macro scales were used as the final results. Although the iteration converged very quickly for this model, other models with strong dependencies on the micro scale TCR may require more cycles to converge. The iteration for this work was performed manually, but it could be automated if desired.

Table 4-6: Total Thermal Resistance for Both Iteration Loops

	Total Resistance Vacuum (K/W)	Total Resistance Air (K/W)	Total Resistance Grease (K/W)
1st Loop	6.2e-2	1.61e-2	3.91e-3
2nd Loop	5.69e-2	1.60e-2	3.90e-3
(2nd – 1st) / 2nd	9% Difference	< 1% Difference	< 1% Difference

4.7 Conclusions

The multi-scale iterative approach for predicting thermal contact resistance which was introduced in the previous chapter was applied to a case study involving a commercial power electronics module with macro and micro scale surface features.

The predicted macro scale contact patterns for the imported surface model was shown to match well with the experimental contact pattern. The results of the imported thermal/ structural analysis on the macro scale with air (R = 1.61e-2 K/W) and thermal grease (R =3.91e-3 K/W) bound the experimental measurements (R = 9e-3 K/W) as expected. The micro scale analysis predicts a thermal contact resistance per unit area that is similar to experimental values from the literature. Hence, the proposed multi-scale iterative finite element model can be used in conjunction with imported surface geometry to predict the thermal resistances of bolted systems, quantitatively study the effects of manufacturing tolerances, and determine rationally how improve system performance.

While the thermal and structural results were qualitatively similar for all three surface models, quantitatively the results differed by up to 98%. In addition, the ideal and idealized surface models do not bound the experimental measurement of total thermal resistance for the PEM. The experimental value (R = 9e-3 K/W) was 20% higher than the upper bound (worse case) simulations with air as the interstitial material ($R_{air,ideal}$ =

7.16e-3 K/W and $R_{air,idealized}$ = 7.32e-3 K/W). This showed that the ideal and idealized surface models cannot be used to predict the thermal resistances for the case study and validated the need for better surface modeling.

References:

1. http://matweb.com
2. C. V. Madhusudana, Thermal Contact Conductance (New York: Springer Verlag, 1996) 101.
3. Song, S. et al., "Experimental Study and Modeling of Thermal Contact Resistance Across Bolted Joints." Proceedings of the 31st Aerospace Sciences Meeting & Exhibit, Reno, NV., Jan. 11-14, 1993. AIAA 93-0844.
4. Yeh, C.L. and Lin, C.T., "Thermal Contact Resistance Correlation for Metals Across Bolted Joints." Int. Comm. Heat Mass Transfer, Vol 30. No. 7 (2003) 987-996.
5. Fukuoka, T. "Finite Element Analysis of the Thermal and Mechanical Behaviors of a Bolted Joint." J. Pressure Vessel Technology, Vol 127 (2005) 402 - 407.
6. http://www.sensorprod.com/pressurex.php
7. J. E. Shigley, C. R. Mischke, R. G. Budynas, Mechanical Engineering Design 7th Ed. (New York: McGraw Hill, 2004) 423.
8. J. E. Shigley, C. R. Mischke, R. G. Budynas, Mechanical Engineering Design 7th Ed. (New York: McGraw Hill, 2004) 423-424.
9. Slocum, A.H., Precision Machine Design, (Dearborn, MI: Society of Manufacturing Engineers, 1992) 375.
10. Kim, J., Yoon, J.C., and Kang, B.S., "Finite element analysis and modeling of structure with bolted joints." Applied Mathematical Modeling 31 (2007) 895-911.
11. ANSYS Contact Technology Guide, Section 3.8.9.1.
12. Gmelin J., "Thermal boundary resistance of mechanical contacts between solids at sub-ambient temperatures," Phys. D: Appl. Phys. 32 (1999) R35.

Chapter 5: Factors Influencing Thermal Contact Resistance

This chapter explores the effects of various geometric parameters, material properties, boundary conditions and assumptions on the micro and macro scale solutions of the iterative multi-scale thermal/structural finite element model.

5.1 Micro Scale Model

The effect of boundary conditions (temperature vs. flux), applied load, surface roughness and thermal boundary resistance on micro scale thermal contact resistance are explored in this section. In addition, the effect of two model parameters (surface sample and imported lateral resolution) are examined to ensure that the simulation results are representative of the system and not a reflection of the assumptions built into the model.

The calculation of thermal contact resistance per unit area on the micro scale in the previous chapter was calculated based on the results from the macro scale analysis. However, it is difficult to compare the results of the three interstitial conditions since the three cases had different applied thermal loads. For this section, each case (except for the discussion of boundary conditions) uses an arbitrary constant applied temperature difference of 10 K. All cases presented vary one parameter while keeping the others constant. The constant values for the non-varying parameters are their nominal values for the as-designed, as-measured PEM case study system. (See Section 4.5 for more details.)

5.1.1 Boundary Conditions

In the previous chapter, it was noted that the thermal load could be applied to the micro scale model as an applied temperature or an applied heat flux (heat flow). For that work, the thermal contact results were nearly identical (within 1%) for the two boundary conditions provided that the applied temperature and heat flux were taken from the average temperature and average heat flux for the elements *in contact* from the macro scale model. If a different temperature difference is used, the model will tend to over predict the heat flux through the interface which can change the results for thermal contact resistance.

5.1.2 Load

Figure 5-1 shows a plot of thermal contact resistance per unit area versus applied load which has been normalized versus the Young's Modulus of the softer of the two materials (aluminum) for the three interstitial materials. The plot shows that there is a threshold

value of applied load. Below the threshold, thermal contact resistance increases dramatically. Above the threshold, the system is relatively insensitive to applied load. It also shows that the thermal contact resistance for vacuum at the interface and air at the interface are very similar. This indicates that solid/solid conduction is the dominant mode of heat transfer at the micro scale unless the thermal conductivity in the gaps is very large.

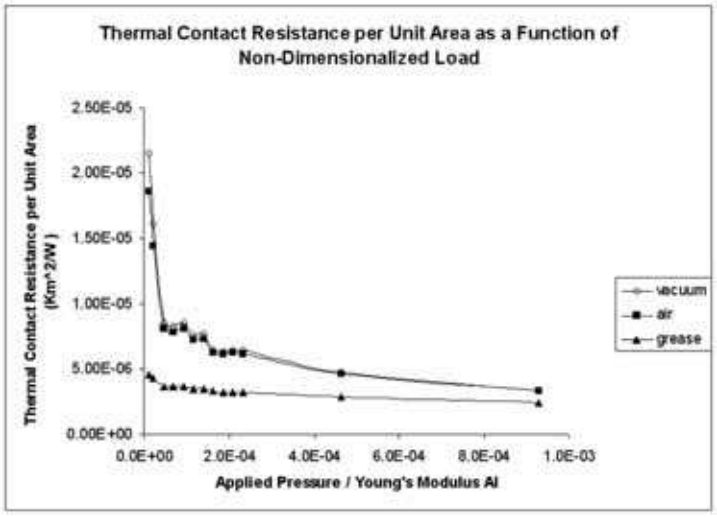

Figure 5-1: Micro Scale TCR vs. Non-dimensionalized Load (P/E)

The threshold value for applied load is likely based on the deformation of the contacting asperities. Below the threshold value, the asperities are rapidly deforming, increasing the real area of contact and bringing more asperities into contact. Above the threshold value, it becomes increasingly difficult to deform the contacting asperities so the real area of contact increases more slowly and the thermal contact resistance decreases more slowly. This is demonstrated very clearly in Figure 5-2a which shows the inverse of the real area of contact plotted against the non-dimensionalized load. This curve has the same basic shape as the TCR curves for the vacuum and air cases, indicating a strong relationship between real area of contact and thermal contact resistance at the micro scale.

The thermal contact resistance with thermal grease at the interface is less dependent on the real area of contact at the interface. Instead, it seems to be a strong function of the average contact gap (Figure 5-2b) which decreases more gradually with applied load.

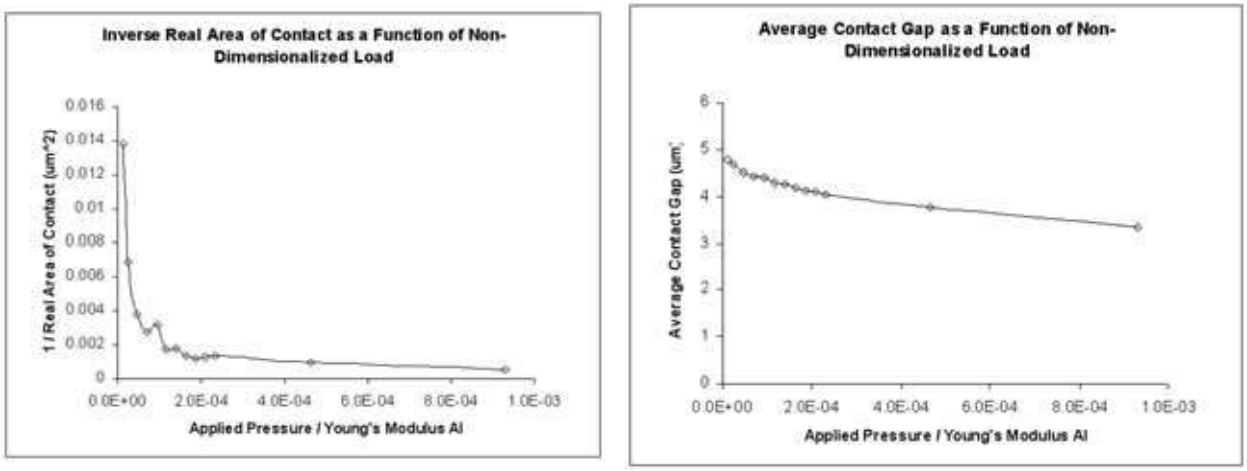

Figure 5-2: Micro Scale Inverse Real Area of Contact (left) and Average Contact Gap (right) vs. Non-Dimensionalized Load (P/E)

5.1.3 Surface Roughness

To study the impact of surface roughness of micro scale thermal contact resistance, the surface data from the measured PEM base plate and test heat sink samples were scaled by factors between 0.3 and 1 down by multiplying the values in the surface data. The applied normalized mechanical pressure for all remaining micro scale parameter studies was 3.23e-4. The results are shown in Figure 5-3. Micro scale thermal contact resistance seems to scale almost linearly with surface roughness for all three interstitial materials, although the slope for the thermal grease case is lower than for the other two cases.

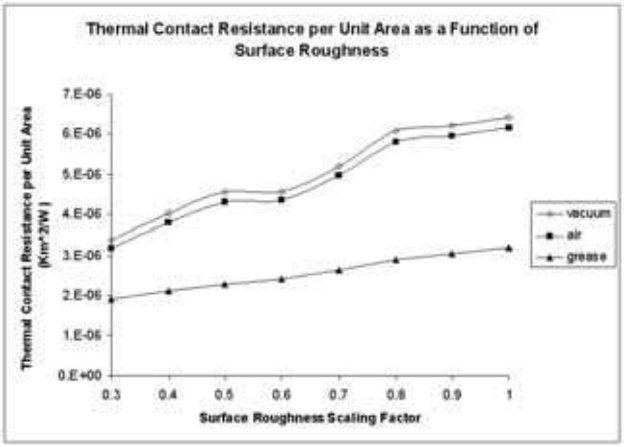

Figure 5-3: Micro Scale TCR vs. Surface Roughness (P/E = 3.23e-4)

As the surface roughness decreases, the real area of contact should increase and the average gap should decrease. In Figure 5-4, it is shown that the inverse real area of contact has an approximately linear relationship with surface roughness and that the average contact gap has a linear relationship with surface roughness. Since the thermal contact resistance for the interstitial materials scale with inverse real area of contact and average contact gap, and the inverse real area of contact and average contact gap scale with surface roughness, it is logical that the thermal contact resistance also scale linearly with surface roughness.

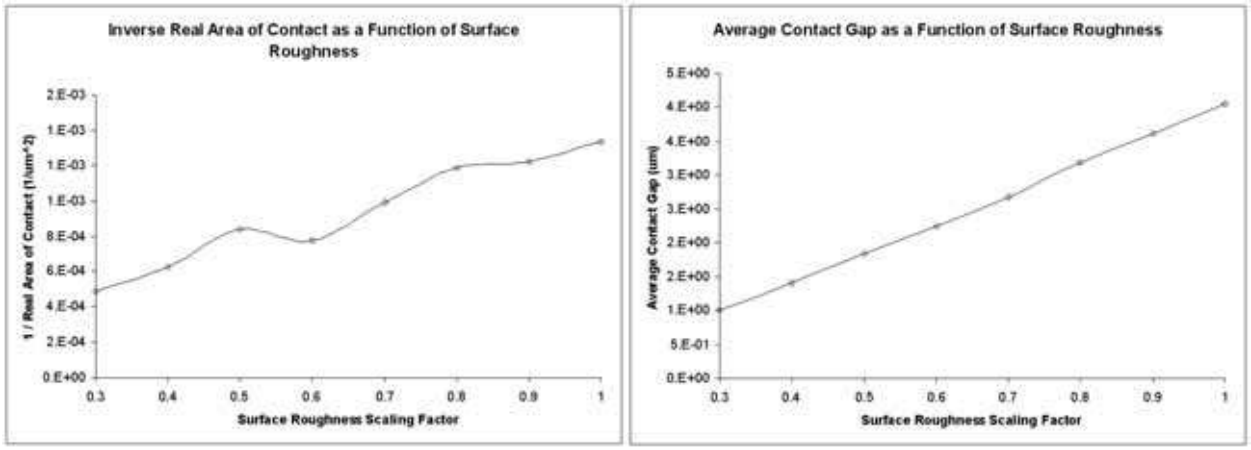

Figure 5-4: Micro Scale Real Area of Contact (left) and Average Contact Gap (right) vs. Surface Roughness (P/E = 3.23e-4)

5.1.4 Thermal Boundary Resistance

Figure 5-5 shows the effect of thermal boundary resistance on the micro scale thermal contact resistance. Like the applied load, the thermal boundary resistance seems to have a threshold value below which the thermal contact resistance changes very little with thermal boundary resistance. This is likely due to a saturation effect where the solid/solid contacts can only transport so much heat at a time regardless of how low the resistance across that interface is. The vacuum and air cases show a greater dependence on the value of thermal boundary resistance because they have a greater dependence on solid/solid conduction than the thermal grease case which has a greater dependence on interstitial conduction. However, thermal grease case does show a small dependence on thermal boundary resistance values, indicating that solid/solid conduction still plays a role in the heat transfer across the interface.

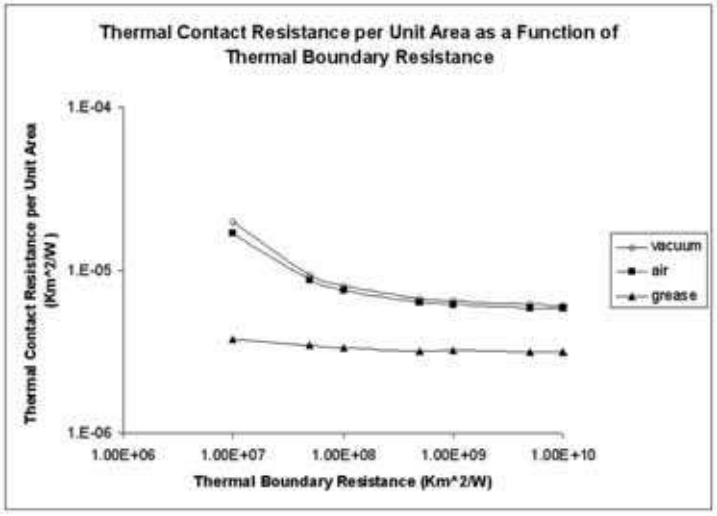

Figure 5-5: Micro Scale TCR vs. Thermal Boundary Resistance (P/E = 3.23e-4)

5.1.5 Surface Samples

The results that have been presented thus far have used a single base plate surface measurement and a single test heat sink surface measurement. However, it was not known if these two samples were representative of the entire surface. Since two measurements of the base plate and heat sink were available, the micro scale model was solved for all four combinations of surface measurement. The results are shown in Figure 5-6.

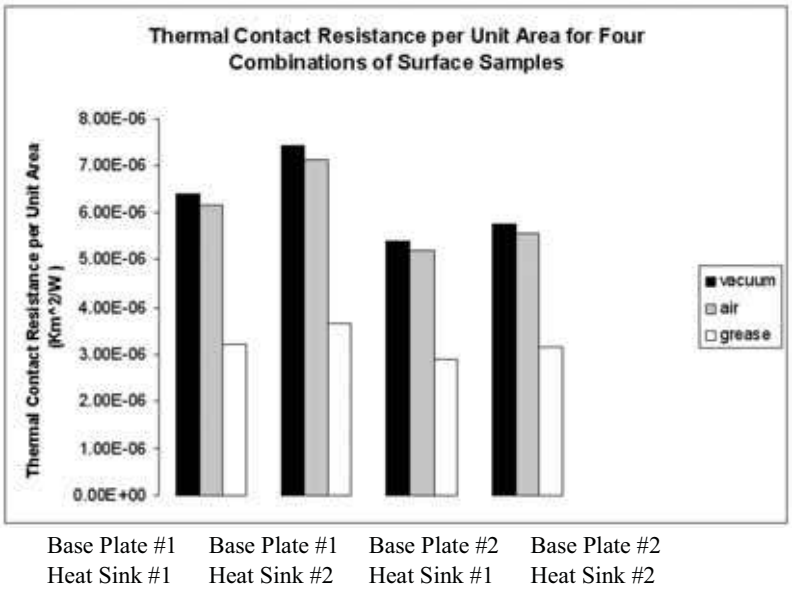

Figure 5-6: Micro Scale TCR vs. Various Combinations of Surface Samples (P/E = 3.23e-4)

The variation in thermal contact resistance across the four combinations for the vacuum and air cases were 27%. The variation in thermal contact resistance across the four combinations for the grease case was 21%. While more data is required to ensure that the surfaces used were representative, it is clear that the choice of surface sample is not a dominant factor in calculating thermal contact resistance for this model.

5.1.6 Imported Lateral Resolution

The base plate surface samples were measured with a lateral resolution of 1.1 um and the heat sink surface samples were measured with a lateral resolution of 0.55 um. However, they were imported into the model with a lateral resolution of 10 um (one data point ever 10 um in the x and y directions).

A reduced lateral resolution is required because there are still limitations on the size of model that can be solved with a PC. For this work, structural contact models with imported resolutions of 3 um have been solved. However, coupled thermal/structural model requires more memory and disk space than the pure structural model and the smallest imported resolution that could be solved for this work was 6 um.

Micro scale thermal/structural models with imported resolutions ranging from 6 um to 10 um were solved to explore the impact of lateral resolution on thermal contact resistance. The results are shown in Figure 5-7.

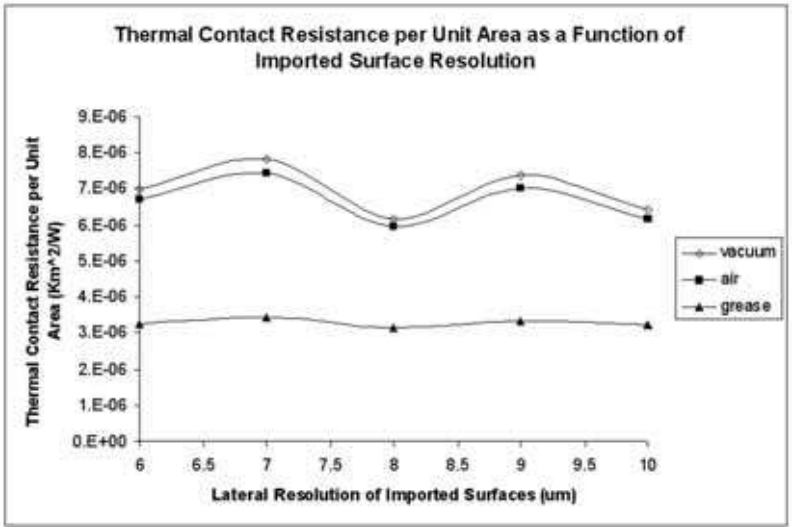

Figure 5-7: Micro Scale TCR vs. Imported Surface Resolution (P/E = 3.23e-4)

The thermal contact resistance for the air and vacuum models seemed to oscillate about a mean value rather than tending towards a specific value or in a specific direction as the lateral resolution was varied. The variation between the minimum and maximum values of thermal contact resistance over the range of imported resolutions was 27% for the vacuum

case and 25% for the air case. The variation for the thermal grease case was only 8%. While the micro scale results have not converged with respect to the imported lateral resolution, the imported lateral resolution does not seem to be a dominant factor in calculating the micro scale thermal contact resistance for this model. Again, more work is required to explore the effects of different measured surfaces and a large range of imported resolutions to ensure that the results are representative.

5.2 Macro Scale Model

The effect of boundary conditions (temperature vs. flux), the contribution of the thermal contact resistance to the total thermal resistance and the validity of traditional one dimensional assumptions for the macro scale thermal/structural model are explored in this section. In addition, the effects of parameters including applied load, thermal conductivity, amplitude of surface bow (surface form), thickness of the base plate and heat sink, and the magnitude of the micro scale thermal contact resistance per unit area are examined to determine the sensitive model parameters for optimization.

5.2.1 Boundary Conditions

Figure 5-8 shows the total thermal resistance and the thermal contact resistance for the as-designed macro scale thermal/structural model for both an applied temperature (425 K) boundary condition and an applied flux boundary condition (600 W) on a linear scale. The values for the vacuum case are on the left, the values for the air case are in the center and the values for the thermal grease case are on the right. Next to each set of values is the percent difference between the calculated resistances for the two boundary conditions.

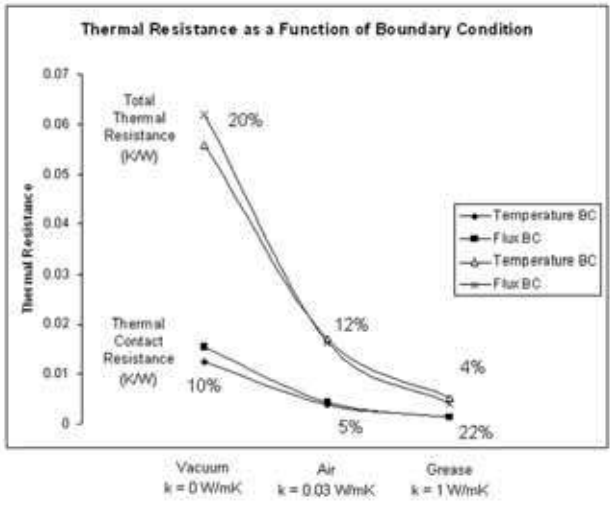

Figure 5-8: Total Thermal Resistance and Thermal Contact Resistance vs. Boundary Conditions (Linear Scale)

The differences between the temperature and heat flux boundary conditions for the total thermal resistance of the system were: 20% (vacuum), 12% (air) and 4% (grease). The differences between the temperature and the heat flux boundary conditions for the thermal contact resistance were: 10% (vacuum), 5% (air) and 22% (thermal grease). So the choice of boundary condition is not a major factor in determining TCR, but it is significant enough to justify applying the proper BC for the system of interest.

5.2.2 Contact Resistance vs. Total Resistance

Figure 5-9 shows the same plot as Figure 5-8 but on a logarithmic plot. The percentages next to the plots show the contribution of thermal contact resistance to the total thermal resistance of the system for both the temperature and heat flux boundary conditions. The smaller percentage represents the difference for the temperature BC and the larger percentage represents the difference for the flux BC.

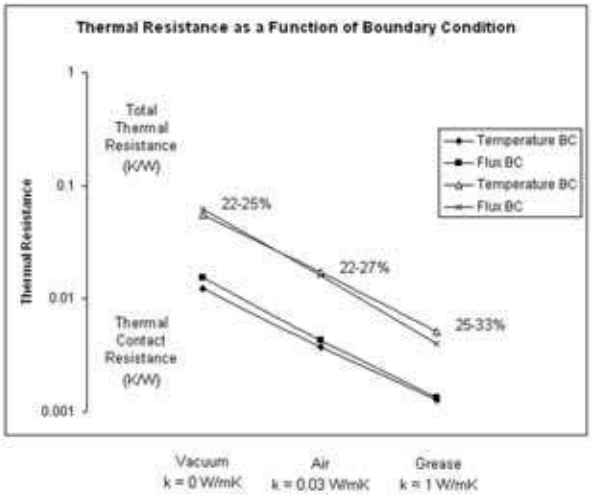

Figure 5-9: Total Thermal Resistance and Thermal Contact Resistance vs. Boundary Conditions (Log Scale)

The plots shows that for both sets of BCs and all three interstitial materials, the thermal contact resistance is approximately 25% of the total thermal resistance of the system. The percentage increases slightly with the thermal conductivity of the material at the interface. This shows very clearly that while the thermal contact resistance is a significant portion of the overall thermal resistance, it is not the dominant resistance. Instead, the thermal resistances through the bulk of the base plate and the heat sink are the dominant resistances. This is a very important result for deciding what aspects of the system to target for optimization to reduce the total thermal resistance in the system and increase the amount of heat that can be removed from the PEM.

5.2.3 One Dimensional Approximations

Figure 5-10 shows the same plot that was used in Figure 5-8 and Figure 5-9. This time, the values for the temperature BC have been excluded. The new line on the plot represents the total thermal resistance which has been calculated using a one dimensional (1D) approximation. Recall from Chapter 3 that the 1D thermal resistance for heat conduction is given by:

$$R_{cond} = \frac{L}{kA} \qquad [5.1]$$

where L is the length or distance that the heat must flow [m], k is the thermal conductivity of the material through which the heat flows [W/mK], and A is the cross sectional area through which the heat flows [m^2]. The thermal resistances for the bulk of the base plate and heat sink were calculated using this relation and added to the calculated thermal contact resistance to compare to the calculated total thermal resistance and determine the validity of the traditional 1D approximation for bolted plate systems.

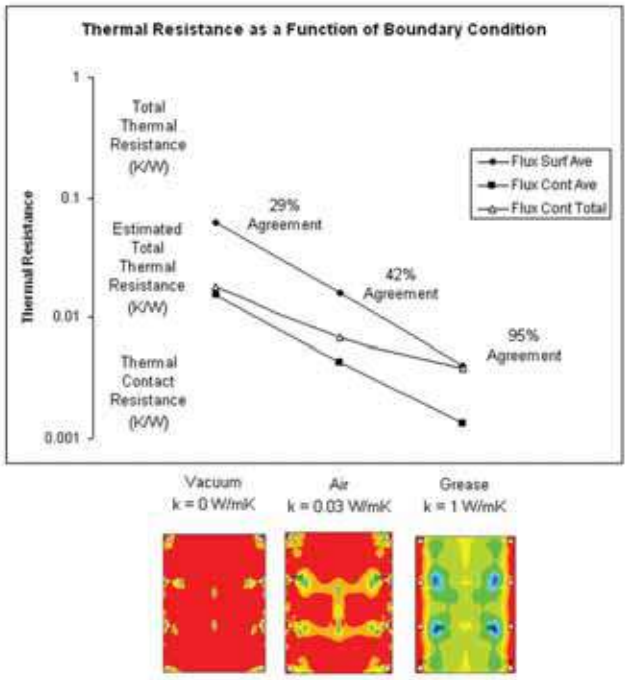

Figure 5-10: Total Thermal Resistance (As-Simulated and 1D Approximation) and Thermal Contact Resistance

The 1D approximation produced a total thermal resistance that was only 29% of the calculated value for the vacuum case, 42% of the calculated value for the air case and 95% of the calculated value for the thermal grease case. This indicates that the 1D approximation is only valid for the case where there is thermal grease at the interface.

The results match well with expectations. For the vacuum case and also for the air case to a lesser extent, the heat transfer across the interface is due to solid/solid conduction. The contact between the two plates is primarily at the center and at the bolt holes so heat generated in regions that are far away from the contact areas have a very long distance to travel through the bulk to reach a contact region. Thus, the path length (L) for the vacuum and air cases is up to twenty times larger (100 mm vs. 5 mm) for the 3D than for the 1D cause. The thermal conductivity for both cases (k) is the same. However, the cross sectional area for the heat path to the contact regions is poorly defined so a comparable 3D resistance cannot be defined. For the thermal grease case, the heat flux is relatively uniform across the surface so the heat transfer is nearly 1D and a quasi-1D approximation is more appropriate.

5.2.4 Load

Figure 5-11 shows the effect of applied load on the macro scale total thermal resistance and thermal contact resistance. The total thermal resistance has four curves: one for the vacuum case, one for the air case, one for the thermal grease case, and one “predicted” curve. The values for the predicted curve were obtained by calibrating the experimental value for total thermal resistance against the values for the air and thermal grease case. Each value on the predicted curve represents the same percent contribution from the air and thermal grease values. The experimental value for total thermal resistance is shown on the predicted curve in turquoise. The dashed line represents the as-designed applied load. All other values represent loads which could be applied to the model and their effect on the thermal resistances in the model. The experimental value for the thermal contact resistance of the PEM system is unknown so the predicted curve has been excluded from these curves.

The thermal resistances at the macro scale show a similar trend as the values at the micro scale. There seems to be a threshold value for applied load. Below the threshold value, the thermal resistances increase dramatically. Above the threshold value, the system is relatively insensitive to applied load. It is likely that the threshold value represents the applied load required to deform the two plates and bring them into contact. Once in contact, additional load is unlikely to increase the contact area significantly. Figure 5-12a demonstrates that the apparent area of contact is approaching an asymptotic value at approximately the same rate as the thermal resistances which confirms this. Similarly, the thermal resistances for the cases with thermal grease at the interface seem to be controlled by the average contact gap (Figure 5-12b).

By increasing the applied load by a factor of four, the performance for the vacuum case can be increased 16%. The improvement for the rest of the cases including the predicted case is less than 2%.

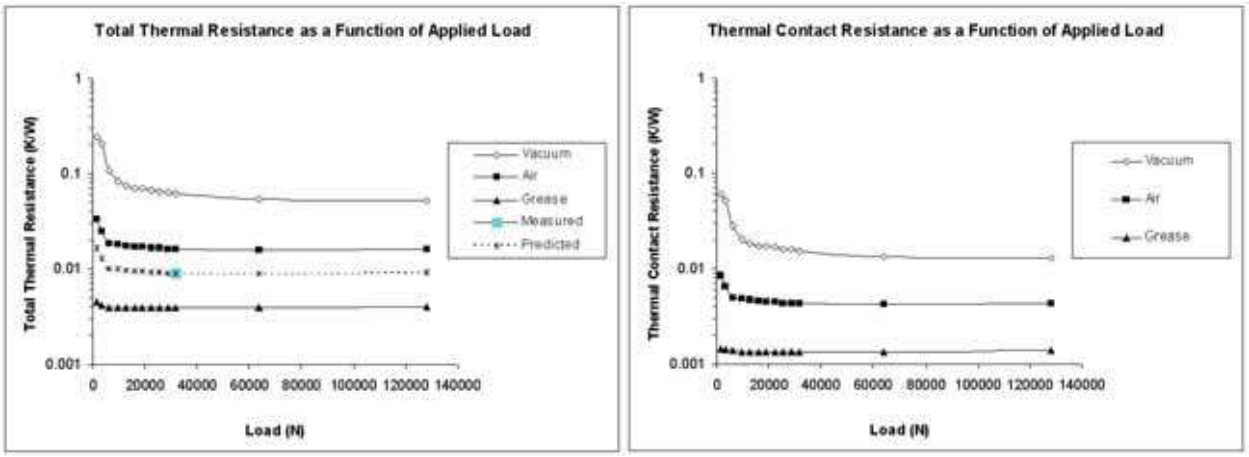

Figure 5-11: Total Thermal Resistance and Thermal Contact Resistance vs. Applied Load

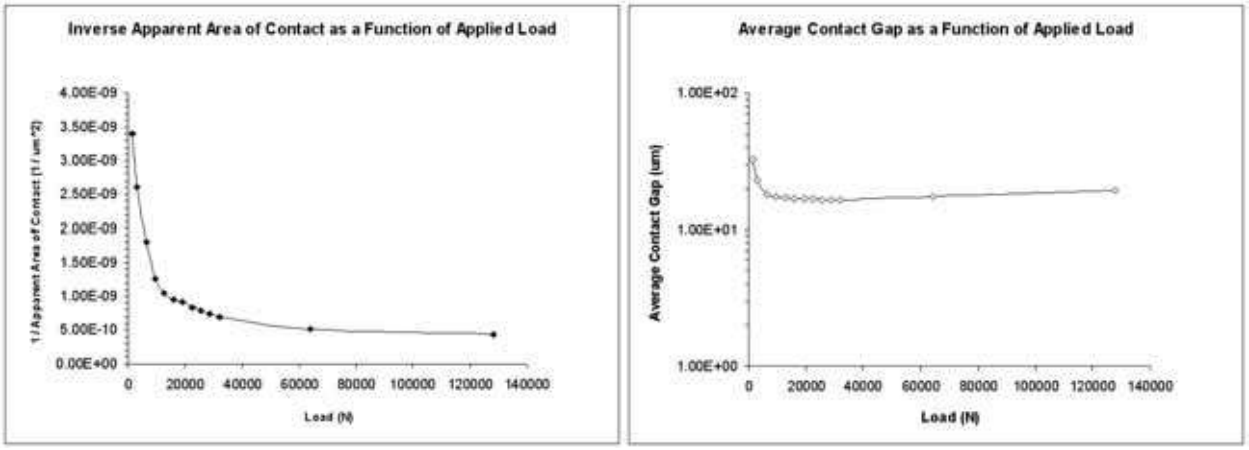

Figure 5-12: Inverse Apparent Area of Contact (left) and Average Contact Gap (right) vs. Applied Load

5.2.5 Thermal Conductivity

In Section 5.2.2 it was shown that the thermal contact resistance is only approximately one quarter of the total thermal resistance in the system. Therefore, it may be valuable to attempt to reduce the thermal resistances in the bulk of the base plate and heat sink by increasing the thermal conductivity of the bulk materials. Since aluminum is a reasonably good conductor of heat, the only economical improvement would be to replace one or both plates with copper. Figure 5-13 shows the total thermal resistance and the thermal contact resistance for the case study system with the original materials (AlSiC and aluminum), with a copper heat sink, with a copper base plate and with copper for both plates.

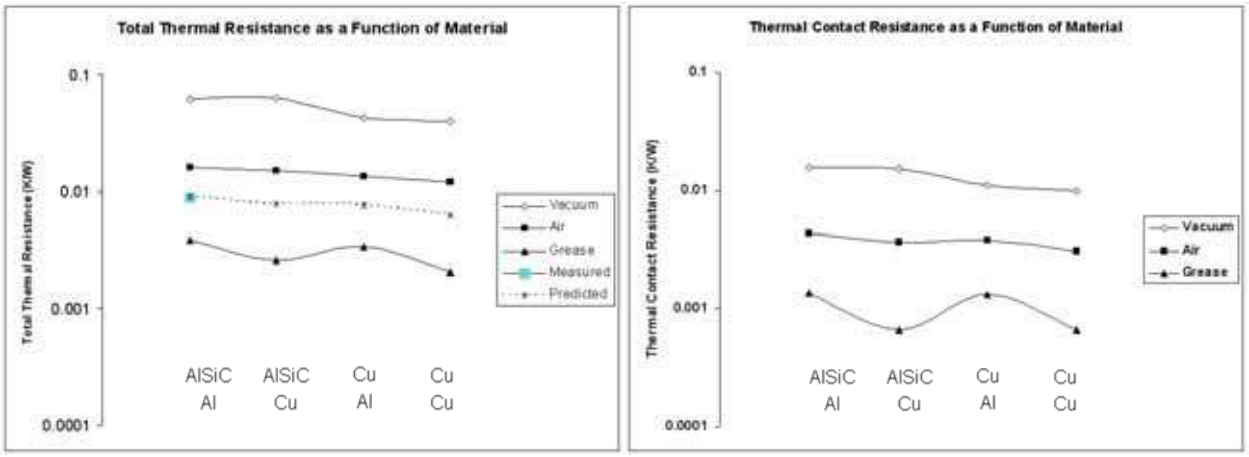

Figure 5-13: Total Thermal Resistance and Thermal Contact Resistance vs. Thermal Conductivity

The results for total thermal resistance and thermal contact resistance highlight the coupled nature of the thermal/structural solution. The copper has a higher thermal conductivity than the aluminum and the AlSiC (385 W/mK vs. 175 W/mK) but it also has a higher Young's Modulus than the aluminum (175 GPa vs. 68.5 GPa). So for the case with an AlSiC base plate and a copper heat sink, the increased thermal conductivity improves the performance for the systems with air and thermal grease but the increased Young's Modulus actually worsens the performance for the system with vacuum at the interface. For all of the other combinations, the copper improves the performance at least slightly.

By replacing both plates with copper, the vacuum case can be improved 36%, the air case can be improved 25%, the grease case can be improved 47%. This results in a predicted improvement of approximately 30%.

5.2.6 Flatness and Surface Form

Figure 5-14 shows the total thermal resistance and thermal contact resistance as a function of the amplitude for the base plate surface form (bow). The air, grease and predicted cases show an overall improvement of 63%, 13% and 50% respectively as the surface form approaches zero. This is because the average contact gap decreases significantly as the surface form is reduced (Figure 5-15) which in turn increases interstitial heat transfer in the presence of air (63%) or thermal grease (13%). However, the performance of the vacuum case actually gets worse for a perfectly flat plate (-11%). This is because the two contact regions that were located in the center of the plate and the contact regions towards the center near the four middle bolt holes disappear as the surface form goes to zero. This increases the path that the heat must travel to find a contact region and thus increases the

thermal resistance. Thus, the plate should be as flat as possible if an interstitial material (air or thermal grease) is present. Otherwise, the plate should be as flat as possible without losing convexity.

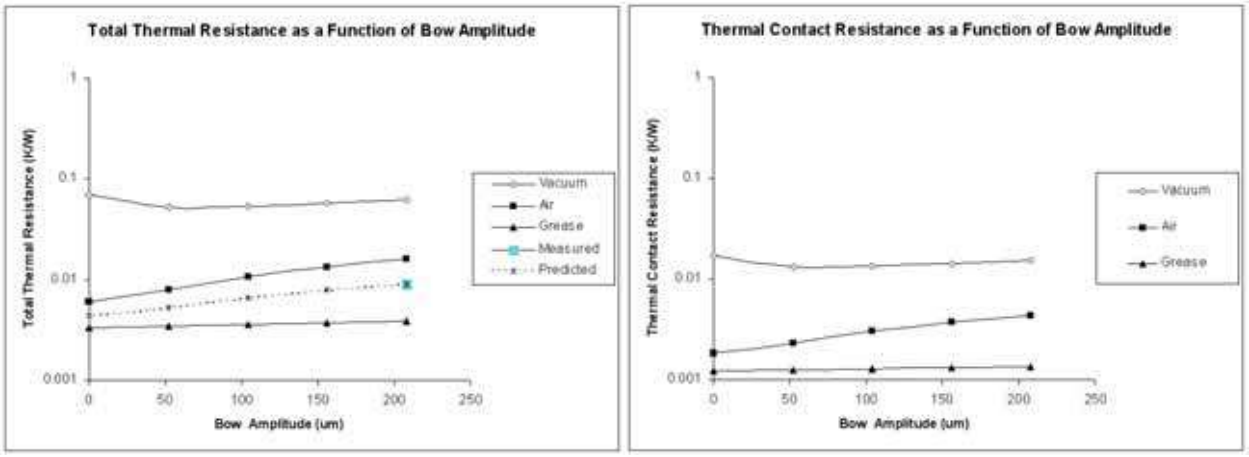

Figure 5-14: Total Thermal Resistance and Thermal Contact Resistance vs. Bow Amplitude

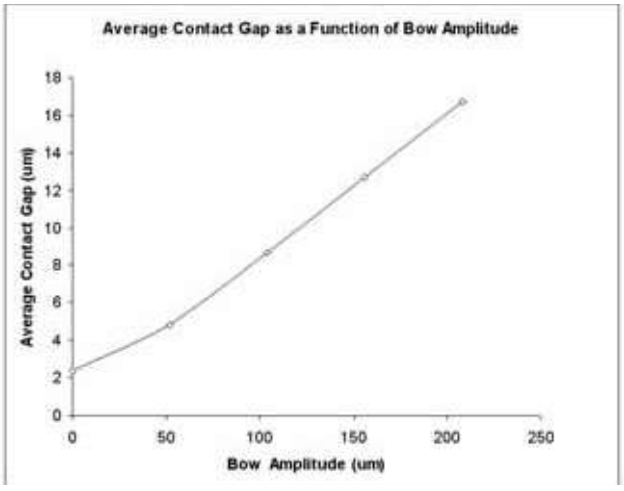

Figure 5-15: Average Contact Gap vs. Bow Amplitude

5.2.7 Base Plate and Heat Sink Thickness

Another option for reducing the total thermal resistance in the system is to reduce the thickness of the base plate and/or the heat sink. Reducing the thickness will reduce the conduction path slightly for the vacuum and air cases and dramatically for the thermal grease case. However, it will also reduce the mechanical stiffness of the plates and change the deformation behavior of the plates which may an unexpected impact on the contact area and average contact gap.

The total thermal resistance and thermal contact resistance as a function of base plate thickness are shown in Figure 5-16. The vacuum and air cases show a significant reduction in thermal resistance by increasing the base plate thickness which corresponds to an increase the real area of contact between the two plates. The thermal contact resistance for the thermal grease also shares this decrease due to a decrease in the average contact gap between the plates. The total thermal resistance for the thermal grease, however, increases with base plate thickness (L) as the 1D thermal resistance to conduction (L/KA) increases. This is another good example of the coupled nature of the thermal and structural contact solutions.

By increasing the base plate thickness from 5mm to 7mm, the total thermal resistance is decreased by 18% for the vacuum case and by 4% for the air case. The total thermal resistance increases by 9% for the thermal grease case and is unchanged for the predicted case. Given the coupled nature of the results for the base plate thickness, it is recommended that this parameter be omitted from optimization.

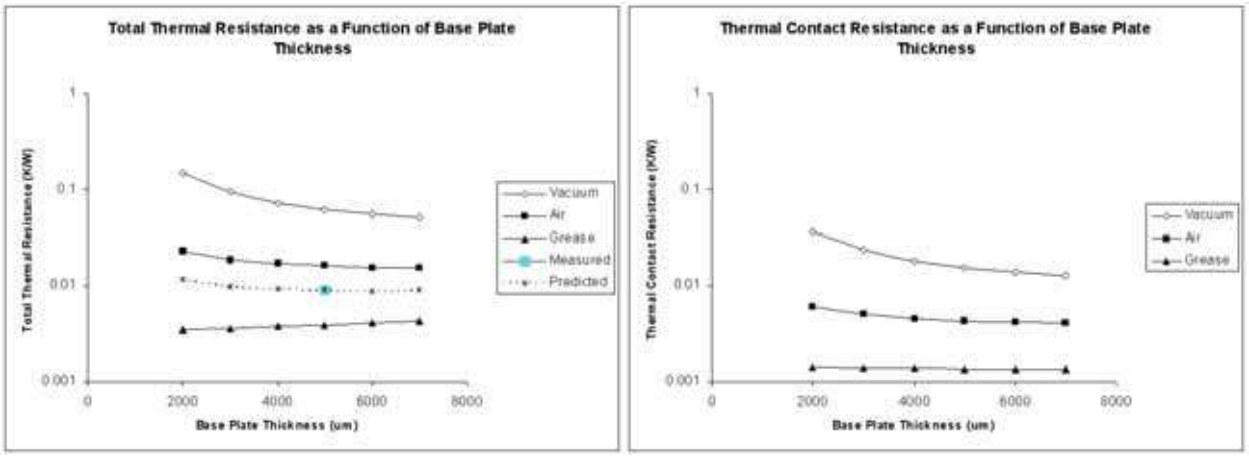

Figure 5-16: Total Thermal Resistance and Thermal Contact Resistance vs. Base Plate Thickness

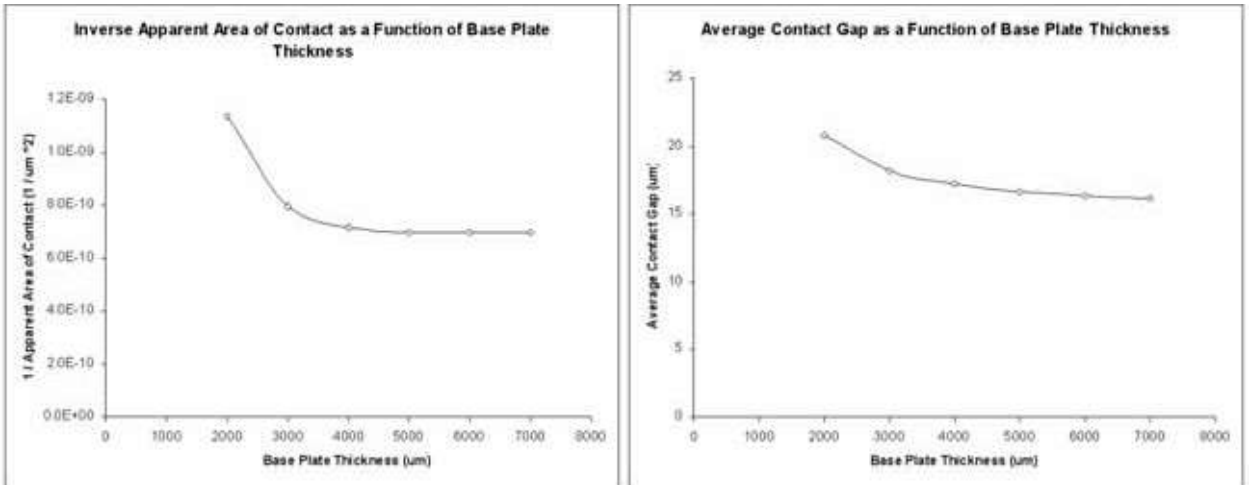

Figure 5-17: Inverse Apparent Area of Contact (left) and Average Contact Gap (right) vs. Base Plate Thickness

In contrast, the total thermal resistance and thermal contact resistances for all three interstitial materials decrease slightly as the thickness of the heat sink is reduced. By reducing the thickness of the heat sink from 10 mm to 5mm, the total thermal resistance of the system may be reduced by: 4% for the vacuum case, 7% for the air case and 30% for the thermal grease case. This leads to an overall improvement of 12% for the predicted case. Since the system seems relatively insensitive to the heat sink thickness, it is suggested that this parameter also be omitted from optimization.

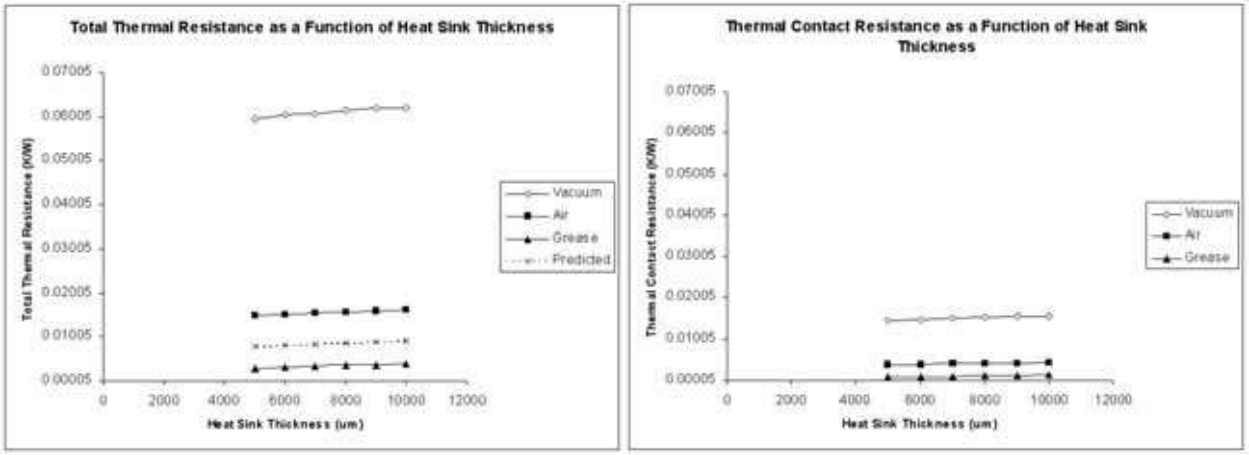

Figure 5-18: Total Thermal Resistance and Thermal Contact Resistance vs. Heat Sink Thickness

5.2.8 Micro Scale Thermal Contact Resistance

Figure 5-19 shows the total thermal resistance and the thermal contact resistance for the macro scale system as a function of the micro scale thermal contact resistance per unit area. (Recall that the micro scale TCR is implemented in the macro scale model as the TCC real constant which is equal to the inverse of micro scale TCR.)

The macro scale system seemed relatively insensitive to the micro scale TCR values with an interstitial material. Over a range from 1e-4 to 1e-7 Km^2/W, the vacuum case improves 62%, but the air case only improves 7% and the thermal grease case improves 2%. The predicted improvement is 6%.

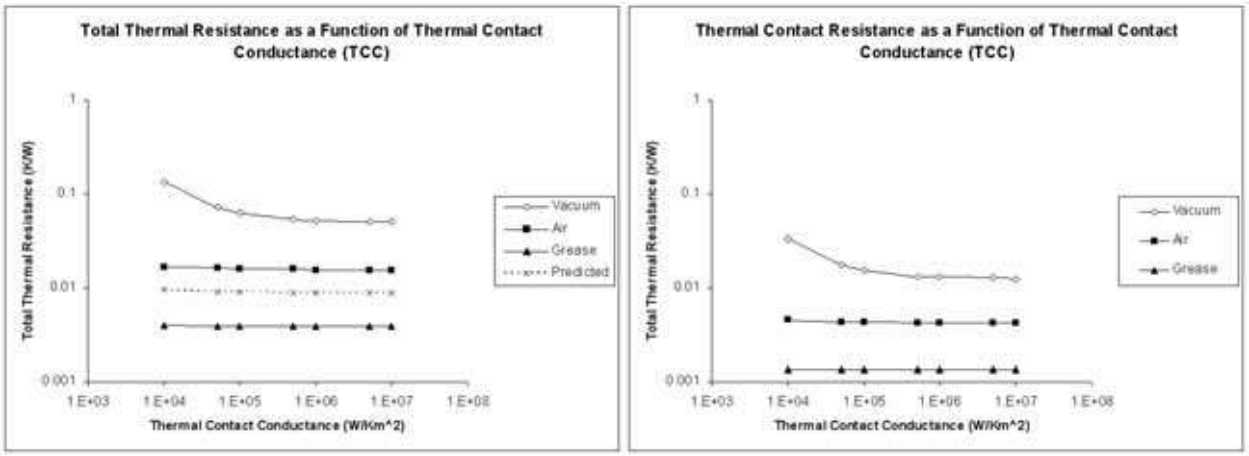

Figure 5-19: Total Thermal Resistance and Thermal Contact Resistance vs. TCC

5.3 Improving PEM Performance

Given the results above, the best possible combination of all parameters would be to:

- Increase the load by a factor of 4 (20 Nm of torque per bolt)
- Eliminate surface bow (perfectly flat) for air or thermal grease case
- Minimize surface bow to maintain convexity for vacuum case
- Replace materials for base plate and heat sink with copper
- Decrease micro scale TCR to 1e-7 Km^2/W by increasing the micro scale mechanical load and reducing the micro scale surface roughness

The results for this combination of parameters are shown in Table 5-1. This shows that the performance of the PEM system can be increased by up to 153% if all of the proposed changes are possible.

Table 5-1: Results for Optimum PEM System Design

	Total Resistance As-Designed [K/W]	Total Resistance Best Case [K/W]	% Improvement
Vacuum	5.69e-2	2.89e-2	97%
Air	1.60e-2	6.84e-3	134%
Predicted	8.98e-3	3.55e-3	153%
Grease	3.90e-3	1.17e-3	232%

5.4 Summary

Table 5-2 shows a summary of the improvements that are possible for the PEM system. Each cell represents the percentage that the total thermal resistance is reduced for each of the three interstitial materials (vacuum, air and thermal grease) and for the predicted performance of the PEM based on the experimental value provided by the manufacturer. Cells that are empty represent total thermal resistances which increased instead of decreased as is desired. Recall that the predicted values were obtained by calibrating the experimental value for total thermal resistance against the values for the air and thermal grease case. Each predicted value represents the same percent contribution from the air and thermal grease values.

Table 5-2: Options for Improving PEM System Performance

	Vacuum	Air	Grease	Predicted
4x Load	16%	< 2%	< 2%	< 2%
Copper Plate / Sink	36%	25%	47%	30%
No Surface Bow	X	63%	13%	50%
7 mm Thick Base Plate	18%	4%	X	X
5 mm Thick Heat Sink	4%	7%	30%	12%
1e-7 Km^2/W $r_{contact}$	62%	7%	2%	6%
Best Case	97%	134%	232%	153%

5.5 Conclusions

It was shown that the micro scale system is insensitive to the nature of the applied thermal load as long as the results from the macro scale model for the elements in contact are used. The micro scale system is sensitive to applied structural load, surface roughness and nano scale thermal boundary resistance. The applied load and thermal boundary resistance seemed to exhibit a threshold type behavior while the relationship between thermal contact resistance and surface roughness seemed to be linear. The thermal contact resistance per unit area for the vacuum and air cases seems to be inversely proportional to contact area, while the TCR per unit area for the thermal grease case seems to be directly proportional to the average interstitial gap size. The choice of surface sample and imported lateral resolution seemed to have a relatively small effect on the model. The effects of the surface modeling parameters will be explored further in future work.

It was shown that the macro scale system is relatively insensitive to the nature of the applied thermal load, the applied structural load, the micro scale thermal contact resistance and the thickness of the heat sink. The thermal resistances are sensitive to base plate thickness, the amplitude of the surface form and the thermal and mechanical material properties of the base plate and the heat sink. The applied load and micro scale thermal contact resistance both exhibited a threshold type behavior. Again, the total thermal resistance and thermal contact resistance for the vacuum and air cases seems to be inversely proportional to contact area, while the TCR for the thermal grease case seems to be directly proportional to the average interstitial gap size. The macro scale system also exhibited strong coupling between the thermal and structural solutions, especially for the surface form amplitude and the base plate thickness, which can make it difficult to predict the effect than altering certain parameters will have on the thermal resistances in the model. It was shown that the thermal contact resistance on the macro scale contributes approximately 25% to the total thermal resistance of the system regardless of interstitial material. It was also shown that one dimensional thermal conduction resistances (L/KA) apply only for the cases where thermal grease is present at the interface.

Finally, it was shown that the PEM system for the case study can be improved by up to 153% if thermal grease is used, the applied structural load is increased by a factor of four, the surface form (bow) is eliminated, the micro scale thermal contact resistance is reduced to 1e-7 Km^2/W and the base plate and heat sink materials are replaced with copper.

Chapter 6: Conclusions and Future Work

6.1 Summary

Chapter 1 presented a summary of the work and the significant results. The choice of finite element program for this work was also presented.

Chapter 2 presented a method for importing surface measurement data into a finite element program and two methods for creating surface geometry using the imported data. It was shown that it is possible to solve relatively small contact problems with real surface geometry on a desktop computer. The results of mechanical contact analyses with imported surface geometry were shown to qualitatively match expectations.

Chapter 3 presented a multi-scale iterative approach to model thermal contact resistance on the macro and micro scale to be used in conjunction with the finite element surface modeling methods developed in the previous chapter. The assumptions and limitations of the model were discussed and future improvements to the model were suggested.

In Chapter 4, a commercial power electronics module (PEM) which exhibited both macroscopic surface form and micro scale surface roughness was analyzed using three different macro scale surface models and three different interstitial materials to demonstrate the method, to verify the accuracy of the model and to demonstrate the impact of geometric surface assumptions. The PEM base plate, which was bolted to an ideal heat sink, was modeled as ideal (perfectly flat), idealized (sinusoidal) and real (imported) with vacuum, air, and thermal grease in the interface.

The predicted macro scale contact patterns for the imported surface model was shown to match well with the experimental contact pattern. The results of the imported thermal/ structural analysis on the macro scale with air (R = 1.61e-2 K/W) and thermal grease (R =3.91e-3 K/W) bound the experimental measurements (R = 9e-3 K/W) as expected. The micro scale analysis predicts a thermal contact resistance per unit area that is similar to experimental values from the literature. Hence, the proposed multi-scale iterative finite element model can be used in conjunction with imported surface geometry to predict the thermal resistances of bolted systems, quantitatively study the effects of manufacturing tolerances, and determine rationally how improve system performance.

While the thermal and structural results were qualitatively similar for all three surface models, quantitatively the results differed by up to 98%. In addition, the ideal and idealized surface models do not bound the experimental measurement of total thermal resistance for the PEM. The experimental value (R = 9e-3 K/W) was 20% higher than the upper bound (worse case) simulations with air as the interstitial material ($R_{air,ideal}$ =

7.16e-3 K/W and $R_{air,idealized}$ = 7.32e-3 K/W). This showed that the ideal and idealized (non-imported) surface models cannot be used to predict the thermal resistances for the case study and validated the need for better surface modeling.

In Chapter 5, the factors influencing the micro and macro scale thermal/structural behavior of bolted plates were examined and recommendations for reducing both contact resistance and the overall thermal resistance of bolted plates were presented. It was shown that the micro scale system is insensitive to the nature of the applied thermal load as long as the results from the macro scale model for the elements in contact are used. The micro scale system is sensitive to applied structural load, surface roughness and nano scale thermal boundary resistance. The applied load and thermal boundary resistance seemed to exhibit a threshold type behavior while the relationship between thermal contact resistance and surface roughness seemed to be linear. The thermal contact resistance per unit area for the vacuum and air cases seems to be inversely proportional to contact area, while the TCR per unit area for the thermal grease case seems to be directly proportional to the average interstitial gap size. The choice of surface sample and imported lateral resolution seemed to have a relatively small effect on the model. The effects of the surface modeling parameters will be explored further in future work.

It was shown that the micro scale system is insensitive to the nature of the applied thermal load as long as the results from the macro scale model for the elements in contact are used. The micro scale system is sensitive to applied structural load, surface roughness and nano scale thermal boundary resistance. The applied load and thermal boundary resistance seemed to exhibit a threshold type behavior while the relationship between thermal contact resistance and surface roughness seemed to be linear. The thermal contact resistance per unit area for the vacuum and air cases seems to be inversely proportional to contact area, while the TCR per unit area for the thermal grease case seems to be directly proportional to the average interstitial gap size. The choice of surface sample and imported lateral resolution seemed to have a relatively small effect on the model. The effects of the surface modeling parameters will be explored further in future work.

It was shown that the macro scale system is relatively insensitive to the nature of the applied thermal load, the applied structural load, the micro scale thermal contact resistance and the thickness of the heat sink. The thermal resistances are sensitive to base plate thickness, the amplitude of the surface form and the thermal and mechanical material properties of the base plate and the heat sink. The applied load and micro scale thermal contact resistance both exhibited a threshold type behavior. Again, the total thermal resistance and thermal contact resistance for the vacuum and air cases seems to be inversely proportional to contact area, while the TCR for the thermal grease case seems to be directly proportional to the average interstitial gap size. The macro scale system also exhibited strong coupling between the thermal and structural solutions, especially for the surface form amplitude and the base plate thickness, which can make it difficult to predict the effect than altering certain parameters will have on the thermal resistances in the model. It was shown that the thermal contact resistance on the macro scale contributes

approximately 25% to the total thermal resistance of the system regardless of interstitial material. It was also shown that one dimensional thermal conduction resistances (L/KA) apply only for the cases where thermal grease is present at the interface.

Finally, it was shown that the PEM system for the case study can be improved by up to 153% if thermal grease is used, the applied structural load is increased by a factor of four, the surface form (bow) is eliminated, the micro scale thermal contact resistance is reduced to 1e-7 Km^2/W and the base plate and heat sink materials are replaced with copper.

6.2 Conclusions

6.2.1 Surface Modeling and Importation

- Historically surfaces were modeled with idealizations and it was assumed to be impossible to use real surface data
- It was shown that it is now possible to import real surface data and create surface geometry using surface data
- Qualitatively it was shown that surface importation is viable surface modeling option
- Quantitatively it was shown that imported surfaces behave differently (up to 98%) from idealized surfaces and succeed in predicting TCR where the idealized surfaces did not

6.2.2 Thermal Contact Resistance for Bolted Joint Case Study

- A multi-scale iterative finite element model was developed to predict thermal contact resistance
- It was confirmed that model produces good results
- Simulated contact for bolted joint systems was primarily around the bolt holes as expected
- The coupled thermal-structural nature of TCR was demonstrate
- It was shown that base plate thickness and thermal conductivity cannot be optimized for both vacuum and grease due to thermal/structural coupling in the system and in the material properties
- It was shown that resistance through bulk dominates performance for the case study system
- It was shown that 1D Assumptions (L / KA) only valid for 1D systems (grease)
- The micro scale model was insensitive to: BCs
- The micro scale was sensitive to: load, surface roughness, $r_{boundary}$
- The bolted systems was insensitive to: load, BCs, $r_{contact}$
- The bolted systems was sensitive to: plate thickness, flatness, conductivity
- TCR for vacuum and air seems to have a strong dependence on inverse RAoC for both scales
- TCR for grease seems to have a strong dependence on average contact gap for both scales

- Could improve PEM performance by ~ 153% by increasing the applied mechanical load by a factor of 4, by eliminating or minimizing the surface bow, replacing the base plate and heat sink materials with copper and by reducing the micro scale thermal contact resistance

6.3 Future Work

The ability to import measured surfaces into finite element models opens up new questions and new opportunities in fields such as surface characterization, tribology, fluid sealing, thermal and electrical contact, and more. The future work section focuses on work that is now possible with the methods presented in this work.

6.3.1 Future Work for Surface Modeling

Surfaces are clearly a function of length scale, however this work has not fully investigated many of the length scale issues in surface modeling. For example, how much surface data per unit area is required to adequately represent the behavior of the surface? The answer will determine the minimum imported lateral resolution of surface models and thus will impact surface modeling. Clearly more surface data would produce a more accurate model, but it would also increase the cost of solving the model. Today we are limited by the size of models that can be solved. Perhaps, some sort of model size limit will always exist. But these limits are decreasing daily and soon it will be a question of efficiency instead of possibility.

How large a foot print is required when measuring micro scale surface topography to obtain a representative surface sample? Will a 10 um x 10 um sample suffice? Is 100 um x 100 um require or more? Does the required foot print vary by material or manufacturing process? Are multiple measurements required?

The relationship between the length scale(s) of the imported surfaces and the length scales of the finite element mesh and the so-called pinball region should also be considered in future work.

Future work should focus on continuing to improve the assumptions in the surface models. This includes the incorporation of advanced material models including plasticity, viscoelasticity, viscoplasticity, etc. This work has only addressed static contact, but sliding contact will be required for tribological applications. Surface coatings and interstitial layers such as metal foils may be added. In the far future, other surface factors including surface chemistry may also be addressed.

It will be important to determine when idealized and characterized surfaces can be used in place of imported surfaces in numerical models. Finally, it may be possible use the imported surface technology to compare current surface modeling techniques and suggest better methods for surface characterization and surface modeling.

6.3.2 Future Work for Thermal Contact Resistance of Bolted Plates

In the future, it may be valuable to consider alternate solutions to reducing the total thermal resistance of the PEM case study system, including using micro and meso scale surface texturing to reduce thermal contact resistance between the two plates; placing a thin malleable metal foil between the contact surfaces to increase contact area and reduce thermal contact resistance; and removing the heat sink altogether and using forced air cooling to remove the heat from the base plate.

It is known that the diameter, arrangement and spacing of the bolt holes in bolted plate systems affects the thermal performance of the system. It would be valuable to investigate the effect of bolt hole geometry on total thermal resistance and thermal contact resistance.

The modeling of the bolted regions of the macro scale system should be improved by including the bolts in the model. Thermal expansion should also be taken into account at the bolted region and elsewhere in the model.

The iterative multi-scale finite element model presented in this work incorporated a number of averaging assumptions. These include the fact that the micro scale model was solved for a single averaged contact pressure and the fact that the TCC value for the macro scale model was applied as a single averaged value. In addition, the macro scale thermal contact resistance was reported as a single averaged value. It would be very valuable in the future to consider removing some of these averaging assumptions and refining the model.

While many historical analytical models and experimental correlations were reviewed in the course of this work, they were not presented in any of the literature searches and the results of this work were not compared to previous work. It would be valuable to determine how well this model compares to those results and what improvement, if any, the numerical model offers to the community.

Finally, it was shown that there are clear relationships between total thermal resistance, apparent area of contact, and average contact gap. It would be very interesting to determine if the derived mechanical solutions from this work (average and maximum contact gap, average contact pressure, etc.) can be used to create new thermal contact models.